Università degli Studi di Torino

PhD Program in Complex Systems for Quantitative Biomedicine

Department of Oncology

Title of the thesis:

"Experimental models of CAR-redirected cellular therapy with CIK lymphocytes against ovarian cancer peritoneal carcinomatosis"

Cycle: XXXVI

Academic years: 2020-2023

PhD Program Coordinator: Prof. Enzo Medico

Candidate: Federica Galvagno

Internal Tutor: Prof. Alberto Puliafito

External Tutor: Prof. Dario Sangiolo

Ai miei genitori

ACKNOWLEDGEMENTS

I would like to express my sincere gratitude to all those who have accompanied me all along my PhD, in various ways and in different roles.

To the two complementary Professors and my thesis supervisors, who scientifically guided me along my work, Professor Alberto Puliafito and Professor Dario Sangiolo. I would like to thank both for giving me the unique opportunity to be a part of their research groups, trusting me and supporting my scientific growth. They contributed to a rewarding PhD thesis experience, through valuable, experienced and constructive scientific advice during the planning and development of this research work and by always encouraging me. It has been a great privilege to work with her at the Candiolo Cancer Institute, surrounded by excellent scientists. In particular, I am very thankful to Professor Puliafito, for his enormous patience in having tough me a central part of what I learned during these years, for his guidance, the suggestions and time he dedicated to my growth.

To Professors Antonio Rosato and Claudia Marchetti who have read and critically reviewed this work.

A special thank goes to my former colleagues of the Experimental Cell Therapy laboratory, Valeria, Annamaria, Chiara, Ramona, Alessia, Letizia, Andrea and Elisa for sharing this experience with me and for providing me indispensable tools to face the doctorate path, with scientific and moral support, even along the most tragicomic moments of my PhD journey.

Likewise, I would also like to thank Professor Luca Primo and my current colleagues, members of the Cell Migration laboratory, Laura, Vanesa, Isabel, Sabrina and Andrea. They motivated my interest towards science and helped me developing scientific critical thinking through laboratory meetings and seminars. Together with Giorgia and Sushant, they support and help me every day in the lab, while interspersing with moments of fun.

My mum and dad, for their constant support, availability and effort, for the possibility they gave me to pursue the PhD, despite the risk of the future that this career brings with it.
To my friends, a sure thing from many years now.

TABLE OF CONTENTS

ABSTRACT

Background

Peritoneal carcinomatosis (PC) from ovarian cancer (OC) has poor prognosis and is in need for optimized therapies. Such a clinical condition displays a composite structure with floating cell aggregates with-in ascites and solid-like masses invading the peritoneum. A deep understanding of the dynamics is thus crucial to optimize the therapeutic strategies and knowledge.

Chimeric antigen receptor (CAR)-based immunotherapies are among the most suited treatments for the compartmentalized pathophysiology of PC. The ex vivo expanded cytokine-induced killer lymphocytes (CIK), intrinsically endowed with HLA-independent antitumor activity, are a valid platform to be exploited against solid tumors. However, appropriate preclinical models recapitulating the clinical hurdles are needed to better tailor the clinical translation and optimize currently available therapies.

Methods

Here, we explored the activity of mesothelin (MSLN) CAR-redirected CIK (MSLN-CAR.CIK) against advanced OC, by developing suitable 3D models resembling the complexity of peritoneal metastasis, where 3D mOC spheroids were co-cultured with MSLN-CAR.CIK, either floating in liquid medium or embedded in a 3D hydrogel. To measure MSLN-CAR.CIK activity we employed imaging-based methods.

Results

MSLN-CAR.CIK resulted functional in both 3D biological models recapitulating the floating as well as solid component of OC PC. Specifically, CAR.CIK were found to localize faster than NTD.CIK in both 3D liquid and solid settings. Recruitment kinetics of CAR.CIK on mOC aggregates in liquid was significantly faster when coupled to fluid flow in shaking cultures, reminiscent of spontaneous patient movement, than in absence of flow, coherently with the relative increase in cytotoxicity. Even in the 3D solid setting, CAR.CIK were functionally more efficient on mOC spheroids than NTD.CIK. However, the solid setting was characterized by slower kinetics and significantly influenced by the distance traveled by the effectors. CAR.CIK antitumor activity was found to be comparable to the liquid condition. Our data indicate that the kinetics of recruitment should therefore be considered when assessing CAR.CIK killing.

Conclusions

Our findings provide therapeutically relevant information on intraperitoneal approaches with CAR.CIK, supporting further developments and improvements for clinical studies in the context of locoregional cell-therapy approaches for patients with PC from OC.

INTRODUCTION

Chapter 1: Chimeric antigen receptor-based cell therapy and peritoneal carcinomatosis from advanced ovarian cancer

1.1 Cancer Immunotherapy

The immuno-oncology field has pointed out the crucial role played by the immune system in counteracting tumor development and progression, while immune evasion by cancer cells has been established as a hallmark of cancer [1,2].

The research focused on restoring patient immune response as well as exploiting the immune system to control and eliminate tumors has thus led to the evolution of cancer immunotherapies [3], that have proven to be effective and prolonged patients survival with otherwise rapidly fatal cancers [4].

In the latest decades, different categories of immune-based therapies have been developed in oncology among which the most important are immune checkpoint inhibitors (ICIs), cancer vaccines and adoptive cellular therapies (ACTs). It is important to underline, how while ICIs have shown promising results mostly in tumors of solid origin, such as lung cancer, melanoma, head and neck cancer, ACTs have gained success prevalently against hematological tumors, such as lymphomas and multiple myeloma [5,6].

1.1.1 Immune checkpoints inhibitors and cancer vaccines

The ICIs are drugs, mostly monoclonal antibodies (mAbs), developed to target ICs. ICs are receptors generally expressed by immune cells that regulate and maintain the immune cell function and homeostasis. ICs act generally as negative regulators of T lymphocytes function, aimed to prevent their hyperactivation and fine-tune their activity. However, tumor cells can acquire the ability to evade immune recognition and elimination by exploiting these regulators. ICIs have therefore the main role of re-activating the impaired cytotoxic T cells in the TME [7].

Examples of ICs are the cytotoxic T lymphocyte antigen 4 (CTLA-4), programmed cell death 1 (PD-1) and programmed cell death ligand 1 (PD-L1).

CTLA-4 is a receptor similar to the co-stimulatory molecule CD28 expressed by T cells, despite with opposing regulatory function [8]. CTLA-4 binds the co-stimulatory molecule B7 on the antigen presenting cells with greater affinity than CD28, thus inhibiting T cell priming and proliferation [9,10]. The first mAb against CTLA-4 approved by the Food and Drug Administration (FDA) was ipilimumab in 2011 for the targeting of melanoma, after reaching effective results in clinical trials [11], and since then, for the targeting of many other solid tumors [12]. Another

example of mAb against CTLA-4 is tremelimumab, which gained first approval in 2022 in combinatorial treatment for unresectable hepatocellular carcinoma [13].

PD-1 is an immune checkpoint generally expressed by T cells that, upon binding with PD-L1/2 molecules expressed on antigen presenting cells, negatively regulates T cell activation [14]. PD-1 on T cells has a central role in cancer immune evasion upon binding with PD-L1/2 ligands on tumor cells, causing effector T cell exhaustion and anergy [15]. mAbs targeting PD-1 such as pembrolizumab and nivolumab have been broadly indicated for the treatment of both solid and blood tumors (i.e. melanoma, non-small-cell lung carcinoma, Hodgkin lymphoma, head and neck squamous cell carcinoma, urothelial carcinoma and gastric cancers) [4]. Considering PD-1 ligands, the mAb atezolizumab targeting PD-L1 has been approved for treatment of different tumors including urothelial carcinoma, non-small cell lung cancer and hepatocellular carcinoma [16-18].

Generally, ICIs success has been mostly related to the so-called inflamed or “hot” solid cancers, rich in tumor-reactive T cells and other inflammatory immune cell types. However, it is very common to observe primary and acquired resistance to this type of treatments [19].

Cancer vaccines have a different molecular rationale than ICIs and aim to prepare and stimulate the immune system to react against tumor-related antigens and therefore protect from tumor cells. Cancer vaccines are categorized into preventive or therapeutic. Preventive vaccines are administered to healthy individuals, to reduce the incidence of viral hepatocellular carcinoma and cervical cancer [20]. Therapeutic vaccines instead stimulate the immune system to recognize and target neoplastic cells when already present, generally by identifying a tumor specific or associated antigen expressed significantly by tumor cells and less by normal tissues [21].

The applicability of this immunotherapy to a broad range of tumors is strictly limited by the identification of the optimal antigen: within a single tumor there may be thousands of somatic mutations turning into neoantigens, with difficulty in predicting which one could provoke the strongest antitumor immune response [22]. Therefore, this technology is currently moving toward the development of personalized design, with a ‘single patient and single disease’ precision [4].

1.1.2 Adoptive cell therapies

ACTs involve isolation, manipulation, expansion and reinfusion of immune cells into a donor patient to generate a more effective immune response against the tumor cells. Immune effectors can be represented by the tumor-infiltrating lymphocytes (TILs), a heterogeneous population of endogenous T cells isolated from patient cancerous lesions, or by mononuclear cells derived from peripheral blood [23,24].

Effectors can be selectively expanded and genetically engineered to induce the expression of a transgenic T-cell receptor (TCR) to recognize specific tumor antigens presented by the major histocompatibility complex (MHC) of the tumor cells. TCR-redirected T cells can recognize intracellular peptides, despite being restricted by the MHC level of expression and matching [25]. Another modality of ACT involves redirection of immune effectors with chimeric antigen receptor (CAR), exclusive for a given extracellular presented tumor antigen and independent of the MHC presentation [26].

Generally, ACTs, in particular CAR-cell therapies, have succeeded in targeting hematopoietic tumors such as B cell leukemia and lymphoma and multiple myeloma, with six drugs approved by the FDA [27].

In solid tumors however, despite a significant number of ongoing promising clinical trials, there are still very limited approved clinical application for ACT [28,29]. A recent promising example is represented by lifileucel (LN-144), an autologous TILs-based ACT approved in 2024 for the treatment of patients with advanced melanoma [30,31]. Of note, US FDA has lately accelerated the additional approval of afamitresgene autoleucel, the first example of engineered cell therapy approved for a solid tumor [32]. Afamitresgene autoleucel is a MAGE-A4-specific TCR T-cell therapy designed for advanced MAGE-A4+synovial sarcoma adult patients with certain HLA types, who have already received chemotherapy [33] . One of the greatest difficulties in reaching a broader range of approval for solid tumors is represented by the tumor microenvironment (TME). Differently from hematological tumors, solid masses present an immunosuppressive TME which prevents the entry and counteracts the activity of immune effector cells [34]. While ACTs are delivered systemically for blood tumors, with easy access to the target, ACT targeting solid tumors must face the tumor stroma, TME, altered vasculature and limited trafficking immune cells. Consequently, research efforts are active in trying to overcome this situation [35].

1.1.2.1 Chimeric antigen receptor-cell therapies: emerging opportunities beyond the practical difficulties for solid tumor

The engineered cellular or cell immunotherapies are a pool of treatments centered on the administration of modified living agents as cells of the immune system to fight tumor cells.

CAR- and TCR- engineered T cells are nowadays the object of promising studies. The immune effectors are obtained from leukapheresis or peripheral blood mononuclear cells (PBMCs), expanded ex vivo and genetically modified [36].

CAR cell therapies consist of genetically engineered immune cells expressing the CAR surface receptor, which specifically redirects the immune effector to recognize targets surface tumor antigens, with consequent immune cell activation and tumor destruction [26].

The complexity of the CAR structure can differ depending on the generation. Most commonly, the CAR is composed of four domains, such as a specific antigen-binding domain, usually a single-chain variable fragment (scFv) derived from a mAb targeting the antigen of interest, a hinge and a transmembrane domain that connect the extracellular domain to the intracellular signaling domains, and the intracellular signaling domains usually comprising of an activation domain (CD3ζ-derived immunoreceptor tyrosine-based activation motif) and one or more co-stimulatory domains (4-1BB or CD28) [37] **(Fig. 1A)**. The first-generation of CAR.T cells was designed to mimic T cell activation but was not highly effective at killing tumor-target, due to the inability to reach a sufficient co-stimulation. Consequently, the second- and third-generation of CAR.T cells were developed to provide additional co-stimulatory signals, through the insertion of a single or double co-stimulatory domains [38,39]. The fourth-generation of CAR.T cells, also known as "armored" CAR and termed T-cells redirected for universal cytokine-mediated killing (TRUCKs) are second-generation CARs engineered to release in an inducible way a transgenic product, commonly a pro-inflammatory cytokine such as interleukin-12 (IL-12), upon CAR activation, to boost CAR.T proliferation and counteract the immunosuppressive TME [40]. Finally, the fifth-generation of CARs are characterized by a single co-stimulatory domain added of a drug-dependent OFF-switch or ON-switch, which modulate CAR molecule to improve therapy safeness and productiveness [41] **(Fig. 1B).**

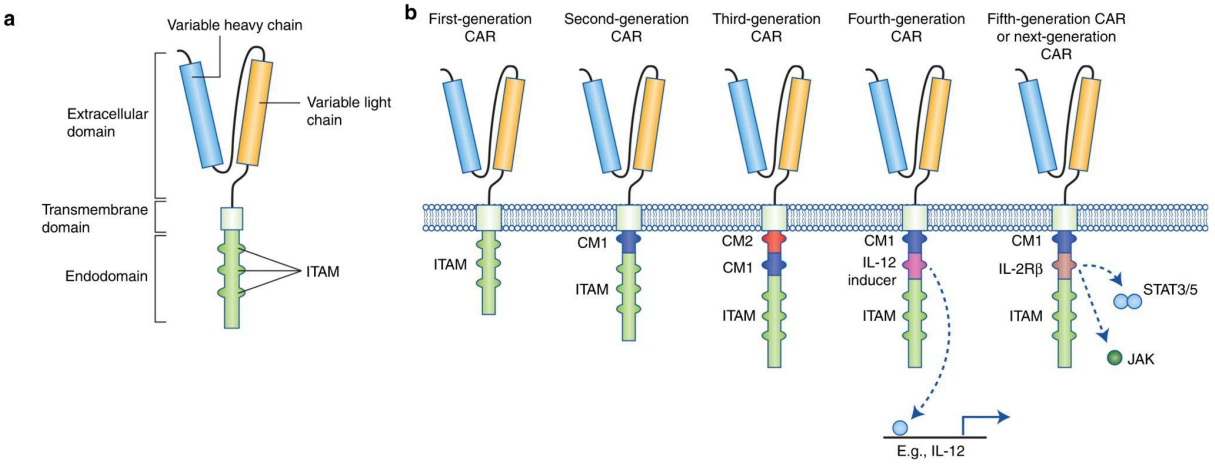

Figure 1. Structure of the CAR molecule from the first to the fifth generation. (A) Basic structure of CAR molecule, characterized by three main components: the extracellular domain composed of a single-chain fragment variant (scFV), a transmembrane domain transmitting the receptor-binding signal, and the endodomain. **(B)** Complexification of CAR molecular structure along the generations. (Modified from Tokarew N. et al., BJC, 2019).

CAR-cell engineering usually exploits viral approaches (lentiviral and γ-retroviral vectors) that enable the CAR-coding gene to integrate into the genome of immune cells [36]. However, the large-scale applicability of viral vectors still presents many difficulties in the affordability and scaling out of the manufacturing, therefore different non-viral based approaches are of current interest. The most known is the gene delivery method based on DNA transposons, for example the Sleeping Beauty technology [42]. The transposons are mobile genetic elements able to integrate themselves and the target gene into the genome of interest, while being cheaper and with a greater performance compared to viral vectors [43].

As already mentioned above, CAR-cell therapies employing T cells reached great results for treatment of hematologic malignancies, reaching approval by the FDA [27]. Therefore, these results have increased the prospect to apply this strategy against other types of malignancies, with intense research efforts currently devoted to translate the success in the challenging field of solid tumors [28]. In this regard, CAR.T cell therapy is object of investigation in a variety of solid tumors including lung cancer [44], pleural cancer [45], central nervous system tumors such as glioblastoma [46], osteosarcoma, peritoneal carcinomatosis (PC) [47] and many clinical trials are currently ongoing or just completed against ovarian cancer (OC) [48,49].

However, CAR-cell based treatments still present several radical limitations when targeting solid tumors, including OC, influencing different aspects of CAR-therapies outcome. The first limitation is the lack of well-defined and homogeneously expressed tumor specific antigens in solid tumors, compared to blood cancers. This limitation has increased the need for development of different strategies that can overcome tumor heterogeneity [50]. Since most of the targeted antigens in the CAR.T therapy of solid tumors are tumor-associated antigens, it is crucial to attempt overcoming on-target off-tumor toxicities, for instance by exploiting CAR targeting domains with a moderate affinity [51,52] or using mRNAs to express transiently the CAR [53,54]. Moreover, the CAR.T production process is expensive and labor-intensive [55], and even difficult when expanding T-cells from pre-treated patients [56]. Additionally, the severe toxicities resulting from CAR.T cell infusion — cytokine release syndrome (CRS) and immune effector cell-associated neurotoxicity - have been documented extensively, and being the focus of different studies to reduce their manifestation [57]. Finally, the application of an “off-the-shelf” allogenic CAR.T cell setting is still challenging [58]. These limitations make the identification of an efficient and optimized immune effector nontrivial, and sometimes make it necessary to find alternative effectors or side-by-side cell therapeutic approaches, in order to overcome some of these obstacles. Therefore, many different approaches other than CAR.T have entered preclinical and clinical testing for both solid and liquid tumor indications. Examples include natural killer (NK) cells [59,60], macrophages [61], γδ T cells, NKT and the cytokine-induced

killer lymphocytes (CIK), all accumulated by an intrinsic MHC-unrestricted antitumor activity [62]. Among them, CIK have been extensively tested in our lab and proved to be promising.

1.1.2.2 Cytokine-induced killer lymphocytes as immune effector for chimeric antigen receptor cell therapies

CIK are patient-derived ex vivo expanded T lymphocytes [63-65], that present a mixed T-NK phenotype. The ex vivo culture can start from different sources including PBMCs, where the CIK precursors are circulating naive T lymphocytes, mainly those with a naive CD3 positive and CD4 CD8 double negative phenotype [66]. A specific expansion protocol for CIK has been developed, involving the timed stimulation by interferon-γ (INF-γ), anti-CD3 antibodies and IL-2 [67,68]. Upon 14 days of expansion, the bulk population is mainly represented by CD3+CD56+ CIK, CD3+CD56- T cells, and a small fraction of CD3-CD56+ NK cells [67] **(Fig. 2A)**.

CIK are intrinsically endowed with MHC-independent antitumor activity, which does not require a prior antigen exposure or priming, but it is consequent to the interaction of their main killing receptor (natural killer group 2 member D - NKG2D) with the stress-inducible targets (MHC class I-related molecules A and B (MIC A/B) and the UL16-binding protein family members (ULBPs 1–6), commonly present on tumor cells [69] **(Fig. 2B)**. The engagement leads to the release of granzymes and perforins by CIK that provoke tumor target cell lysis [70].

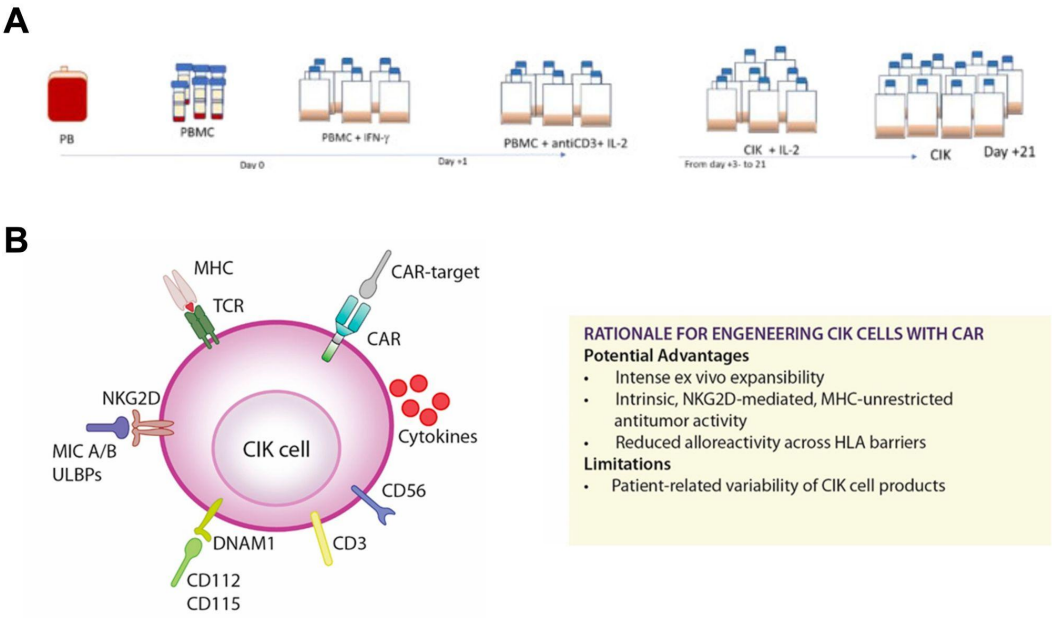

Figure 2. Main features of cytokine Induced killer lymphocytes (CIK). (A) Main steps of the ex vivo expansion protocol to obtain the CIK (Mareschi K.et al., Pharmac (Basels), 2020). **(B)** Main potential advantages and limitations of CIK for CAR engineering (Modified from Rotolo et al., Int J Mol Sci, 2019).
Abbreviations: PBMC, peripheral blood mononuclear cell; MHC, major histocompatibility complex; TCR, T cell Receptor; CAR, Chimeric Antigen Receptor; CD, Cluster of Differentiation; NKG2D,

Natural Killer Group 2D receptor; MIC A/B, MHC class I chain-related gene A/B; ULBPs, UL16 binding proteins; DNAM-1, DNAX Accessory Molecule-1; CIK, Cytokine Induced Killer.

Different preclinical and clinical trials against solid tumors, including hepatocellular carcinoma, lung cancer and renal cell carcinoma, outlined relevant safety and efficacy exerted by CIK therapy [71-76].

CIK have been also exploited as compelling immune actors for CAR-cell therapy upon genetic modification, generating bi-potential killers endowed with a higher potency and tumor-killing performance, that already showed promising results against different solid tumors. CAR.CIK cell therapy could bring improvements where conventional CAR.T cells present a poor therapeutic efficacy [62,77,78], thanks to their ability to exert anti-tumor activity both by intrinsic NKG2D-mediated and CAR-specific targeting [77,79,80].
CAR-engineering of CIK has been recently reported in several preclinical settings, including OC, by our and other groups [81-89]. Concurrently, initial evidences are now available from early clinical trials where CAR-engineered CIK have been administered for the treatment of blood cancer patients [80,90-92].

1.1.2.3 Chimeric antigen receptor-cell therapies limitation in reaching solid tumor: locoregional deliver as a potential advantage

As explained above, differently from the hematological malignancies, CAR-cell therapy application to solid tumors is crucially limited by the physical tumor barriers and immunosuppressive TME, that limit the ability of CAR-cells to traffic to and infiltrate in [28]. An attempt to ameliorate these limitations is through the utilization of locoregional delivery instead of the systemic route. Ideally, the locoregional delivery eliminates the need for CAR.T cells to traffic to disease sites, increasing numbers of CAR.T cells within the tumor and their proliferation, while limiting the CAR.T cells on-target off-tumor toxicities, as well as immune-related systemic toxicities, while at the same time reducing the initial dosage required [50]. Moreover, the regional delivery increases the depth of penetration reached by CAR.T cells, generating a local immune response that further translates in a systemic immunity by inducing changes in the tumor immune microenvironment that promote a systemic elimination of the disease. On the contrary, the systemic delivery results in sequestration of CAR.T cells in non-specific organs, such as the lungs, with shallow penetration into the tumor [93].

Nowadays, the number of preclinical and phase I clinical studies applying CAR.T cell locoregional delivery to treat solid tumors spanning different body areas is increasing **(Fig. 3A-B)** [94].

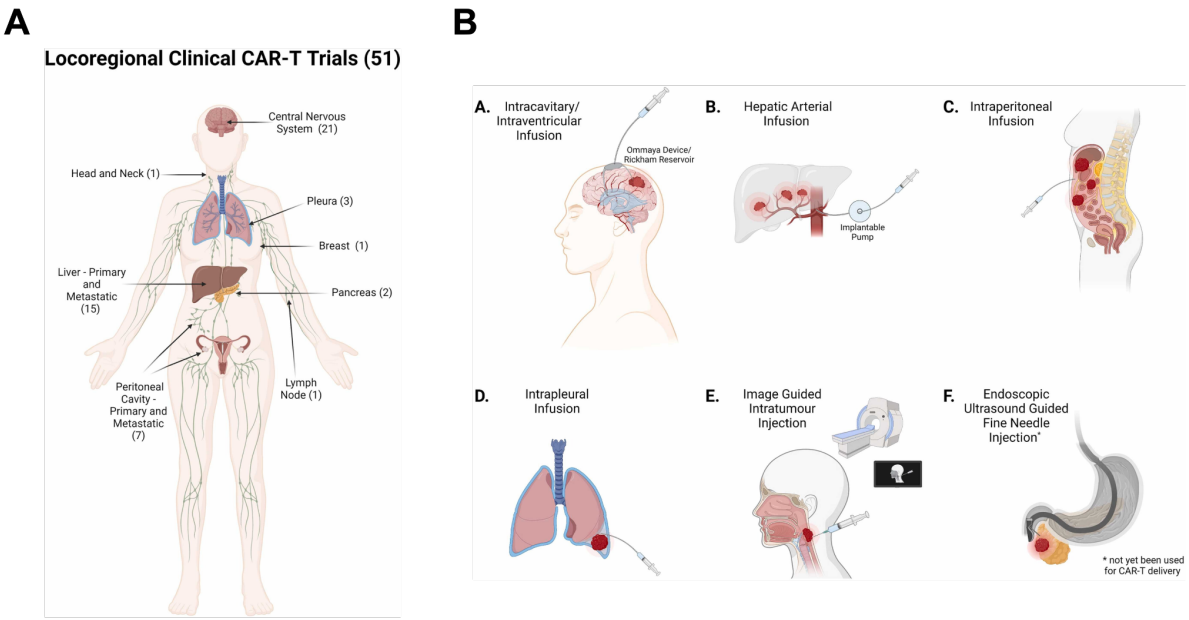

Figure 3 Locoregional delivery for CAR-cell therapies. (A) Numbers of clinical trials exploiting local delivery for CAR.T cell therapies grouped per body areas. **(B)** Regions and related techniques to apply regional CAR-cell delivery (Modified from Sagnella S. M. et al., Pharm Resear, 2022).

In particular, great improvements were reached in the treatment of recurrent adult glioblastoma, pediatric brain tumors, and brain metastasis and/or leptomeningeal disease with the intracerebroventricular delivery, where CAR.T cells managed to access tumors by passing the shield represented by the blood brain barrier and obtained a considerable tumor regression, more effectively and safely than the results obtained by intravenous delivery [95-97]. Likewise, the intrapleural and intrahepatic delivery of CAR-cell therapies targeting pleural and hepatic tumors reached consistent results in phase I clinical trials [45,98]. As an example, the phase I study of regionally delivered mesothelin (MSLN)-targeted CAR.T cell therapy followed by pembrolizumab administration led by the trial investigator Prasad Adusumilli showed the feasibility and safety, as well as evidence of antitumor efficacy in patients with malignant pleural diseases [45].

The peritoneal cavity has become an additional central point of locoregional investigation for all the primary or metastatic tumors that spread within the abdomen, including gastric cancer, pancreatic cancer and OC [94].

1.2 Peritoneal carcinomatosis: clinical condition from advanced ovarian cancer

PC is a cancerous clinical condition that affects the peritoneal serous membrane that lines the internal abdominopelvic cavity, defined as peritoneum [99]. The peritoneum is a serous organ of

mesodermal origin, divided into the parietal layers covering the anterior and posterior abdominal walls, and into the visceral layers covering the organs. The peritoneum is the largest and most complex serous membrane of a body, generally consisting of glycocalyx, a
single layer of mesothelial cells supported by a basal lamina, submesothelial stroma, and the elastic lamina. It exhibits both mesenchymal and epithelial features **(Fig. 4)** [100].

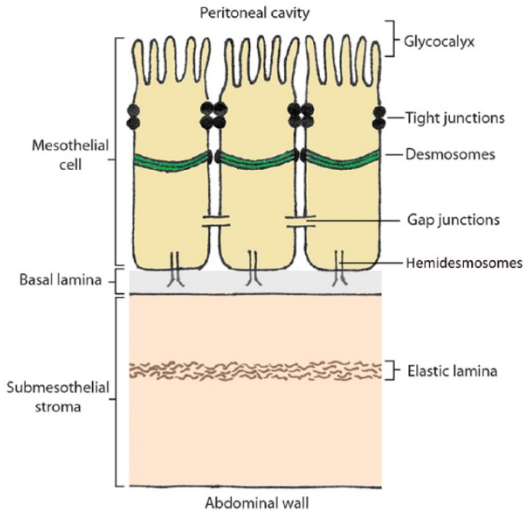

Figure 4. Composition of the peritoneum. The peritoneum is composed by a layer of mesothelial cells (mesothelium) supported by a basal lamina laying over a submesothelial stroma.
(van Baal JOAM et al., J Histochem Cytochem, 2017).

PC can originate as primary tumor (peritoneal mesothelioma and primary peritoneal cancer) or consequent to the metastatic dissemination of tumors originating from intraperitoneal organs. When arising from the metastatization, the commonest origin are the tumors of the digestive tract, with gastric cancer as the highest, at 15–43% [101], and of the gynecologic reproductive tract, particularly OC [99,102], as well as from sarcoma or extraperitoneal tumors (lung, breast and kidney tumors) [103].

OC is the most fatal tumor among the gynecological cancers in women, with a 5-year relative survival rate around 48.6% [104-106].
The most common origin for OC is the ovary itself, but it can also arise from other nearby structures including the fallopian tubes [107]. OC refers to a comprehensive plethora of tumors with different histological subtypes, which differ on the type of cell presenting the initial neoplastic mutation and on the consequent clinical behavior [108], albeit the majority (90-95%) originate from the epithelial surface of the ovary [109]. Despite the favorable prognosis at early stages, OC is frequently diagnosed in advanced stages (stages III and IV) [110], where it is already widespread at the intra-abdominal level with accumulating peritoneal metastases, a characteristic feature of PC [99]. The relative incidence of the peritoneal metastases (60–70%) in OC is the highest with respect to other gynecological malignancies (<10%) [111] and PC is most often identified linked to the epithelial OC (EOC), particularly to the serous carcinoma subtype and less frequently to the mucinous or endometrioid subtype [112].

The prognosis of PC originating from OC is typically very poor and the survival rates have only modestly improved over the past few decades [99,113]. The main causes imply the late diagnosis and the limited clinical response to conventional therapeutic options [103]. Indeed, OC patients

generally present periods of remission and relapse that may result in the development of chemotherapy resistance [114]. Recurrence manifests in more than 80% of OC patients, and more than 50% of them die in less than five years post-diagnosis [115].

PC originates from OC through a multistep process where the cancerous cells metastasize intra-abdominally, giving rise to numerous small-sized lesions [99,102] and overall resulting in a highly confined and complex disease. Differently from other solid tumors that spread predominantly through lymph and bloodstream, OC cells shed from the primary tumor into the peritoneal cavity [116], where they are passively transferred via the peritoneal fluid to the peritoneum. Cells then implant onto the mesothelium of the peritoneal cavity, by interacting with the peritoneal cells, as well as on the omentum, a layer of adipose tissue laying over stomach and bowel and covered by visceral peritoneum [117]. The preferentially colonized regions of the peritoneum are the diaphragm and the small bowel mesentery [102,118,119] **(Fig. 5)**. Just a limited fraction of these tumor depositions invade at deeper levels the abdominal muscles and the serosa of the visceral organs [99].

Mechanistically, OC cells undergo epithelial-to-mesenchymal transition (EMT), downregulating surface adhesion molecules, such as E-cadherin, while upregulating other cadherins, including platelet (P)-cadherin and N-cadherin as well as vimentin [120], and detach through exfoliation from the primary tumor site, supported by the high interstitial fluid pressure [121-123].

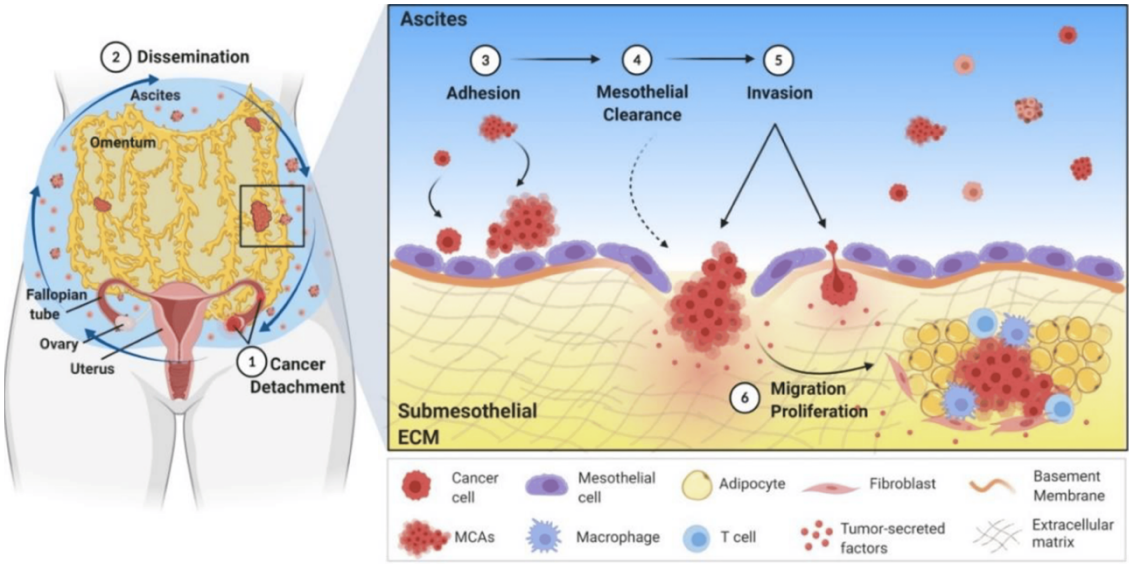

Figure 5. PC originates from OC dissemination in peritoneal cavity. Through a multistep process, OC cells detach from the primary tumor as single cells or MCAs, floating in the ascites. By disseminating throughout the peritoneal cavity, tumor cells form many metastatic implants by adhering to and implanting on the peritoneum and peritoneal organs, over the mesothelium until penetrating the submesothelial extracellular matrix (ECM) (Yang J. et al., Cancers 2020).
Abbreviations: MCAs, multicellular aggregates; ECM, extracellular matrix.

The tumor cells attach to the mesothelial cells of the peritoneum and to the underlying submesothelial stroma through integrins that interact with the molecules of fibronectin exposed on mesothelial cells [124]. Upon interaction, the mesothelial cells upregulate inflammatory mediators (i.e. tissue necrosis factor (TNF)-α, IFN-γ, IL-1β and IL-6), generating a TME even more supportive to the invasive behavior of OC cells [125].
Beyond these solid-like masses invading the peritoneum, PC from OC displays a composite structure characterized as well by the presence of floating cell aggregates within the malignant ascites [119].

1.3 Ovarian cancer dissemination through the abdominal cavity: composition and role of malignant ascites

OC cells detached from their primary origin are passively transferred to the peritoneal cavity via the peritoneal fluid in between the visceral and parietal peritoneum.
In physiological conditions, a limited and constant volume of peritoneal fluid composed of plasma transudate, tubal fluid, ovarian exudate and retrograde menstruation, permits the friction-free bowel movements and the exchange of immune cells and other substances with plasma [100].
However, this homeostasis is lost during the OC advancement. Indeed, it is very frequent the OC manifestation through the progressive and excessive accumulation of peritoneal fluid in the peritoneal cavity, defined as malignant ascites. Ascites manifests in more than 30% of OC patients at initial diagnosis and in almost all cases of relapse, reaching significant volumes [126-129].

The main pathophysiological reason of this accumulation is the impaired fluid drainage (disequilibrium between fluid production and reabsorption) [128], caused by the obstruction of the lymphatic portals by tumor cells [130] and/or to an increased net filtration due to cross-sectional area of microvessels around the peritoneal cavity [131]. Concurrently, OC cells secrete inflammatory mediators that may further increase the ascitic fluid production [132]. The vascular endothelial growth factor (VEGF) is instrumental in the pathogenesis of ascites, since it affects the permeability of the peritoneal membrane [133].
Within malignant ascites, OC cells are continuously exposed to an intra-abdominal fluid flow also generating a continuous flow-induced shear stress (FSS). The FSS results from the movement of the respiratory apparatus (i.e. diaphragm), the effects of gravity, the continuous bowel peristalsis and abdominal pressure changes, as well as from the same ascites build-up [116]. Through this flow, the peritoneal liquid is repetitively transferred along specific pathways, therefore spreading OC cells to preferred areas for metastases [134,135].

It is worth noting that the flow generated within the peritoneal cavity is thought to remain laminar [136], meaning that the fluid particles flow in parallel layers, following the same trajectory, and that viscous forces prevail over the inertial ones [137]. Moreover, it is likely that the maximum FSS values for peritoneal flow are comparable to the slower flows encountered in venous arteries [138]. These aspects are relevant in the hypothesis of a locoregional therapy (either cell-based or not).

Ascites represent a unique pro-inflammatory TME that influences tumor cells at cellular and molecular levels, thus playing a central role in favoring the aggressiveness and progression of the disease [139]. The ascitic fluid composition spans a range of cellular and non-cellular components, variable across patients **(Fig. 6)**.

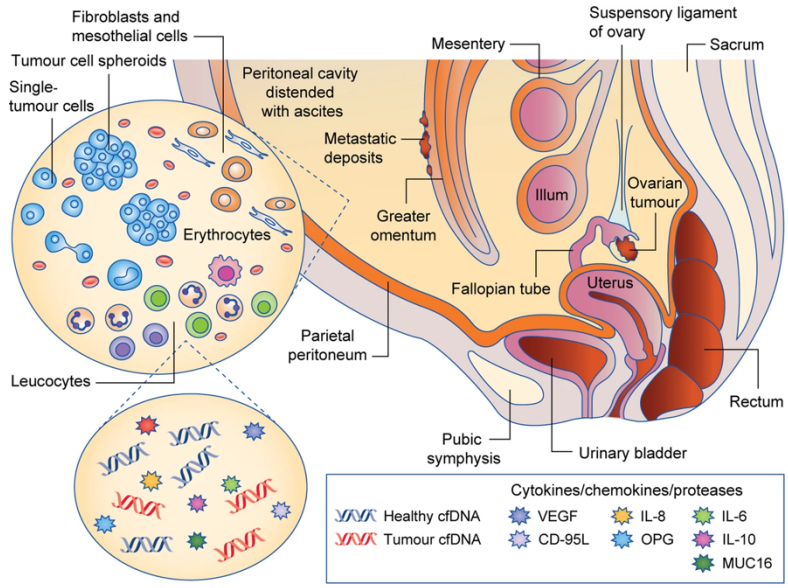

Figure 6. Cellular and acellular composition of malignant ascites in OC. Malignant ascites consist of tumor and non-tumor cells, including mesothelial cells, fibroblasts, adipocytes, endothelial and inflammatory cells, in addition to cell-free DNA and a variety of signaling molecules (Ford C.E. et al., BJC, 2020).
Abbreviations: cfDNA, circulating free DNA; CD-95L CD-95 ligand; OPG osteoprotegerin.

The non-cellular elements consist of cell-free DNA and various signaling molecules, including chemokines, growth factors, proteases, tumorigenic and pro-inflammatory cytokines such as IL-1β, IL-6, IL-8 and TNF-α, as well as the anti-inflammatory cytokine IL-10 and extracellular vesicles [140,141].

Concerning the cellular compartment, tumor cells acquire the ability to survive in the cavity as anchorage-independent single cells and multicellular aggregates (MCAs or spheroids), highly abundant in patients with advanced disease but variable in size, circularity, and concentration. These tumor spheroids probably represent the invasive intermediate and the main source of metastasis, with a greater ability to adhere and invade the peritoneal layer of mesothelial cells with respect to single tumor cells, as well as to resist anoikis [142]. Their presence has been also correlated with resistance to platinum-based chemotherapy [143]. However, MCAs are usually described as heterogeneous structures, made of a small number of malignant cells in addition to diverse non-malignant cell types [143-145]. Indeed, the tumoral front represents just a limited fraction of the total cellular composition, from 1% to approximately 8% of the total ascitic

volume in some patients [128,146]. Generally, the non-tumoral cells present in the ascites mostly include mesothelial and immune cells, as well as fibroblasts, endothelial cells and adipocytes [128,147].

1.4 Advanced ovarian cancer current management

The treatment management for PC from advanced OC include the cytoreductive surgical techniques against the macroscopic lesions [148]. However, cytoreductive surgery does not always completely remove all the PC lesions, often too extensive and numerous [99]. Therefore, it is commonly coupled with the intravenous administration of first-line chemotherapy of carboplatin and paclitaxel, to address the microscopic residual disease [149]. The 5-year survival rate of patients at advanced stages undergoing optimal cytoreductive surgery plus systemic chemotherapy is close to only 50% [150].

Unfortunately, response to platinum-based chemotherapy for OC patients is not univocal but can involve refractoriness, resistance or sensitivity [151]. Moreover, most of the patients frequently develop recurrence (70% of probability) within 2 years despite the initial high response rate [152-154]. This condition has thus led to the subsequent approval of several maintenance therapies. Among them, target therapies commonly in use are the poly ADP-ribose polymerase (PARP) inhibitors targeting homologous recombination deficiency, including olaparib and rucaparib, which showed efficacy when used in combination therapy [155,156] and the VEGF-inhibitor, bevacizumab, to inhibit tumor blood vessel growth [157].

Concerning specifically the management of the malignant ascites, particularly for the unmanageable and treatment-resistant and recurrent form, patients are subjected to paracentesis, as a palliative [158,159]. Additionally, bevacizumab comes in help to control ascites [158].

However, the outcome of these therapies in OC patients with peritoneal tumor spread is limited, due to the limited therapeutic efficacy reached by the intravenously-delivered chemotherapy, caused by the peritoneal-plasma membrane which acts as a barrier and prevents the diffusion of most of the drugs [160].

1.4.1 Locoregional treatment: taking advantage of the peritoneal carcinomatosis pathophysiology

An opportunity to improve PC management comes from its own pathophysiology. Being simultaneously spread all over the abdominopelvic cavity as well as highly localized within it, the locoregional administration of drugs could enhance exposure over tumor cells as well as reduce toxicity [160].

In this regard, the single intraoperative procedure defined as Hyperthermic Intraperitoneal Chemotherapy (HIPEC) has been tested in several early-phase trials to improve patient response as a parallel therapeutic approach. HIPEC consists of a direct delivery of chemotherapy into the abdomen of patients with PC, through a temporally limited fluid flow-based drug delivery system [128,161-163]. The hyperthermia functions to increase chemotherapy penetration at the peritoneal surface and tumor' sensitivity to the drug, as wells as to activate heat-shock proteins that serve as receptors for NK cells, inhibit angiogenesis and promote protein denaturation, all resulting in tumor cytotoxicity and apoptosis [164,165]. The need to translate to an intraperitoneal therapeutic delivery arises from the low concentrations reached in the peritoneum by chemotherapies when administered intravenously, as already mentioned [166]. On the other hand, the direct intraperitoneal delivery enables micrometastasis to be directly exposed to the drug. Altogether, the advantageous consequence is an increased spatial and temporal exposure of the drug which thus increases the absorption and susceptibility of cancer cells, reducing at the same time the systemic drug absorption and the consequent systemic toxicity [160].
However, there are currently major limitations to reach the full approval of HIPEC for the treatment of OC globally, due primarily to the difficulties in the standardization of the procedures, the fact that the promising data have been derived from limited number of cases, the logistics and the associated toxicity [108,160,167].

Beyond HIPEC, a new intraperitoneal delivery system called Pressurized IntraPeritoneal Aerosol Chemotherapy (PIPAC) was introduced in 2011 [168]. PIPAC is based on the application of a polydisperse aerosol drug nebulization into the peritoneum [169], that can be further improved by applying an electrostatic field during or after aerosolization of chemotherapeutic agents to increase the uptake by tumor cells, which favor their electrostatic precipitation on tissues [170].

Altogether, the advancement of delivery and efficacy for locoregional therapeutic approaches is a very active research frontier for this type of cancer. In particular, a promising avenue in this context is currently represented by the locoregional translation of cell-based immunotherapies.

1.5 Immunotherapy for advanced ovarian cancer

OC has not been uniquely identified about its immunological TME phenotype. Almost half of OC manifest T cell infiltration and immunogenic features that correlate with an improved overall survival [171], while the presence of tumor-specific lymphocytes in TME and ascites has been linked to an improved survival after treatment [172,173].

Nevertheless, OC also tends to have a highly immunosuppressive TME and a low to intermediate mutational burden [174-176], the latter considered generally as an indication of low immunogenicity and limited responsiveness to immune therapies [177].

The major immuno-therapeutic approaches evaluated for OC include vaccines, IC antagonists and immune cell therapies [178,179]. Generally, depending on the OC subtypes, diverse responses to immunotherapy have been outlined, depending on the proportion and quality of the TILs present [180].

Cancer vaccines did not result in substantial clinical benefit in women with OC owing to their TME [181]. Several recombinant vaccines have been developed to target the tumor-associated antigen NY-ESO-1 [182,183], but generally just a fraction of patients tends to exhibit spontaneous strong immune responses, likely due to low levels of antigen expressed in OC [184,185]. Nevertheless, a positive promising prospect is represented by the autologous personalized cancer vaccine vigil, for treatment of late-stage OC. Vigil resulted in educating T cells against clonal tumor neoantigens and in increasing peripheral circulating CD3 + /CD8 + T cells, when applied in combination with ICIs [186].

The ICIs, such as anti-PD-1, anti-PD-L1 or anti-CTLA-4 Abs, obtained limited overall response rates in OC patients and failed to demonstrate significant activity, in contrast with other gynecological malignancies [187,188]. However, ongoing studies are exploring the possibility to improve their efficacy through combination with the PARP inhibitors, in order to potentiate OC immunogenicity, favoring neoantigen release, TME immunomodulation and upregulation of PD-L1 [189,190].

Currently, the only FDA-approved immunotherapeutic options for the management of OC are targeted Abs, such as the already mentioned bevacizumab, mirvetuximab soravtansine which targets the folate receptor (FR) pathway [191], and the trifunctional mAb catumaxomab for the treatment of malignant ascites, which presents two different antigen-binding sites and it is delivered directly intraperitoneally [192].

Concerning the branch of the immune ACTs, there have been promising results in OC patients both in the adjuvant [193] and metastatic setting [194]. Different immune effectors have been tested, among which CIK have shown positive results in various works [71,195,196]. We have provided evidence that CIK activity is significant against EOC in a preclinical setting, against OC cells (pdOVCs) derived from metastatic ascites of patients and Patient Derived Xenografts (PDX), even in the platinum-resistance context. In fact, CIK generated from EOC patients effectively killed *in vitro* the autologous pdOVCs, even upon pre-treatment with carboplatin, and showed the ability to home and target EOC PDX models *in vivo* **(Fig. 7A-B).** However, CIK antitumor activity was less evident at unfavorable effector/target (E:T) ratios **(Fig. 7A)**, thus representing a significant limitation in the perspective of a clinical translation [197]. In order to increase their antitumor potency, CIK population could be redirected with a CAR specific to recognize and target OC.

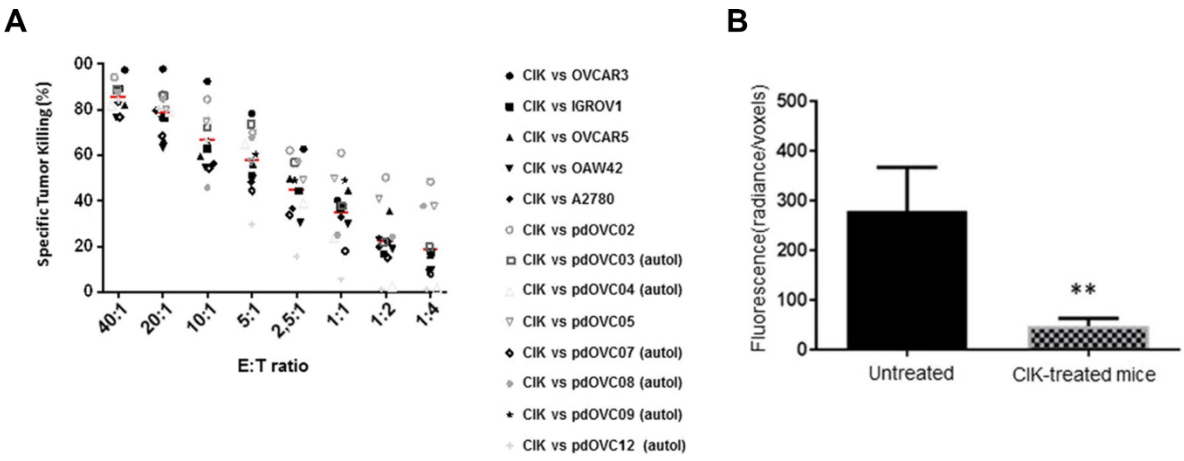

Figure 7. CIK lymphocytes are effective against EOC. (A) CIK lymphocytes effectively kill *in vitro* OC cell lines obtained from metastatic ascites. **(B)** CIK anti-tumor activity against *in vivo* model of patient-derived high grade serous OC PDX model. (Modified from Capellero S. et al., Sci Rep, 2020). Abbreviations: CIK, Cytokine Induced Killer; E:T, effector/target ratio; pdOCV, patient-derived ovarian cancer cells.

Among the CAR-redirected ACTs, different CAR.T therapies have been investigated for their safety and therapeutic efficacy against OC both at preclinical and clinical level, even if with limited efficacy and some side effects in the latter case [198-200]. As already mentioned above, a central subject of investigation for CAR-ACTs is the identification of a qualified target antigen and the most commonly investigated for advanced OC include mucin-16 (MUC16), MSLN, ErbB2 and FRα [198,201].

Another key feature is to find strategies to overcome the inefficient trafficking of the immune redirected cells to tumor site. The locoregional intraperitoneal delivery of CAR.T therapies showed superior efficacy compared to systemic administration in targeting PC deriving from metastatic colorectal and gastric cancers [202,203]. Moreover, it has been shown that CAR.T cells

targeting ErbB2 when delivered intraperitoneally improve survival and safety profile [204]. In a study led by Murad and colleagues, xenograft models of peritoneal OC were treated with CAR.T cells, either delivered in the peritoneum or intravenously, and the intraperitoneal delivery was shown to reach significantly higher reduction in tumor growth and a prolonged survival, even more evident when CAR.T cells were administered repetitively. However, it is worth noting how some cases manifested tumor recurrence, which was most likely associated with the detected antigen escape post CAR.T therapy [205].

Indeed, as already pointed out, the regional delivery of CAR-redirected cell based therapies could help to overcome the inefficient transfer of CAR-redirected immune cells to the solid tumor sites commonly reached by the intravenous transfer, with improved and positive responses against peritoneal metastasis reached with intraperitoneal delivery of CAR.T cells compared with intravenous route [205,206]. In fact, CAR.T treatment delivered intraperitoneally managed to avoid homing process through intravenous infusion and showed dramatic antitumor effect in pre-clinical models of EOC [207].

Here, CAR.T cells achieved better trafficking and infiltration, greater tumor reduction and a more durable effect. Of note, the local peritoneal administration also conferred a systemic effect and enhanced protection against local relapse and distant metastases, probably due to an abscopal effect like the effect associated with locoregional radiotherapy. The abscopal effect is defined as an effect that occurs at sites distant from the original locally irradiated site [208]. Upon regional delivery of CAR-cells, the effect arises consequent to the release of tumor antigens by tumor cells destroyed by CAR.T cells. Antigens are then cross presented by the antigen presenting cells, therefore triggering immune responses against molecules not targeted by the CAR [202,209,210]. Additionally, the consequent cytokine release stimulates the innate immune response. Results from locoregional CAR.T delivery in treating PC from OC improved CAR.T cell trafficking and infiltration, increased the tumor reduction and the effect, as well as increased survival.

Currently, there are different clinical trials ongoing testing CAR.T cell therapies delivered locoregionally in OC patients. Among them, the NCT05316129 is comparing the intravenous and intraperitoneal delivery of autologous CAR.T cells redirected against the follicle stimulating hormone receptor in patients with recurrent or persistent OC, aiming to identify the maximum tolerated dose and overall survival [211]. The phase 1 clinical trial NCT05225363 is designed to treat intraperitoneally patients with platinum resistant EOC with CAR.T cells redirected against the antigen TAG72. The study is intended to test primarily the therapy safety and tolerability as well as CAR.T cells persistence in blood and in peritoneal cavity upon delivery, patients response criteria and phenotypic analysis of immune and tumor cells [212]. Similarly, the study NCT04670068 is intended to treat OC patients not positively responsive

to common treatments, with CAR.T cells redirected against the B7-H3 antigen delivered in the abdomen [213].

The terminated NCT03608618 clinical trial tested MSLN targeted CAR.T cells delivered intraperitoneally for treatment of OC and peritoneal mesothelioma, reporting no dose-limiting toxicities or neurotoxicities, limited adverse effects probably related to on-target/off-tumor effects, and stable disease in a subgroup of treated patients for six months [214,215].

The results of these studies will be crucial to assess possible toxic and adverse effects as well as the ability of the therapy to control disease and improve patient response.

1.6 Peritoneal carcinomatosis and MSLN-CAR.CIK interplay: the role of mesothelin

The identification of a valid target antigen is central for CAR-redirected therapy targeting solid tumors.

MSLN is a suitable and promising tumor target antigen for cell-based immunotherapy against solid cancers, particularly for tumors expressing high MSLN levels, including OC [216,217]. MSLN is a glycosylphosphatidylinositol membrane glycoprotein. It is expressed on the mesothelial cells lining the pleura, pericardium and peritoneum, and minimally on the of the surface of epithelial cells lining the ovaries, tunica vaginalis, rete testis and the tonsillar and fallopian tube epithelial cells [218,219]. Whereas in solid tumors, MSLN is highly and aberrantly expressed in many malignancies [220] including mesotheliomas [221], OC [217,221], pancreatic cancer [222] as well as lung, esophageal, gastric, biliary, endometrial, thymic, colon, and breast cancers [223-226], therefore being identified as tumor-associated antigen.

MSLN function has been not fully understood but seems not essential for normal tissues, since mice with knockout of MSLN gene exhibit normal development or reproduction [227]. Original hypothesis linked MSLN to a cell adhesive role [221]. In contrast, in tumors MSLN seems to play a function in both the development of a malignant phenotype and tumor aggressiveness by promoting cancer cell proliferation as well as resistance to apoptosis induced by cytotoxic agents [228], by promoting the activation of NFκB, MAPK, and PI3K intracellular pathways [229,230]. Specifically in the context of OC, evidences support its contribution to the malignant local implantation and intraperitoneal spread of the OC cells, probably thanks to the binding with MUC16 that presents the repeating peptide epitope CA125 [231,232], favoring the consequent development of PC [233,234], with a role in promoting the expression of matrix metalloproteinase 7 (MMP-7) [234], similarly to what has been shown in other malignancies [230,235]. Moreover, in OC MSLN maintains a homogeneous expression between primary and peritoneal metastatic lesions [236].

Structurally, the MSLN mature form arises from the 71 kDa cell-surface protein precursor, after the cleavage of the amino terminus by the furin protease, which generates a 40-kDa C-terminal fragment, which remains attached to the plasma membrane, and a soluble and released 31-kDa N-terminal fragment, named megakaryotic-potentiating factor (MPF) [237] **(Fig. 8)**.

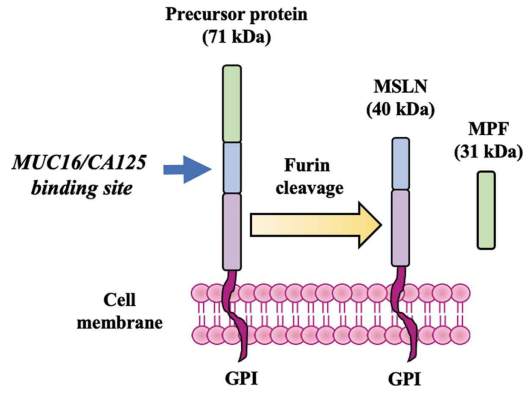

Figure 8. MSLN molecule maturation. The precursor protein of MSLN is proteolytically cleaved by protease furin into its mature form, containing a MUC16/CA125 binding site, and the soluble mature MPF (Sagnella S. M. et al., Pharm Resear, 2022).
Abbreviations: MUC16, mucin-16; CA125, cancer antigen 125; MPF, megakaryocyte potentiating factor.

MSLN has also been detected in its soluble form in the sera of patients affected by solid tumors, like mesothelioma [224,238]. The so called soluble MSLN-related protein (SMRP) is thought to have originated from alternative splicing or by proteolytic cleavage of the MSLN mature form [239]. It is therefore concerning the possible interference that the soluble/shedded form of MSLN may have on the ability of the scFv portion of the CAR to bind the membrane version of the glycoprotein, by MSLN-CAR-cell therapies. Particularly, in OC patients, OC cells secrete high levels of the soluble form of MSLN, which is therefore significantly present in serum or ascites fluid [240-242]. However, *in vitro* and *in vivo* analysis highlight how even high levels of SMRP seemed to not alter MSLN-CAR.T cell efficiency. For example, Lanitis and colleagues assessed *in vitro* how anti-MSLN-CAR.T cells were not inhibited by tumor-secreted form of MSLN. They detected an activation of the CAR.T cells upon engagement with the immobilized form of MSLN protein, but not with the soluble form, probably due to the need for cross-linking of a significant number of CAR receptors on the T cell surface which is provided by immobilized, but not soluble MSLN, and suggested that the CAR's ability to resist soluble antigen-mediated blockade could lie in its ability to disengage soluble MSLN at physiological temperature [243].

Altogether, the activation of CAR.T cells redirected against MSLN depends on the expression of the glycoprotein on the cell surface and not by its soluble form [209,244], most likely due to the higher avidity of the CAR for the membrane-expressed version of the antigen, that is further sustained by the increased concurrent interactions among CAR-redirected cells and tumor cells (i.e. adhesion molecules) [245]. It is worth to note how the engineering of the CAR to recognize the juxtamembrane epitope of MSLN and not binding the shed MSLN seems to

further overcome the presence of the shed glycoprotein and improve the performance of CAR.T cells [246].

Chapter 2: Experimental models of chimeric antigen receptor-based cell therapies in solid tumors

2.1 3D models for chimeric antigen receptor-cell therapies: why it is important to investigate *in vitro* the immunotherapeutic dynamics

In the past decade, cancer research has focused on the necessity to better recapitulate and understand tumor complexity through the development of three-dimensional (3D) *in vitro* systems. 3D models aim to overcome the shortcomings of 2D cultures: the lack of the 3D spatial environment, the lack of several distinctive components (i.e. extracellular matrix (ECM), soluble factors released, stromal cellular components of and metabolic features) and the inability to mimic cell interactions [247]. A careful examination of the effects of anti-cancer agents and personalized cancer treatments should therefore be assessed in more realistic experimental settings.

Concerning the immune-oncology field, suitable preclinical models are necessary to recapitulate the biological complexity of the disease and its dynamic interplay with the immune compartment. The possibility to incorporate concurrently patient-derived cells and a spatial 3D structure has turned the *in vitro* 3D modeling into a useful biological tool to assess interactions between immune and cancer cells, both at the cell and at the environment level as well as in a space and time, a number of observations which are not easily applicable in 2D approaches [248]. In the specific case of the advanced stages of OC, the peculiar complexity of the pathophysiology requires developing suitable preclinical models to recapitulate the biological and clinical complexity of the disease and its dynamic interplay with immunotherapies, especially cell therapies [249].

With a focus on CAR-based cell therapies, at the preclinical level CAR.T cells anti-tumor activity has been mostly probed *in vitro* against singularized cells obtained from cell lines established from solid tumor at E:T ratios which are not achievable in humans and in animal models, where the inoculated tumor cell lines form tumor lesions not resembling the primary human tumors [250]. In 2D settings, CAR.T cell efficacy has been intensively evaluated taking the cytokine production, the tumor cell lysis and T cell exhaustion as proxies in short-term assays [251,252]. Moreover, 2D assays tend to overestimate the immune-mediated cytotoxic effect and do not recapitulate the realistic oxygen gradients and how they may affect T cells [253,254].

3D models enable instead to focus on how cytokines, factors and chemoattractant gradients can influence the processes of CAR-redirected lymphocytes migration and infiltration of tumors, with the possibility to control TME factors (gradients, hypoxia and matrix stiffness) [249].

The aim is to understand how immune cells are recruited to or excluded from solid lesions, and therefore improve their trafficking [255], all features that by definition are not accessible in 2D assays due to the geometry which bring the two cell types in proximity by construction. Along the same line, the 3D engineered *in vitro* models can help to dissect the dynamics of immune-cell activation and cytotoxic activity against solid tumors, while following the events over time [256].

Generally, 3D cell culture approaches involve the use of multicellular tumor aggregates, most commonly termed cell spheroids or tumor organoids depending on the origin of the sample. Tumor spheroids are generally obtained by assembling cancer from single cell suspensions derived from cancer cell lines. Experimental methods allow to easily control tumor spheroid size, to scale up production and grant high reproducibility and handling, therefore being suitable for high-throughput systems [257]. When spheroids reach large dimensions (i.e. several hundreds of microns of diameter) they may be divided into metabolically different layers, with an inner necrotic core with limited availability of nutrients and oxygen [258]. Tumor spheroids can be cultured with or without the support of ECM and integrated of other cell types from the TME (e.g. CAFs, immune cells, endothelial cells) to better recapitulate the complexity and heterogeneity of solid TMEs [259]. When constituted by multiple cell types, spheroids are known as heterotypic spheroids [260] **(Fig. 9).**

Tumor organoids or patient-derived organoids (PDOs) or tumoroids are instead multicellular structures obtained from stem or progenitor cells. These models have the ability to self-organize and self-renew, retaining features of the original tumor specimen, such as phenotype as well as mutational diversity and patient response to treatment [261,262]. In these regards, PDOs can be employed to predict clinical outcomes in patients, therefore bridging the gap between the *in vitro* and the *in vivo* settings [263]. Nevertheless, similarly to tumor spheroids, tumor organoids do not include cellular components of the TME, hence different types of co-cultures have been experimented [264]. Aiming to understand mechanisms underlying the interplay between tumor and immune cells, tumor organoids and autologous or allogenic

immune cells could be a valuable platform, exploiting submerged hydrogel cultures or microfluidic 3D or air-liquid interface cultures [265-267] **(Fig. 9).**

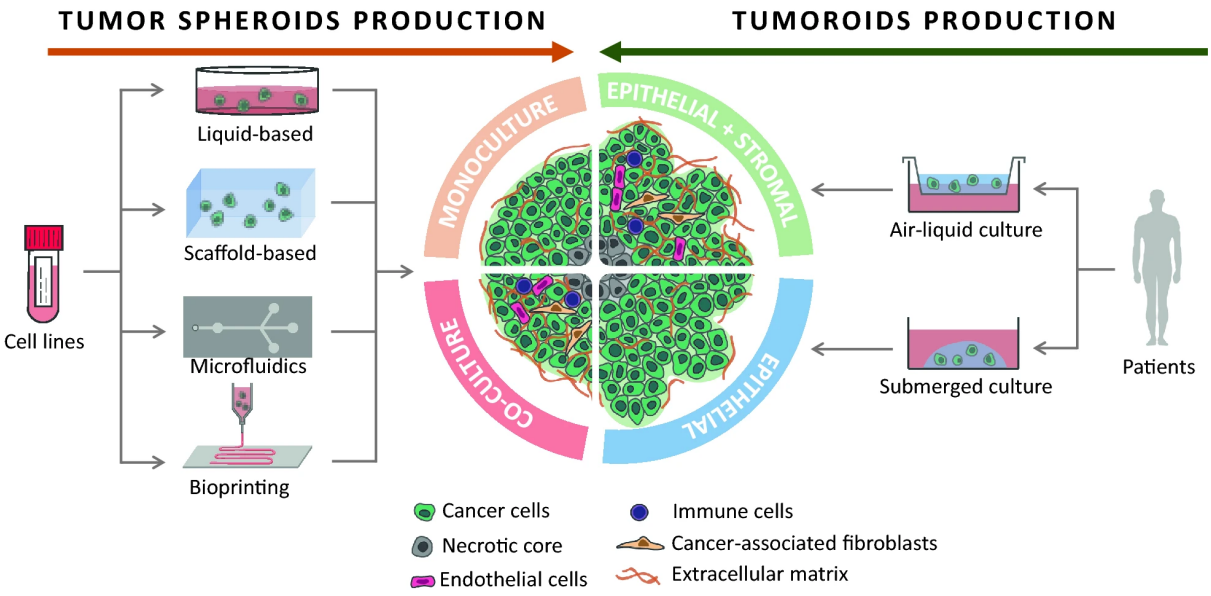

Figure 9. 3D cell culture models: spheroids and organoids ways of generation. 3D tumor spheroids can be obtained through different methods and be homotypic or heterotypic, when cultured with other cell types **(left).** 3D PDO or tumoroids are complex structures directly generated from cancer patients' samples **(right)** (Jubelin C. et al., Cell & Bioscience, 2022).

Microscopically, it is critical to shed light on the parameters which can positively control CAR-redirected lymphocytes behavior and function towards tumor regression, in order to better design, optimize, and evaluate CAR-cell therapies. A deeper understanding is needed on how CAR-cells encounter tumor cells, the consequent dynamics of immune-mediated killing (whether led by an individual immune effector or in cooperation with others) and the optimal density reached in the TME to obtain an effective eradication of the tumor lesions. For example, advancements were made by Galeano Niño, Pageon, Tay et al., that employed 3D tumoroids embedded in a matrix to track the movement of T or CAR.T cells. Within their models, researchers demonstrate how the activation of the CAR promoted the creation of a homotypic positive chemokine feedback, thereby amplifying the recruitment of additional CAR.T cells to the tumor target [255].

As already mentioned, macroscopically, CAR.T cell therapy are limited in their trafficking and infiltration against solid tumor lesions. Those abilities are necessary for complete disease eradication and for the preservation of the function upon massive antigen encounter, but are not exhaustively accessible within the 2D culture methods [268]. The complex architecture, composition and mechanics of the stroma in solid tumors strongly influence lymphocytes

effective infiltration and distribution throughout [269]. The presence of aligned fibers of ECM guides the infiltrated T cells in solid tumors, which generally migrate exploiting a fast amoeboid movement with low adhesion pseudopodia, squeezing through pre-existing matrix gaps by changing their shape [270]. This ameboid phenotype can couple to a more mesenchymal-like phenotype with adhesive spreading, defining the amoeboid-mesenchymal plasticity [271,272]. However, the complexity of those mechanisms requires to deepen the knowledge on the regulation of CAR.T cell migratory behavior or further enhance their motility in physically complex microenvironments. Indeed, although 2D models helped to study lymphocyte motility in the past [273,274], they lack the capacity to facilitate steric cell–microenvironment interactions from textured and aligned ECMs. Thus, 3D platforms that incorporate disease-relevant ECM architecture (i.e. with variable stiffness) and allow quantitative analysis of motility for large numbers of cells necessary to point out the drivers of CAR.T cell migration and provide suggestions for immune cell engineering. Moreover, 3D models have enabled to inspect which could be the crucial chemoattractants and soluble factors affecting lymphocyte recruitment or exclusion from tumors and how to exploit them in order to improve the performance [255,275].

Different ways are currently exploited to construct *in vitro* 3D immune-oncology models. Generally, 3D tumor spheroids or organoids have been the current starting point to determine CAR.T function (i.e. cytotoxic effect), in various challenging set-up (i.e. hypoxia) [256,276,277]. Tumor PDOs have recently been advanced to incorporate immune cell components of different origin, for several aims including immunotherapy testing. Most commonly, PDOs are co-cultured with exogenously introduced immune cells [256,278].

The models can be further organized within different platforms. Among them, the microfluidics-associated technologies have increased their popularity in cancer research, with a great potential for immune cell therapy advancements [279]. Microfluidic chips enable to mimic complex and dynamic TMEs at high throughput level coupled with real-time observation by live-microscopy, while demanding a low amount of biological sample [280,281]. For example, through microfluidic models it has been possible to assess how T cells interact with tumor cells or monocytes [282], as well as the effect of ECM and hypoxia on T cell cytotoxic activity [283].

The improvement of the 3D models is also related to the introduction of biomaterials as scaffold materials which recapitulate the ECM composition of tumors and structurally support the attachment and growth of tumor cells [284]. Biomaterials differ on their physicochemical and biological characteristics, depending on how they have been functionalized. One direction of development along this line is to engineer biomaterials that favor anti-tumor immune responses, improve therapeutic efficacy, target drug-delivery, and reduce adverse effects, therefore becoming central for tumor immunotherapy research [285]. Smith and colleagues developed a biopolymer scaffold system loaded of CAR.T cells, vaccine adjuvants and several

stimulatory or pro-survival factors, to deliver CAR.T cells directly to tumor surfaces, which results in improving the resistance of heterogeneous solid tumors in mouse models to CAR.T cell therapy [286].

Altogether, 3D models are useful in several immunotherapy settings, including the redirected cell therapies, with fundamental implications in their therapeutic optimization. Moreover, the potential of the 3D models is not limited to the mechanistic and structural investigations but allows more direct conclusions in the translational direction thanks also to their robustness, simplicity and reproducibility.

2.2 How to investigate 3D models dynamics: role of imaging and image analysis methods

The 3D *in vitro* models are advantageous tools to mimic the interaction between tumor cells and immune cells, and provide information about migration, infiltration and killing ability of immune cells against solid tumors.

Nevertheless, in order to exploit the power of 3D models, it is useful to couple them with adequate advanced experimental techniques that allow to follow the cellular mechanisms and interactions without losing the spatial structure and the dynamics, and with a suitable throughput. Indeed, it is worth noting how, despite the advantages of the 3D models, there are experimental limitations when trying to translate experimental methods proper of the 2D set up.

In particular, if interested in detecting immune-tumor cell interactions in space and time, optical 3D imaging coupled with up-to-date quantitative image analysis solutions enables to visualize and characterize events of cell motions and cellular interactions. Indeed, 3D microscopy has the ability of providing information on the heterogeneity at tumor cellular level, thus elucidating how tumors respond to treatment and cancer-targeting drugs works, even regarding immune-cell therapies.

IMAGING: Optical microscopy, and in particular 3D imaging, plays a crucial role in displaying information on the tumor cellular and structural composition, as well as to appreciate mechanisms of cancer progression and treatment outcomes. Although the application of brightfield imaging in 3D does not typically allow a fine spatial axial resolution, the progresses of fluorescent microscopy techniques have come in help, concomitantly to their acquired advantage of having minimized the cellular damage arising upon prolonged exposure or intense light illumination when applied in live imaging [287]. Through live-cell imaging, it is possible to follow the cellular processes occurring in viable and preserved structure over

extended periods of time with minimum or no alteration of cell activity [288]. Currently, a plethora of fluorescent probes or genetically encoded proteins are available to label specific cellular components or highlight particular cellular events for real-time tracking [289]. While biosensors are most commonly genetically encoded, live-cell dyes or Abs labeling reduce sample manipulation, with faster applicability even for large-scale testing. However, the limited lifetime of live-cell dyes has also prompted the development of different label-free imaging approaches that instead rely on the intrinsic biophysical properties of the sample and couple with specialized label-free imaging technology instead of exogenous labeling [290-292]. Additionally, to overcome the limits imposed by the fluorescence spectra, a variety of approaches referred as "multiplexing imaging techniques" have been investigated to improve resolution, including multispectral fluorophores [293], markers which are specific at the subcellular level, optical microscopy techniques to detect specific patterns in wavelength intensities and spectral barcodes combined with signaling reporters [294].

Different microscopy modalities have improved their applicability for imaging of 3D structure, such as wide-field, confocal, light-sheet and multi-photon microscopy [287] **(Fig. 10).**

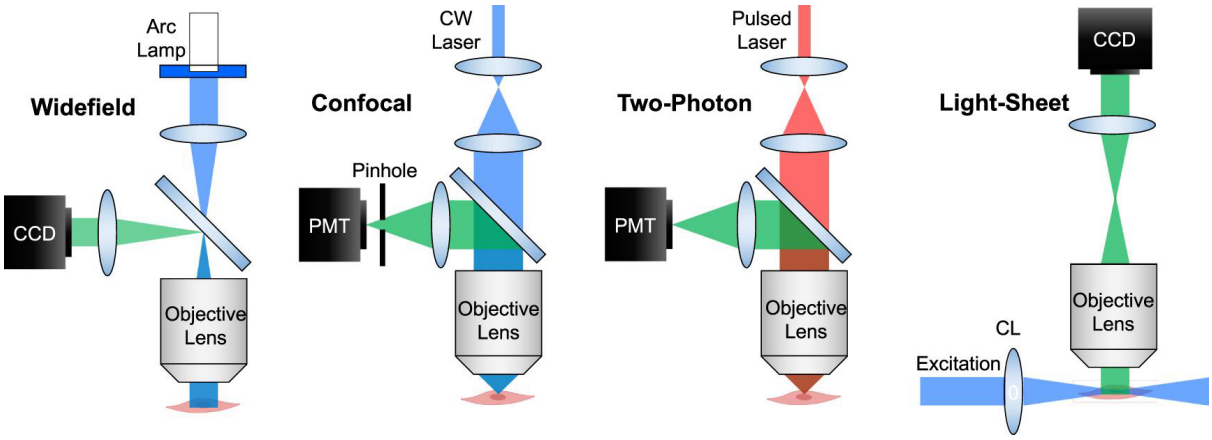

Figure 10. Comparison of wide-field, confocal, two-photon, and light-sheet microscopy. Wide-field microscopy excites the whole sample and emission fluorescence originates from both inside and outside the focal plane. In confocal microscopy defined regions of interest can be exposed to a fluorescent light source and the pinhole blocks all out-of-focus light to reach the detector therefore allowing just in-focus fluorescence to be collected. Multiphoton microscopy delivers light in short pulses from near-infrared, which allows a deeper penetration of the tissue. In light-sheet microscopy, excitation and emission are orthogonal and the sample field of interest is imaged as a thin slice illuminated perpendicularly to the observation (Mannam V. et al., JPhis, Photonics, 2020).
Abbreviations: CCD, charge-coupled device; PMT, photomultiplier tube; CL, cylindrical lens.

Concurrently, microscopy hardware has evolved to require less illumination intensity but still providing a better signal-to-noise ratio. Finally, imaging modalities with faster scanning speeds have become popular in live-cell fluorescent microscopy, due to the ability to detect multiple fluorophores, with a temporally limited sample illumination and thus reduced phototoxic burden [295].

Common readouts include cell interactions among different cell types (i.e. engineered T cells with tumor cells) and the recording of tumor cell cytotoxic effects induced by treatment. Indeed, by providing a high spatio-temporal resolution and readouts for cellular dynamics, morphology and signaling, live imaging has shed light on the mode of action of a variety of cancer treatments, including immune-cell therapies [256,296].

Among the 3D models most suitable for the investigation through imaging-based methods are tumor organoids, already introduced in the previous sections. By live imaging, we can carry out drug screenings [297] or evaluate the function of immune-cell therapies when challenged in co-cultures [256,296]. For example, Dekkers and colleagues followed the dynamics and molecular signature of serial killing mediated by T cell therapies against PDOs by integrating live imaging with transcriptomic profiling, revealing a significant behavioral heterogeneity in engineered T cells when targeting tumor organoids, considerable to fit patient-specific combinatorial treatment to reach an optimized response to cancer immunotherapies [278].

In a different set-up, Schnalzger et al. set-up a co-culture workflow to test the efficacy and safety of CAR-redirected immune effectors (NK-92) against solid cancer within a tissue-like environment, through a 3D live imaging confocal protocol that monitored effector cell recruitment and cytotoxicity at a single organoid level [256].

QUANTITATIVE IMAGE ANALYSIS: The advanced microscopy technologies have led to the generation of a large amount of images and data, which requires the help of computational and mathematical solutions to manage their analysis and interpret the results [298]. Indeed, if those processes are performed manually, they are time consuming, difficult, generally error-prone and limited in the throughput. Moreover, segmenting, annotating and tracking objects through consequent time points manually may be difficult to scale for biological images, and expert annotators may be therefore required to check their interpretation. These limitations have led to the development of different automatic or semi-automatic methods for image analysis, therefore joining the expertise of computer vision with biology.

Scientific images analysis generally requires different types of knowledge. Beyond the underlying scientific question, it is important to be aware of the experimental setup and the imaging hardware exploited, as well as how the images are represented and stored [299].

The main steps in performing quantitative image analysis involve preprocessing of images (i.e. deconvolution), pixel classifications, detection of objects, image segmentation, tracking of same objects over time-lapse in live imaging (i.e. tracking of single cells or multicellular objects such as PDOs or spheroids), counting of object properties of interest, classification/prediction of cell types and cell motility, visualization, semi-quantitative image analysis and results interpretation **(Fig. 11)** [300-304]. Commonly, workflow in image analysis programs exploits machine-learning-based image processing functions.

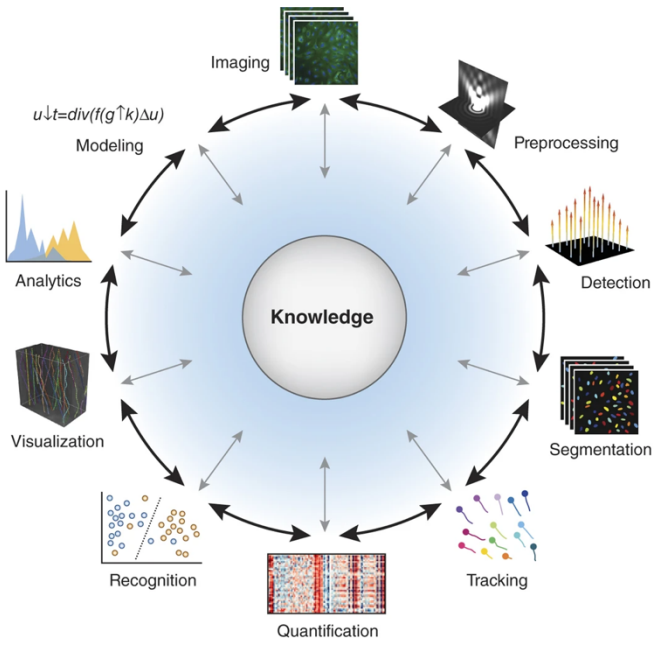

Figure 11. Bioimage analysis workflow. (Meijering E. et al., Nat Biotechnol, 2016)

Image analysis processes require algorithm parametrization. This step can be done by user supervision, i.e. making programs learning from training datasets, which is the principle of supervised machine learning [305]. However, the main limitation is usually represented by the large amount of initial data on which the programs need to be trained, in order to define the whole set of features of the space.

Pixel classification is applied to segment and generate binary images, and can be done by choosing a user-defined class label to each pixel of the image [306]. Upon user-providing examples for each class of label in the training data set, programs subsequently estimate for each image pixel the probability of belonging to a defined semantic class. The resulting probability maps can be used directly for quantitative analysis or adapted to other image analysis steps. The segmentation-based methods separate the task of cell detection from tracking, processing the spatial and temporal information stepwise [306-308].

In order to classify objects and discriminate between similar objects such as single cells or structures within *in vitro* co-cultures or ex vivo patient models, based for example on their shape, the probability maps obtained upon pixel classification are subject to smoothing and thresholding, calculating then the features of interest for each segmented object. It is possible to segment objects in a semi-automatic modality, taking as a reference their boundary information [309].

Computational approaches have also been exploited to discriminate among cell types [310] and their states or fates in microscopy analysis [311,312].

Altogether, thanks to these performing computational tools, it is now possible to broaden what and how we can detect in living systems, even at the intra-cellular level.

2.3 3D models of peritoneal carcinomatosis: biophysical and biological features

The advances available nowadays in the 3D *in vitro* models allow to infer concurrently various biophysical and biological features of a given solid TME, in order to understand their role and better mimic tumor complexity.

The interplay among OC cells and malignant ascites generates a peculiar environment where tumor cells are influenced in their morphology, phenotype, migration, as well as in the structure of the spheroids [313]. Given the substantial influence that ascites have on OC cells due to their composition and the concomitant FSS [314], it is therefore important in 3D experimental models of OC to mimic the intrinsic dynamic fluid environment characteristic of the peritoneal cavity, so overcoming the static behavior characterizing the majority of current tested platforms.

As already introduced in the sections before, ascites expose tumor cells to a high concentration of ECM proteins that directly influence the cell-ECM interactions [315]. This condition, referred to as macromolecular crowding (MMC), impacts OC cells phenotype. Bascetin and colleagues used two inert crowders to mimic the MMC and questioned how it could affect the actin organization of OC cell lines. They detected a decrease in cell spreadness, therefore supporting previous evidence depicting ascites viscosity as a marker of the degree of cancer invasiveness and with the concentration of cells floating in the ascites [316,317].

During the advanced stages of the disease, OC cells are exposed to mechanical stresses which manifest both as interstitial fluid pressure and FSS. FSS intensity depends on the ascites build-up of the volume in every patient. The FSS characteristic of the ascitic fluid is estimated to be in the 0–1 Pa range, strictly dependent on the individual increase of ascites volume in the patient's cavity [136,318]. The increase in the liquid volume triggers an increment in the intraperitoneal pressure to which OC cells are subjected, reported to be on average of 2,9x10^4 Pa [319], and results in a flow-induced mechanotransduction that alters cytoskeleton organization and cell proliferation, and therefore the adhesive and invasive phenotype of cells [320]. In this regard, cells can perceive mechanical changes and biomechanical force in the

extracellular milieu and react by converting them into biochemical signals and cellular responses, in order to maintain tensional homeostasis [321,322].

Different studies have already tried to simulate the FSS and / or compression raised from malignant ascites on OC 3D structures, generating FSS in different ways. For example, Klymenko and colleagues evaluated the impact of high intraperitoneal ascites-induced pressure on EOC progression, particularly on MCAs, by developing two *in vitro* systems useful to assess short-term and long-term compression-induced mechanotransduction and the resulting cellular responses related to dissemination. Results showed changes in the expression of genes related to EMT as well as increment in the migratory phenotype of compressed MCAs on hydrogels, compared to the control uncompressed 3D structure [323]. Similarly, EMT-linked markers were modulated by the flow on 3D OC nodules when tested in a microfluidic platform [324].

The addition of low amounts of FSS has been also evaluated in a microfluidic model mimicking the peritoneum with 3D OC spheroids, where it was reported to promote the stem-like and chemoresistant properties of OC cells [325]. FSS-induced chemoresistance was also highlighted in a chip perfusion model of 3D OC nodules [326].

The biophysical properties of ascites do not manifest just on tumor cells but may also impact the OC treatments tested, including CAR-based cell therapies. Therefore, it is fundamental to assess the therapy performance in 3D preclinical models recalling those biomechanisms.

AIM OF THE STUDY

The central aim of my PhD project was to model CAR-based cell immunotherapy exploiting CIK lymphocytes as immune effectors, mimicking a locoregional setting against advanced OC. In order to dissect how the composite structure of PC may affect cell-based immunotherapy and explore the complexity of the structural, dynamic and quantitative features, we have developed reductionistic 3D models of both the solid and the liquid component of PC.

The intent was to split the main complex problem in different simple and adaptable models that could be addressed independently and quantitatively, and then discussed together in the prospect of a translational logic. The underlying rationale considered the hypothetical different mechanisms driving immune effectors recruitment in the two contexts: an active directional migration, consequent of a chemotaxis-driven localization within an ECM in the 3D solid-like model, and a fluid flow driven localization of CAR.CIK, that generated a passive CAR.CIK transport in the floating-like environment.

The work has been divided in different specific objectives comprehensive of (a) the generation and characterization of CIK lymphocytes with anti-MSLN-CAR and the evaluation of their tumor interactions in 2D settings, (b) the set-up of reductionistic 3D preclinical assays, decomposed into I) floating-like and II) solid-like tumor models and the (c) spatio-temporal analysis of MSLN-CAR.CIK dynamics by means of live imaging techniques, to dissect the mechanisms determining localization in “solid” vs “floating” environments in 3D.

The perspective of our work is to shed light on the portability of MSLN-CAR.CIK locoregional therapeutic approaches into the context of PC from OC and thus provide translational bases to optimize the clinical studies exploring the intraperitoneal delivery of a cell-based immunotherapy with CAR.CIK.

In the next chapter, I will discuss in detail the results obtained.

MATERIALS AND METHODS

1. Metastatic ovarian cancer cell lines

The commercially available metastatic ovarian cancer (mOC) cell lines OVCAR-3 and OVCAR-4 were purchased from National Cancer Institute (NCI), OAW28, COV362 and OAW42 from the European Collection of Authenticated Cell Cultures (ECACC) while SK-OV-3, and the control cell lines Caco-2, HeLa and MRC-5 were purchased from American Type Culture Collection (ATCC, Manassas, VA, USA). All cell lines were kept in stock in our institute's cell culture facility, except Caco-2, previously obtained from an established collection of CRC cell lines [327]. Upon request of the scientists, the personnel in the facility thaws certificated vials of frozen cells, which are expanded and handed out for research were obtained from the different biological resources centers as well as re-authenticated by the facility every 6 months, by applying the PowerPlex16 Cell-ID assay (Promega, Madison, WI, USA), based on the analysis of 16 genomic STR markers plus amelogenin and tests for *Mycoplasma* contamination, with a PCR *Mycoplasma* Detection kit (Applied Biological Materials Inc., Richmond, BC, Canada). All cell lines have been characterized by the provider and maintained as suggested.

OVCAR-3 and OVCAR-4 were cultured at 37 °C under 5% CO2 humidified atmosphere in RPMI-1640, COV362 in DMEM low glucose, SK-OV-3 in McCoy, while OAW28 and OAW42 in DMEM low glucose supplemented with 20 IU/l Insulin. Culture media (all purchased from Sigma-Aldrich, St. Louis, MO, USA), unless specified, were supplemented with 10% fetal bovine serum (Thermo Fisher Scientific, Waltham, MA, USA), 100 U/mL of penicillin, 100 µg/mL streptomycin and 2 mM L-Glutamine (Sigma-Aldrich, St. Louis, MO, USA).

Co-cultures either starting from single tumor cells or from spheroids with immune effectors were carried out in standard tissue culture plastic dishes (Falcon), multiwell plates (Corning Inc., New York, NY, USA) or imaging dedicated supports (Cell imaging plate, 96-well, black-walled, glass-bottom, tissue culture treated, Eppendorf AG, Hamburg, Germany; PhenoPlate 96-well, black, optically clear flat-bottom, ultra-low-attachment (ULA)-coated, PerklinElmer Inc., Waltham, MA, USA; µ-slide 18-well chamber slide 81816, ibiTreat IBIDI, GmbH, Gräfelfing, Germany).

2. Generation and *ex-vivo* expansion of MSLN-CAR.CIK

CIK were generated from PBMC of patients with advanced stage tumors, at Candiolo Cancer Institute and San Luigi Hospital, after releasing written informed consent according to internal institutional review board (IRB)-approved protocols (no. 225/2015; no. 125/2022).

PBMC were isolated by density gradient centrifugation (Lymphosep, Aurogene, Roma, Italy) and seeded in cell culture flasks at a concentration of 2 × 10^6 cells/mL in RPMI-1640 medium (Gibco BRL, ThermoFisher, Waltham, MA, USA), consisting of 10% fetal bovine serum (Sigma-Aldrich, St. Louis, MO, USA), 100 U/mL penicillin and 100 µg/mL streptomycin (Gibco BRL, ThermoFisher, Waltham, MA, USA) and 2 mM L-glutamine (Sigma-Aldrich, St. Louis, MO, USA). We added IFN-γ (Miltenyi Biotec, Bergisch Gladbach, Germany; 1,000 U/mL) on day 0 and after 24 hours we activated PBMC using anti-Biotin MACSiBead Particles loaded with CD2, CD3, and CD28 Abs (Miltenyi Biotec, Bergisch Gladbach, Germany) and human IL-2 IS (Miltenyi Biotec, Bergisch Gladbach, Germany, 300 U/mL). On day +3, stimulated PBMC were transduced with third-generation bidirectional lentiviral vector [328] encoding for second-generation anti-MSLN-CAR containing 4-1BB co-stimulatory domain (Creative Biolabs Inc., Ramsey Road Shirley, NY, USA) and GFP reporter gene, by overnight incubation. In detail, the fragment obtained by PCR-amplification from a plasmid encoding for the anti-MSLN-CAR (Creative Biolabs Inc., Ramsey Road Shirley, NY, USA) was cloned in frame into a lentiviral vector with a bidirectional expression cassette carrying a cDNA encoding the eGFP (enhanced Green Fluorescent Protein) in the antisense position with respect to the internal promoter hPGK [328]. Paired NTD.CIK were used as control. For selected experiments, activated PBMC were transduced with an irrelevant third-generation dNGFR/GFP-bidirectional lentiviral vector. Cells were expanded over 4 weeks. Fresh medium supplemented with IL-2 (300 U/mL) was replaced every 2–3 days as needed and the cell density was maintained at 1.8 × 10^6 cells/mL. Transduction efficiency was evaluated by detecting GFP or CAR positivity of membrane expression by flow cytometry with an anti-F(ab')$_2$ fragment Ab (Jackson ImmunoResearch Europe Ltd).

3. Tumor and MSLN-CAR.CIK characterization by flow cytometry

Conjugated CD3, PD-1 (BD Pharmingen, San Diego, CA, USA), and CD314 (anti-NKG2D), CD8, CD56 (Miltenyi Biotec, Bergisch Gladbach, Germany) mAbs were used to characterize phenotype of MSLN-CAR.CIK. MSLN-CAR.CIK were stained with a conjugated anti-F(ab')$_2$ fragment Ab (Jackson ImmunoResearch Europe Ltd) to detect CAR expression. mOC cells were stained with conjugated mAbs for the expression of CIK NKG2D ligands, MIC A/B (BD Pharmingen, San Diego, CA, USA) and ULBP-2,5,6 (R&D Systems Inc. Minneapolis, MN, USA). mOC were stained with 1 µg/mL MSLN-Ab (Sigma-Aldrich, St. Louis, MO, USA), then washed and incubated with rabbit anti-rabbit IgG-AlexaFluor 647 Secondary Ab (Invitrogen, ThermoFisher, Waltham, MA, USA).

Labeled cells were read on two different flow cytometers (CyAn ADP, Beckman Coulter, Brea, CA, USA and Celesta, BD Life Sciences, San Jose, CA, USA) and analyzed using Summit

Software (Beckman Coulter, Brea, CA, USA). Gating criteria were set to secondary Ab/unstained controls.

4. Cancer cell spheroid formation

Three-dimensional (3D) mOC spheroids were generated from multiple mOC cell lines by using the hanging drop technique. The protocol was adapted from the published method [329]. A methylcellulose stock solution was prepared by dissolving 6 g of autoclaved methylcellulose powder (M0512; Sigma-Aldrich, St. Louis, MO, USA) into 250 mL of preheated (60 °C) serum-free culture medium, for 2 hours with a sterile magnetic stirrer. 250mL of complete culture medium was added to a final volume of 500 mL, to obtain a final concentration of 10% fetal bovine serum, and then mixed overnight at 4 °C. The solution was then centrifuged at 5000 g for 2 hours at room temperature. The supernatant was collected and used as described below. To generate mOC spheroids, cells were detached, counted and mixed with 80% culture medium and 20% of methylcellulose-prepared solution, to obtain a final concentration of 0.24% methylcellulose. Drops of 20 µL were pipetted down onto the inner part of a 100- or 150-mm Petri dish lid. The lid was carefully reversed to let the spheroids form in the hanging drops under non-adherent culture conditions. After 3-4 days, spheroids were carefully harvested by washing out the drops with PBS and collecting the solution into 15 mL tubes. Spheroids were gently spun down at 600 r.p.m. for 5 min and mixed with medium or Cultrex BME (CultrexTM Basement Membrane Extract; R&D, Minneapolis, MN, USA). Spheroids premixed with Cultrex BME were seeded as described in the following paragraph. The number of cells per drop changed depending on the type of 3D assay. Generally, OVCAR-3: 200-750; SK-OV-3: 200-500-750; COV362: 200-750.

5. 3D floating-like and solid-like models

We cultured 3D mOC aggregates employing two different experimental settings: (I) to mimic floating metastasis, we set up a 3D floating-like model in which spheroids and MSLN-CAR.CIK were cultured in liquid medium, where the flow was enforced by mechanical shaking of the plate (using the BioTek Cytation3, Cell Imaging Multi-Mode Reader). (II) The 3D solid-like model was realized by embedding both spheroids and MSLN-CAR.CIK in a 3D hydrogel or seeding MSLN-CAR.CIK on top of the hydrogel.

(I) 3D floating-like models

For the 3D floating-like co-cultures, pre-assembled spheroids were cultured in 75 µL of culture media in ULA 96-well flat-bottomed plates (PerklinElmer) 3 days upon spheroids growing in hanging drop. The next day, MSLN-CAR.CIK were added in 75 µL of culture media with a final volume of 150 µL and IL-2 concentration of 300 U/mL. Differently from 2D assays, in the 3D

case the effective number of E:T ratio was expressed in terms of volume densities rather than absolute numbers. The number of immune cells to be seeded in the culture medium was estimated by calculating the density of effector cells that could fit into a spherical shell (1000 µm radius) surrounding each tumor spheroid, in order to approximately generate a theoretical 1:1 E:T ratio in the volume around all spheroids.
The co-cultures were either maintained static or in the presence of a fluid flow for 24-36 hours continuously, to generate a fluid flow (shaking was stopped for a short time only for acquiring images, when needed).

(II) 3D solid-like models
For the 3D cell solid cultures, the pre-assembled spheroids were resuspended in a defined volume of Cultrex BME in order to reach a concentration of approximately 10 spheroids every 45 µL of hydrogel per well, always keeping the tube on ice.
In the 3D-solid embedded culture, MSLN-CAR.CIK were pre-mixed with the spheroids into the hydrogel at densities c.a. 2 × 10^6 cells/mL. Similar to the 3D floating-like models, the number of immune cells to be seeded in the gel was estimated by calculating the density of effector cells that could fit into a spherical shell (390-450 µm radius) surrounding each tumor spheroid, in order to approximately generate a theoretical 1:1 E:T ratio around all spheroids. 45 µL of the embedded mixture supplemented with 300 U/mL of IL-2 was pipetted per well into a black-walled, glass-bottom, 96-well imaging plate (Eppendorf) and allowed to polymerize for 30 min in the incubator at 37 °C, 5% CO2. After polymerization, the scaffolds were covered with 150 µL of RPMI-1640 supplemented with 300 U/mL of IL-2.
In the 3D-solid top culture, spheroids were embedded in 45 µL of Cultrex BME alone and covered with a volume of 150 µL of RPMI-1640 plus IL-2 (300 U/mL) with a given number of MSLN-CAR.CIK.

To evaluate immune effector infiltration, the 3D-solid embedded culture was re-adapted to fit in a µ-slide 18-well chamber slide (IBIDI). MSLN-CAR.CIK were pre-mixed with the spheroids into the hydrogel at densities c.a. 14 × 10^6 cells/mL. The number of immune cells to be seeded in the gel was estimated by calculating the density of effector cells that could fit into a spherical shell (150 µm radius) surrounding each tumor spheroid. 40 µL of the embedded mixture was pipetted per well and allowed to polymerize for 30 min in the incubator at 37 °C, 5% CO2. After polymerization, the scaffolds were covered with 100 µL of RPMI-1640 supplemented with 300 U/mL of IL-2.

6. **Back of the envelope estimation for passive vs active recruitment of immune effectors *in vitro***

We aim at studying the difference between the recruitment in a 3D ECM of immune effectors on tumor targets (spheroids of mOC cells) *vs* in floating cultures, either forced with a fluid flow or not.

First off, we need to consider the typical effective diffusion coefficient induced in a 3D environment. To this aim, we start by saying that the typical recruitment time (of the order 10 hours, as estimated by Iaia et al, Cancers, 2021 [296], and coherent with our data) needs to be compared to the typical distance between spheroids and effectors set to be under 300 *μm*. These estimates would lead to an effective diffusion coefficient in 3D of

$$D \lesssim \frac{(300\mu m)^2}{10 \cdot 60 \cdot 60s} \sim 2.5\mu m^2/s$$

In a fluid flow the typical time and spatial dimension might be of the order of (estimating the mixing of an ink droplet in a 96-well plate well)

$$D = \frac{L^2}{T} \sim \frac{0.5^2 cm^2}{20\ s} = \frac{25 \cdot 10^4 \mu m^2}{20s} \sim 12.5 \cdot 10^3 \mu m^2/s$$

The typical time for effectors to get on target depends on the average distance between the two species by adding the transport due to the fluid flow. For rough estimates one can reason that tumor spheroids are considered like cells and effectors as diffusible entities, with a diffusivity that depends on the type of transport involved.

Let us start with the densities. Effectors are seeded in a volume density such that in any sphere of diameter 300 *μm* there should be around 100 effectors, this maps into a density of

$$\rho_e = \frac{100}{\frac{4}{3}\pi R^3} = \frac{100}{\frac{4}{3}\pi 0.15^3 mm^3} \simeq 7.1 \cdot 10^3 cells/\mu L$$

The typical distance of effectors from a spheroid will be then of the order of 100 *μm*. By taking as a reference the maximum distance of an effector, i.e. 300 *μm,* the typical time to get a spheroid and an effector together in a fluid flow described above is then estimated as:

$$t \sim \frac{L^2}{D} = \frac{(300\mu m)^2}{12.5 \cdot 10^3 \mu m^2/s} = \frac{10^4 \mu m^2}{4.2 \cdot 10^3 \mu m^2/s} \simeq 7.2s$$

Therefore, typical times of recruitment in solid vs floating environments are significantly different. It is worth noting that this argument does not take into account the timing of chemical bonding but only that related to mixing.

A more refined analysis can be applied following ref. [330]. The typical time for a diffusing particle released at a given distance from a cell (or an absorber, in our case a cell spheroid) of radius *R* sitting in the origin to reach the cell can be estimated as a function of the diffusion coefficient *D*, of the distance from the cell l and of the size of the cell/spheroid. Assuming effectors to be much further away from the target, for example at a distance of 1 cm from the spheroid the mean capture time (l>>*R)*, is of the order of

$$t \sim \frac{l^3}{3RD} \sim \frac{(10^4)^3 \mu m^3}{3 \cdot 10^2 \mu m \cdot 12.5 \cdot 10^3 \mu m^2/s} = \frac{10^{12} \mu m^3}{37.5 \cdot 10^5 \mu m^3/s} = 74\ hrs$$

For typical distances and effectors well mixed in the liquid these times are obviously much faster coherently with previous estimations, for example when l=300 μm:

$$t \sim \frac{l^6}{3DR(l^3 - R^3)}\left(1 - \frac{9R}{5l} + \frac{R^3}{l^3} - \frac{R^6}{5l^6}\right) \simeq 3s$$

Such estimates also ignore that both spheroids and effectors might be dragged along by the fluid flow, determining times which can be much faster than when spheroids are for example attached to the peritoneal wall.

7. 2D tumor cell killing assays

We assessed the tumor-killing ability of patient-derived MSLN-CAR.CIK and NTD.CIK against mOC cell monolayers in 2D using flow cytometry.

Target cells were stained with the live dye PKH26 (Sigma-Aldrich, St. Louis, MO, USA), according to the manufacturer's protocols. Immune-mediated killing was analyzed by Flow Cytometry (Cyan ADP, Dako) and measured by the DAPI permeability of target cells (PKH26+ gate). CIK cells were co-cultured at different effector to target cell ratios (5:1, 2.5:1, 1:1, 1:2 and 1:4) in complete growth medium supplemented with 300 U/mL IL-2 at 37 °C and 5% CO2 for 72 hours. Target cells were also tested separately from CIK as control to assess their spontaneous mortality. The percentage of mOC-specific lysis for each E:T ratio was calculated using the following formula:

$$\%Tumor\ killing\ = \frac{experimental - spontaneous\ tumor\ mortality}{100 - spontaneous\ tumor\ mortality} \times 100$$

8. 2D tumor treatment withdrawal assays

Treatment withdrawal experiments were carried out in phases (I) and (II).

(I) For the first 72 hours, tumor cells (29.400 cells/well for OVCAR-3, SK-OV-3 and COV362) were co-cultured with MSLN-CAR.CIK or the control NTD.CIK or maintained untreated in 12-well plates at effector target ratios spanning from 2:1 to 1:2 depending on the cell line, in 2 mL of complete growth medium supplemented with 300 U/mL IL-2 at 37°C and 5% CO2. After 72 hours, tumor cells were washed twice in PBS, trypsinized and counted. The amount of viable cells was assessed with trypan blue and Counting chamber, Bürker-Türk (VWR).

(II) For the following 72 hours, tumor cells (8000 cells/well for OVCAR-3, SK-OV-3 and COV362) were re-plated from each treated and untreated condition in 48-well plates without effector cells in 400 uL of complete growth medium at 37°C and 5% CO2. At the end of the essay, tumor cells were washed in PBS, trypsinized and counted, to obtain the amount of

viable cells. The number of cells after each 72 hours were normalized to the corresponding number of cells at seeding time point for each untreated and treated condition.

9. 3D floating-like tumor cell killing assays

In 3D floating-like models, mOC spheroids were seeded at a concentration of 5spheroids/well in ULA 96-well flat bottom plates. MSLN-CAR.CIK and NTD.CIK were plated at a given volume density recapitulating a E:T ratio of 1:1 in culture medium with 300 U/mL IL-2, 25 mM HEPES at 37 °C 5% CO2. Immune-mediated cytotoxicity against mOC spheroids was determined using Promega CytoTox 96 Non-Radioactive Cytotoxicity Assay kit upon 24 hours of continuous mechanical shaking of the co-culture (freq. 150 r.p.m.). Briefly, the supernatant was incubated with CytoTox 96 reagent (Promega) at room temperature for 30 min in the dark, followed by addition of stop solution (Promega) and absorbance was measured at 490 nm. The average optical density (OD) of untreated cells was subtracted from each experimental well. The mean OD value in the medium was subtracted from all measurements. The mean OD values of control lysed cells were considered 100% cytotoxic and used to calculate the percent cytotoxicity deriving by MSLN-CAR.CIK, as recapitulated by the following formula:

$$\%\, Tumor\ cytotoxicity\ = \frac{experimental\ -\ CIK\ spontaneous\ -\ tumor\ spontaneous}{tumor\ maximum\ -\ tumor\ spontaneous} \times 100$$

Non-adhering co-cultures in the presence of a fluid flow were compared to the respective static co-cultures employed as control conditions.

10. Imaging methods for 3D cultures

We employed imaging-based methods to extract semi-quantitative measurements. In order to discriminate MSLN-CAR.CIK and tumor cells and to dynamically monitor recruitment and the efficacy of effector cells in time-lapses, cells were stained with different commercially available non-genetic transient fluorescent dyes after performing the hanging drop technique and during the setting up of the experiments. mOC spheroids were stained with nuclear live staining NucBlue (Invitrogen, ThermoFisher, Waltham, MA, USA) after one hour incubation in 1 mL of medium at 37 °C, while MSLN-CAR.CIK cells were stained with fluorescent dyes PKH26 (Sigma Aldrich) or PKH67 (Sigma Aldrich), following the manufacturer's instructions.

By making use of imaging glass-bottom plates and combining such labeling techniques, we were able to image targets and effectors with different space and time resolution, depending on the experimental question, as detailed in what follows.

mOC spheroids were cultured in different ways depending on the model of interest with MSLN-CAR.CIK.

For the 3D floating-like models one to maximum three mOC spheroids were seeded per well in ULA PhenoPlate-96 black-walled, glass-bottom imaging plates, as described above.

Imaging was performed using a cell imaging multi-mode microplate reader (Cytation3, BioTek, Winooski, VT, USA) equipped with a 4× objective, a mechanical shaker and an incubator with controlled temperature and CO2 concentration. Imaging was performed alternating cycles of 16 minutes mechanical shaking (freq. 180-270 cpm) followed by a halt for image capturing lasting about 11 minutes, for an overall framerate of one image every 30 minutes. 3D static floating model imaging was performed either using the Cytation3 with no mechanical shaking or with an inverted widefield microscope Nikon Ti2 (Nikon Instruments, Melville, New York, NY, USA) with a 4× dry objective, a wide field of view (25 mm) monochromatic camera (IRIS 15; Photometrics, Tucson, AZ, USA) and an incubator to keep the plate stably at 37 °C and 5% CO2. The Nikon Ti-2 is equipped with a SpectraX LED light source with excitation wavelengths of 470 nm and 555/585 nm, associated with filters LED-FITC-A-000, LED-mCherry-A-000 and CY3-4040C-000, depending on the excited fluorophore. Images were taken every hour. The same microscope was used for the 3D solid models with a lens of dry 20× 0.75 NA objective, acquiring images every three hours. Z-stacks of fluorescence images were maximum-intensity projected and brightfield images were projected using Extended Depth of Focus. Time-lapse microscopy assay for 3D solid-like models lasted 72 hours and 24-36 hours for 3D floating-like models. Images were then processed with custom-written Matlab (The Mathworks, Natick, MA, USA) or Fiji/ImageJ [331] scripts.

11. 3D solid-like tumor cell killing assays

In 3D solid-like models, NucBlue positive mOC spheroids and PKH67 (Sigma Aldrich) positive MSLN-CAR.CIK or NTD.CIK were cultured for 72 hours. Upon staining with propidium iodide (Sigma-Aldrich), fluorescence images were acquired with a dry 20× 0.75 NA objective on a Nikon Ti2 inverted microscope. Killing activity was determined as positivity of propidium iodide. Untreated mOC spheroids were used to evaluate spontaneous mortality, whereas a part was lysed with 5% *(v/v)* Triton X-100 as a control for the maximum cytotoxicity.

12. Confocal Microscopy

3D cultures were grown in µ-Slide 18 Well Glass Bottom, Ibidi 81816 (IBIDI, GmbH, Gräfelfing, Germany), employing as reference the 3D-solid embedded model, as described above. Briefly, 10 mOC spheroids per well, stained with PKH26 (Sigma-Aldrich), were embedded in 40 µL of hydrogel, together with MSLN-CAR.CIK or NTD.CIK labeled with PKH67 (Sigma-Aldrich). 100 µL of RPMI-1640 with 300 U/mL IL-2 filled the wells. After 16 h, the co-cultures were washed twice with PBS and fixed with 4% PFA for 30 minutes. After three washes with PBS, the PFA was removed and samples were kept in PBS at 4 °C until subsequent imaging. Images were acquired with a confocal microscope (Leica SP8 with white light laser and AOBS, Leica microsystems, Wetzlar, Germany) with a water immersion 40× objective.

13. Image Processing

Recruitment of MSLN-CAR.CIK cells on spheroids was quantified by segmenting the fluorescent signal coming from the tumor cells with Ilastik [306]. Binary images were then used as masks to calculate the corresponding signal coming from the fluorescence of CIK, normalized to the relative background, as described in **Fig. 12**.

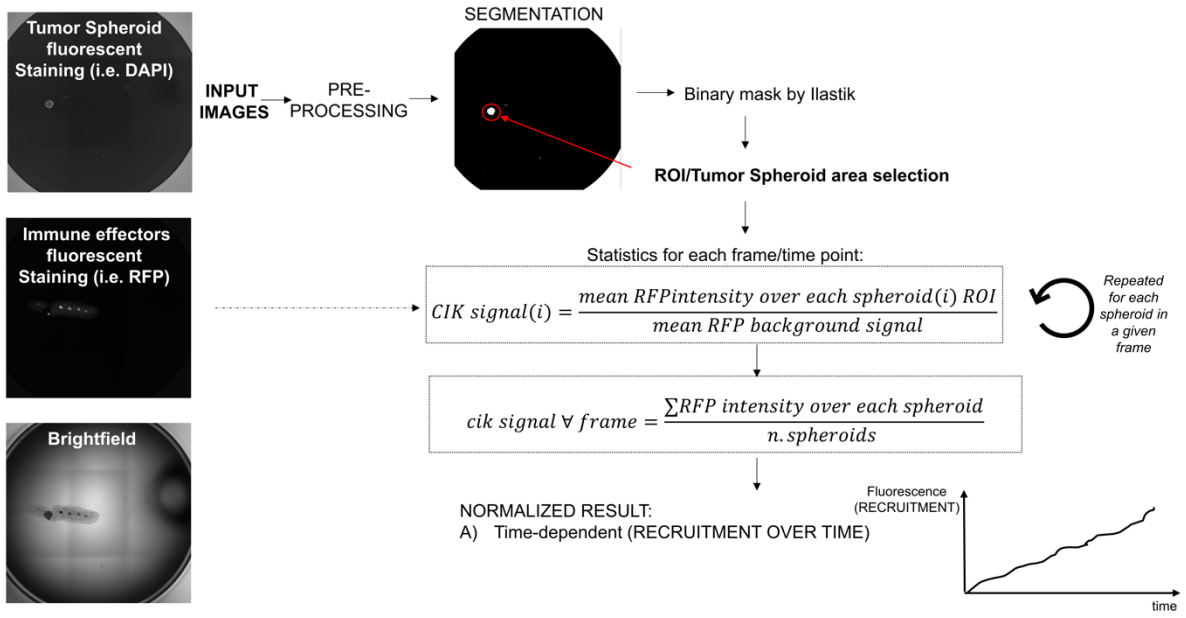

Figure 12. Image analysis procedure to quantify immune effector localization over spheroids, in function of time.

In order to quantify the time taken by recruitment, we performed a fit of recruitment signal coming from each spheroid with a sigmoidal function of the form:

$$S(t) = A + B\frac{e^{k(t-tau)}}{1 + e^{k(t-tau)}}$$

and used the lag-time to reach half the maximum height of the sigmoid as a measure of recruitment time. Profiles were fitted with Matlab (The Mathworks, Natick, MA, USA).

As a quantitation method for assessing killing in 3D, tumor cells and effectors were segmented with Ilastik and the corresponding masks obtained were used to calculate the mean intensity of propidium iodide staining in the corresponding regions, using a lysing agent (Triton X-100) as positive control. Aggregation of data was performed by normalizing with respect to the untreated case for each experiment.

Infiltration of immune effectors into 3D spheroids was performed by segmenting the tumor volume corresponding to the signal intensity coming from tumor cells, which was then filled and morphologically closed. Infiltrated cells were also segmented in 3D and the infiltration percentage was calculated as the percent of volume corresponding to each spheroid occupied by immune effectors.

The fraction of immune effectors on the cell surface was also obtained segmenting a defined volume close to the spheroid surface ("surrounding shell") corresponding to the signal intensity coming adjacent to the outer tumor cells. Immune cells were also segmented in 3D and their percentage was calculated as the percent of volume corresponding to each spheroid surface occupied by immune effectors.

For preparation and visualization of figures and movies we used Fiji/ImageJ. In order to better appreciate intensity variations in fluorescence images, the same contrast adjustments were used in each experiment.

14. Statistical and data analysis

Statistical analyses of data were performed using GraphPad Prism 10.0 (GraphPad Software) or Matlab (The Mathworks, Natick, MA, USA). Descriptive data are presented as mean or median values and all error bars represent standard deviation (SD). To find statistical significance in the comparison between means of two groups, we used two-tailed unpaired Student's t tests. A $P \leq 0.05$ was considered significant. Significance is represented on graphs as *, $P \leq 0.05$; **, $P \leq 0.01$; ***, $P \leq 0.001$; **** $P \leq 0.0001$.

RESULTS

1. Preliminary evaluation: advanced ovarian cancer as a valid target for MSLN-CAR.CIK

1.1 Metastatic ovarian cancer characterization

In order to explore the potential clinical relevance of targeting PC from OC with MSLN-CAR.CIK, we first assessed the levels of expression of MSLN in OC tumors by exploiting public databases of RNA-sequencing **(Fig. 13A)** [332]. Expression of MSLN in OC cell lines is found to be significant and comparable to mesothelioma cell lines and is instead typically non expressed in cell lines originating from other tumors such as melanoma. Furthermore, a detailed analysis of MSLN protein expression in human tumors shows that OC is among the tumors with the highest expression of MSLN [219,222,226].

In order to build a reliable set of biological models, we selected 6 human cell lines derived from patients with mOC, representative of the heterogenous MSLN expression that can be found in PC patients: OVCAR-3, OVCAR-4, SK-OV-3, OAW42 and OAW28 (all derived from ascites) and COV362 (derived from pleural effusion) (data were retrieved from https://www.cellosaurus.org/index.html). To explore the clinical relevance of mOC cells as a target of MSLN-CAR.CIK, we first characterized by flow cytometry our mOC cell line panel confirming an expected variable/heterogeneous expression of the glycoprotein MSLN on the cell surface, as shown in **Fig. 13B**. A high MSLN membrane expression was observed in OVCAR-3, OVCAR-4, COV362, OAW28 and SK-OV-3 cell lines, while a slightly lower expression was found to characterize OAW42, exhibiting a lower mean fluorescence intensity (MFI). The colorectal cancer Caco-2 cells were used as negative membrane expression control while the cervix cancer HeLa cells as the positive control. Further, we confirmed that mOC cell lines expressed variable levels of the main ligands recognized by the NKG2D CIK receptor, MIC A/B (median 92%, SD 38%) and ULBPs-2/5/6 (median 56%, SD 25%) **(Fig. 13C)**.

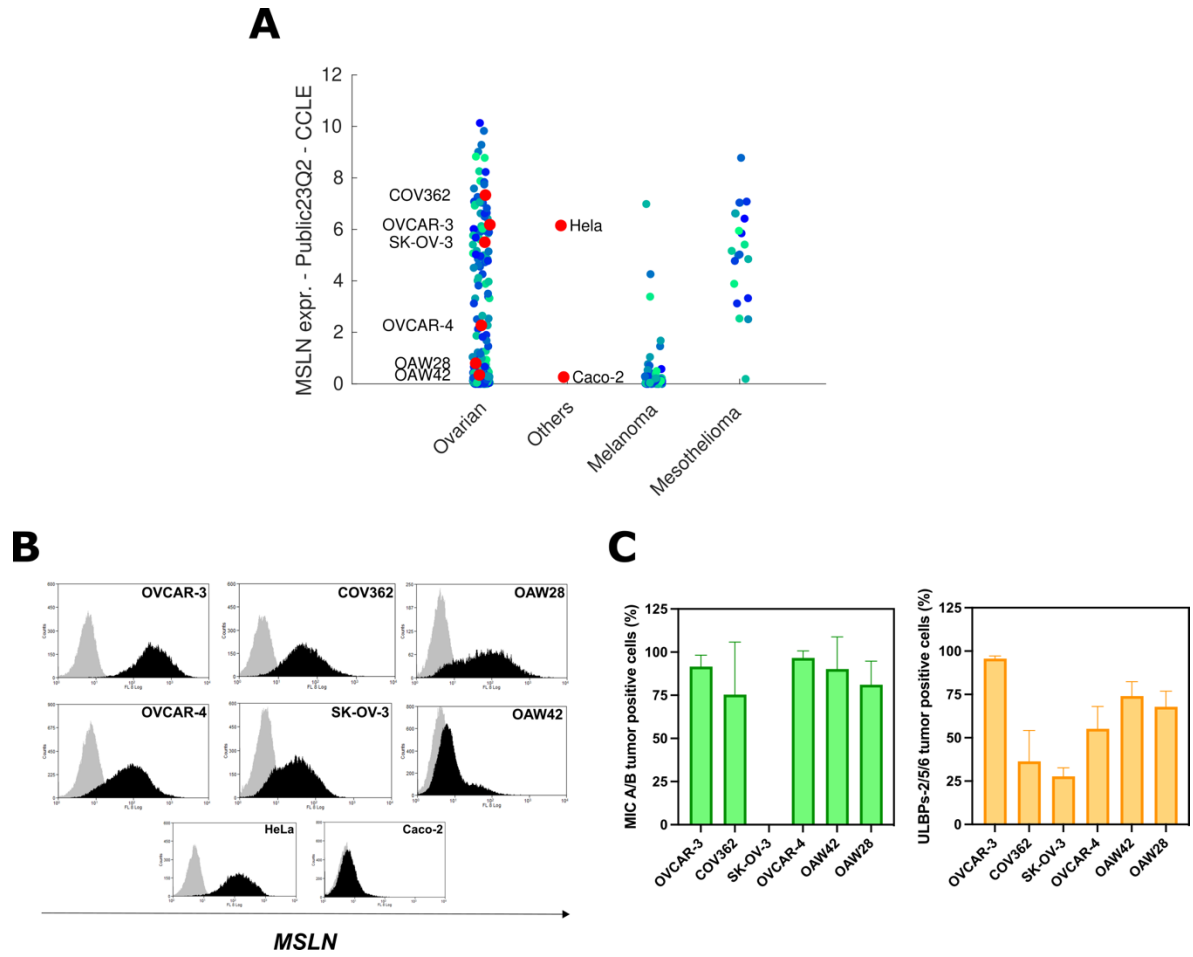

Figure 13. mOC characterization for MSLN and other relevant targets for MSLN-CAR.CIK based therapy. **(A)** MSLN mRNA expression in a panel of OC cell lines from CCLE database. MSLN expression in OC cell lines was comparable with that observed in mesothelioma cell lines, although with greater heterogeneity. RNA-sequencing expression data were selected and downloaded from the CCLE datasets Public23Q2. **(B)** MSLN expression was confirmed in mOC cell lines by flow cytometry. A representative flow cytometry histogram is reported for each mOC cell line. The Caco-2 colorectal adenocarcinoma cell line that lacks MSLN surface expression and HeLa that highly express MSLN were used for comparison. Isotype controls are shown in gray. **(C)** Flow cytometry analysis of surface expression of the main known ligands recognized by the NKG2D receptor on CIK (MIC A/B, ULBPs-2/5/6) on the panel of cell lines. Values from at least 3 biological replicates are reported (mean ± SD).

1.2 Generation and characterization of patient-derived MSLN-CAR.CIK

MSLN-CAR.CIK were generated ex vivo from PBMCs of patients with advanced solid tumors of various origin and engineered with second-generation MSLN-CAR with 4-1BB co-stimulation domain by lentiviral transduction at the 3rd day of culture. After ex-vivo maturation (three weeks), the mean expression of MSLN-CAR on engineered CIK (MSLN-CAR.CIK) was 40±12% (mean±SD) as assessed by flow cytometry **(Fig. 14A)**. Overall, the MSLN-CAR.CIK phenotype was comparable with that of control unmodified non transduced CIK (NTD.CIK), expressing the main CIK markers **(Fig. 14B).**

A

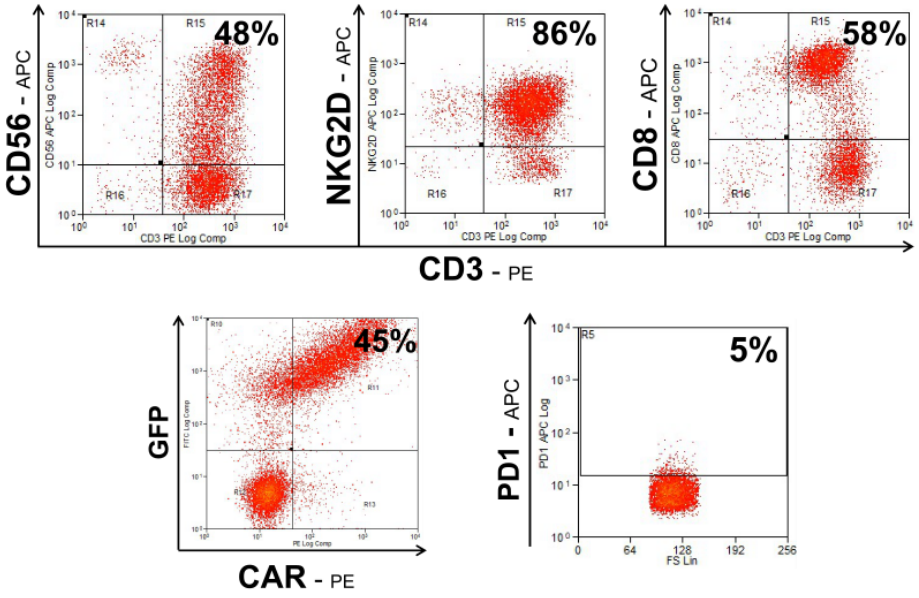

B

Cancer #Pt		CD3 (%)	CD3/CAR (%)	CD3/CD56 (%)	CD3/CD8 (%)	NKG2D (%)	PD-1 (%)
#Pt1	CAR.CIK	99	40	15	56	53	6
	NTD.CIK	99	/	13	44	40	4
#Pt2	CAR.CIK	99	54	19	75	83	3
	NTD.CIK	98	/	20	76	85	3
#Pt3	CAR.CIK	96	45	49	63	92	5
	NTD.CIK	98	/	43	70	89	5
#Pt4	CAR.CIK	99	29	31	79	86	6
	NTD.CIK	99	/	30	81	89	6
#Pt5	CAR.CIK	99	48	41	74	83	3
	NTD.CIK	99	/	47	70	80	4
#Pt6	CAR.CIK	99	21	78	74	88	10
	NTD.CIK	99	/	75	73	78	8

Figure 14. Phenotypic characterization of MSLN-CAR.CIK. (A) Representative flow-cytometry dot-plots showing characteristic patient-derived MSLN-CAR.CIK phenotype. **(B)** Paired patient-derived MSLN-CAR.CIK and respective NTD.CIK immunophenotypes characterization are reported in the table.

1.3 MSLN-CAR.CIK are effective against mOC cells in 2D cell culture

Firstly, we explored in two-dimensional assays the anti-tumor killing ability of MSLN-CAR.CIK against mOC cell lines with significant expression of MSLN, by incubating effector and target cells at different ratios (E:T) from 5:1 to 1:4. MSLN-CAR.CIK effectively killed the tested mOC cell lines at all E:T ratios, significantly superior to that of NTD.CIK and with an intrinsic variability most likely consequent of the specific phenotype of each tested mOC cell line **(Fig. 15A)**.

We evaluated the activity of MSLN-CAR.CIK on targets expressing different levels of MSLN on OC cell surface, by using the OVCAR-3 cell line, with high MSLN level, and the OAW42

cell line, with a lower one. As expected MSLN-CAR.CIK–mediated tumor toxicity was strongly dependent on the level of surface expression of MSLN on tumor cells as shown by comparing mOC cell lines negative or positive for MSLN **(Fig. 15B)**.

In order to assess the ability of cells to regrow following treatment with MSLN-CAR.CIK, we performed a drug-release experiment. Growth of residual mOC cells, following treatment with CAR.CIK, was significantly impaired (72 hours after treatment) as compared with tumor cells exposed to control unmodified NTD.CIK or to untreated condition as shown in **Fig. 15C**.

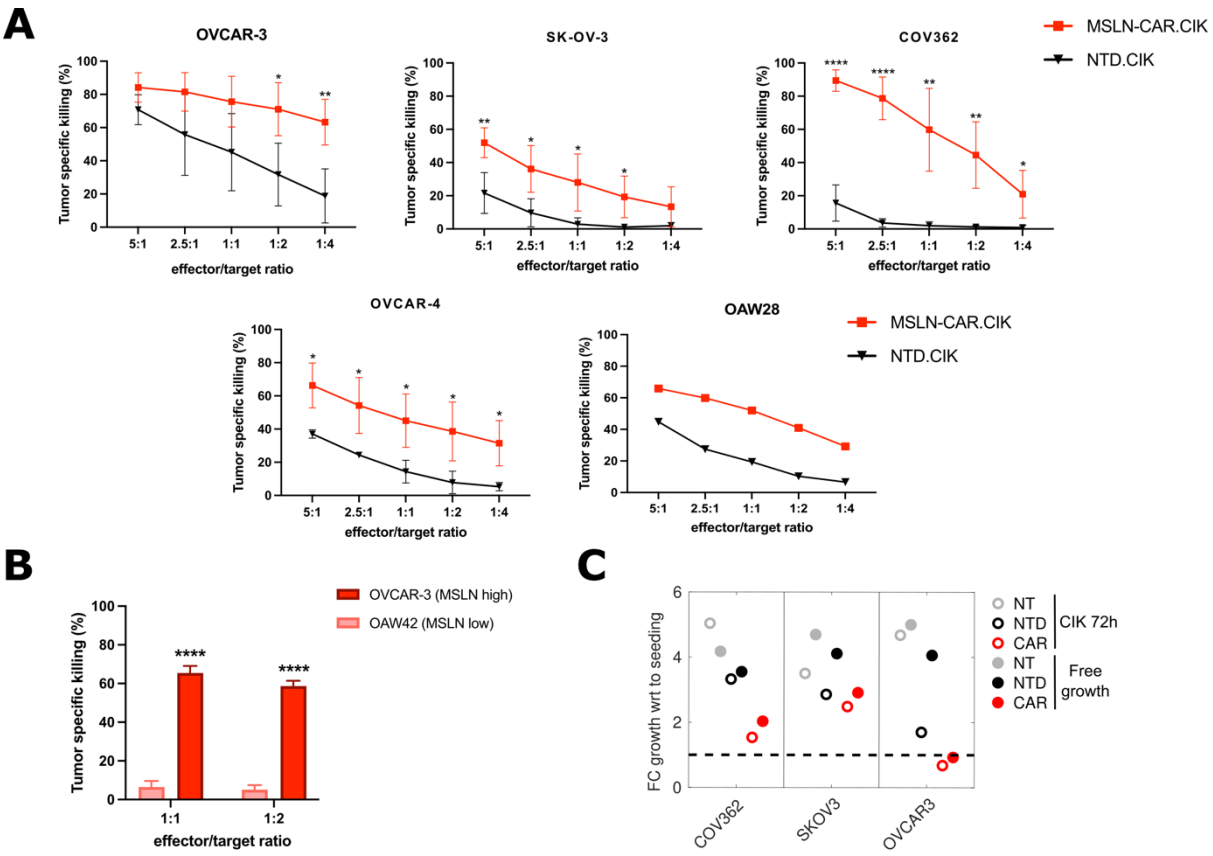

Figure 15. MSLN-CAR.CIK effectively and specifically kill mOC cells in 2D. (A) MSLN-CAR.CIK killed mOC cell lines more specifically than NTD.CIK. Tumor cell–specific cytotoxicity values from 3 or 4 biological replicates are reported, except for single read of OAW28 (mean ± SD). **(B)** MSLN-CAR.CIK killing of mOC cells depends on MSLN expression levels at therapeutically relevant E:T ratios (n=3) (mean ± SD) (OVCAR-3 chosen as MSLN^{high} cell line, while OAW42 as MSLN^{low}). (* P ≤ 0.05; ** P ≤ 0.01; *** P ≤ 0.001; **** P ≤ 0.0001). **(C)** The capability of residual mOC cells of growing upon MSLN-CAR.CIK withdrawal was significantly delayed compared to NTD.CIK (n=1-3).

As a relevant aspect of the proposed therapy, we also explored different controls to check different aspects related to the specificity of the anti-tumor activity exerted by MSLN-CAR.CIK. In this regard, CIK were engineered with an irrelevant dNGFR/GFP-bidirectional lentivirus. MSLN-CAR.CIK showed a higher cytotoxic activity than dNGFR/GFP.CIK and NTD.CIK which was retained even at lower E:T ratios **(Fig. 16A)**. Consistently, MSLN-CAR.CIK and NTD.CIK

showed comparable cytotoxicity against the MSLN-negative control colorectal cancer Caco-2 cell line **(Fig. 16B)** and against the fibroblast cell line MRC-5 **(Fig. 16C)**.

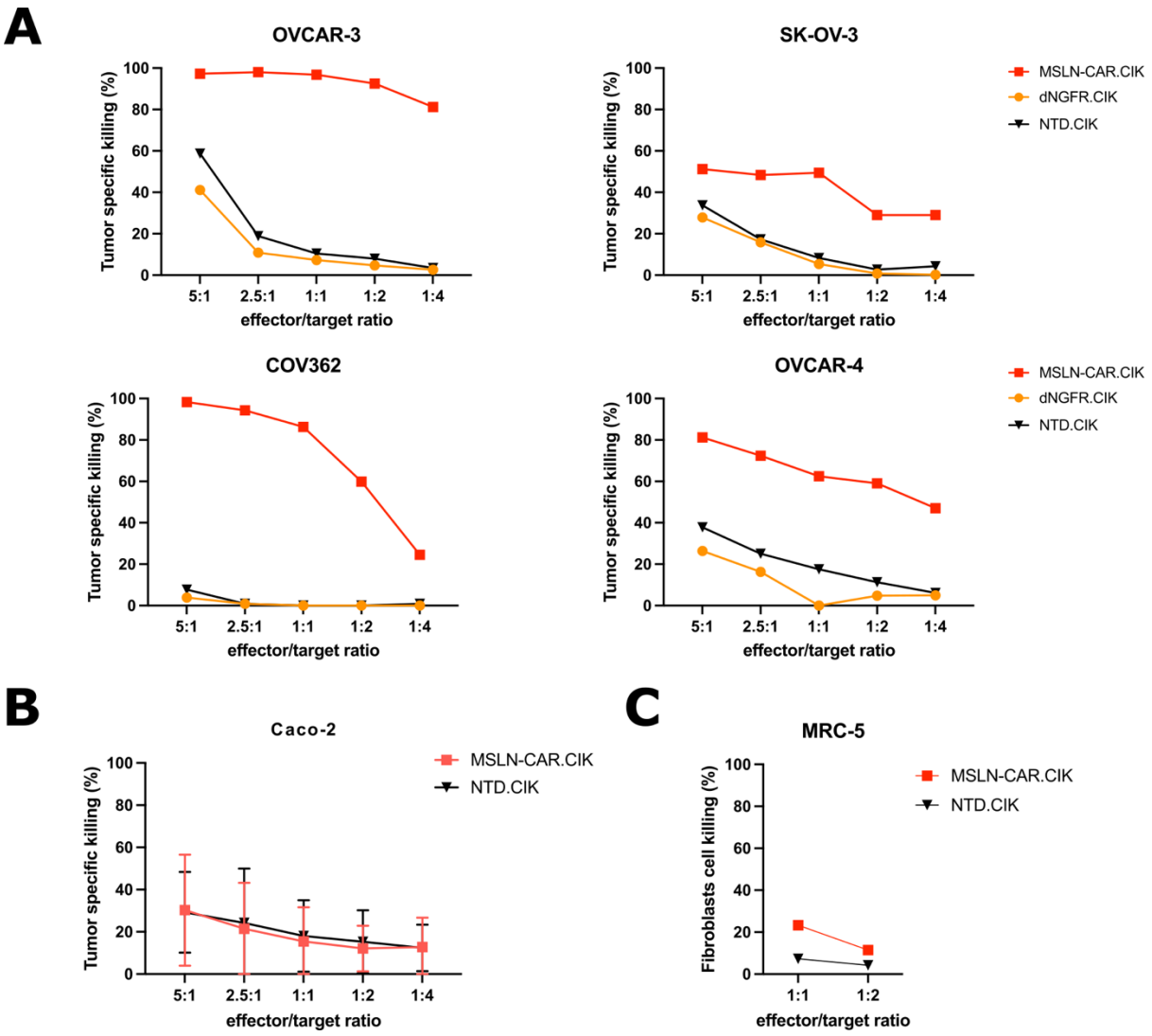

Figure 16. MSLN-CAR.CIK specifically kill mOC cells in 2D. (A) Cytotoxic activity of control CIK engineered with control dNGFR/GFP-bidirectional lentivirus against mOC cell lines was comparable with that of NTD.CIK (mean ± SD). **(B)** MSLN-CAR.CIK and NTD.CIK showed similar cytotoxic activity against colorectal adenocarcinoma cell line Caco-2 not expressing MSLN (n=3). **(c)** MSLN-CAR.CIK–mediated tumor toxicity at therapeutically relevant E:T ratios was low on normal fetal lung fibroblasts, indicating low off-target cytotoxicity (n=1).

2. MSLN-CAR.CIK are functional in 3D biological models recapitulating the complexity of peritoneal carcinomatosis

In order to recapitulate the clinical complexity of peritoneal metastasis and to be able to appreciate the dynamical interactions between MSLN-CAR.CIK and tumor cells, we developed reductionistic experimental settings for the floating-like and solid-like components of PC, splitting the main complex problem in different simpler and adaptable models that could be challenged independently and quantitatively. The ability of killer lymphocytes to reach and kill the different 3D mOC targets were identified as the more relevant point of interest for cell therapy evaluation.

We generated 3D tumor cell aggregates from different mOC cell lines (n=3; OVCAR-3; SK-OV-3; COV362) employing the hanging drop technique (see Methods, section 4). The solid-like context was mimicked by embedding mOC spheroids in a hydrogel and seeding effectors with access to the matrix, giving mechanical support and allowing nutrient exchange to spheroids while enabling immune effectors migration as well as the necessary practical advantages for cell culture. The floating component was instead modeled with liquid shaking co-cultures (see Methods, section 5). The two cellular components were independently followed by means of different fluorescent labeling and using brightfield as a reference and monitored over-time by time-lapse microscopy.

Further, aiming to determine the suitability of fluid flow and the density of both spheroids and effectors, we have carried out “back of the envelope” calculations, by approximating the movement of MSLN-CAR.CIK with respect to targets by an effective molecular diffusion taking as a reference the theories of Berg and Purcell [330], where we estimated the associated diffusion coefficients. Preliminary estimations indicate that fluid mixing is much more efficient than 3D migration in the ECM and that mixing might significantly improve the recruitment, compared to the corresponding case in absence of the flow. Details on this argument can be found in **Fig. 17A** and in the Methods, section 6.

A

$$D_{\text{liquid}} = \frac{l^3}{3Rt} \sim 10^6 \frac{\mu m^2}{s} \cdots\cdots\rightarrow \text{t} \sim \text{sec} \qquad D_{\text{solid}} = \frac{l^2}{t} \sim 10 \frac{\mu m^2}{s} \cdots\cdots\rightarrow \text{t} \sim \text{hours}$$

Figure 17. Rough estimates of MSLN-CAR.CIK-tumor contact timescales predict that flow-induced mixing is much faster than 3D migration in an ECM in promoting their physical interaction. (t = typical timescale for MSLN-CAR.CIK-tumor contact; l = typical MSLN-CAR.CIK-tumor distance; R = tumor spheroid radius; D = diffusion coefficient) (Berg, Purcell 1977).

2.1 Floating component of mOC

2.1.1 MSLN-CAR.CIK localize over the floating component of mOC

In order to mimic the floating metastasis subjected to fluid flows potentially generated by body-movement, we cultured mOC spheroids and MSLN-CAR.CIK in liquid medium, where the flow was enforced by mechanical shaking of the plates as sketched in **Fig. 18A**.

By means of proper fluorescent labeling of the cellular components and by exploiting live imaging, we were able to monitor and measure the localization of MSLN-CAR.CIK on mOC spheroids as a function of time. MSLN-CAR.CIK localization on mOC spheroids was significantly faster and stronger in the presence of fluid flows as compared with the absence of flow, as shown in the snapshots presented in **Fig. 18B-C**, comparing MSLN-CAR.CIK or NTD.CIK treatment to untreated condition, and in **Supplementary Video S1-S2**. Furthermore, MSLN-CAR.CIK localized more intensely on mOC spheroids than unmodified NTD.CIK, regardless of the presence of the flow **(Fig. 18D-E).**

In order to quantitatively appreciate the localization dynamics and extract information from the shape of the recruitment curves, we resorted to the measurement of the lag time, i.e. the time elapsed to reach half the maximum localization, as detailed in the Methods, section 13. Localization of MSLN-CAR.CIK in shaking conditions took on average (3.2±1.0) h and (4.5±2.7) h for control NTD.CIK **(Fig. 18F)**. The absence of flow greatly increased the average localization lag time, with an average localization of (13.1± 2.0) h for MSLN-CAR.CIK and (12.9±5.1) h for NTD.CIK **(Fig. 18F)**.

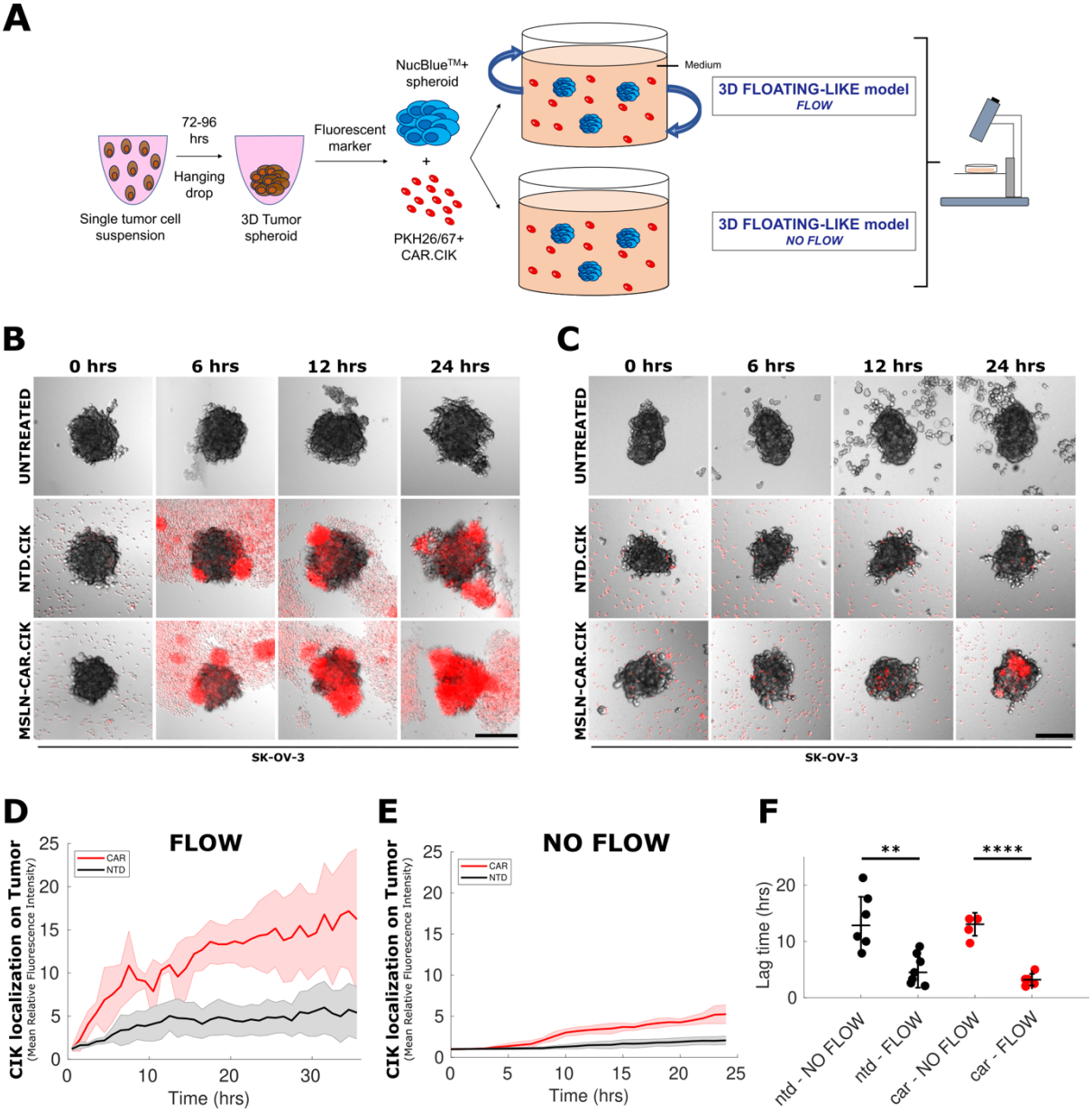

Figure 18. MSLN-CAR.CIK are more stably localized on the floating target when coupled with fluid flow in liquid cultures. (A) Sketch of the reductionistic experimental 3D models recalling floating peritoneal metastasis. 3D tumor spheroids were generated by hanging drop technique. Both 3D tumor target and immune effectors were labelled with different fluorescent dyes, and co-cultured in 3D floating-like models. Tumor spheroids and effectors were cultured in liquid medium in presence **(top)** or absence **(bottom)** of a forced flow, obtained by mechanically shaking of the plate. Live imaging and data mining were used to monitor the assays. **(B-C)** MSLN-CAR.CIK cells were monitored by time-lapse imaging with **(B)** and without **(C)** flow, compared to NTD.CIK. Representative time-lapse microscopy images refer to snapshots at indicated timepoints for brightfield and fluorescence, the latter corresponding to effectors only. Scale bar: 200 µm. **(D-E)** Measure of the intensity of fluorescence signal in the regions of the image corresponding to the spheroids. The plot shows the localization of effector cells on mOC spheroids in the presence **(D)** or absence **(E)** of a fluid flow at different times after the addition of MSLN-CAR.CIK. Each line represents the mean of many single spheroids (CAR flow N = 3; NTD flow N = 3; CAR no flow N = 5; NTD no flow N = 3), while shades represent SD. **(F)** Quantitative analysis obtained from localization data: localization time extracted by fitting the localization time sequences as fluorescent signal localized onto the tumor

spheroids for MSLN-CAR.CIK vs NTD.CIK in the presence or absence of a flow. In floating-cultures, mean and dispersions were (3.20 ± 1.02) h for MSLN-CAR.CIK (N = 5 spheroids), compared with NTD.CIK (4.50 ± 2.72) h (N = 7 spheroids). Localization time in static cultures had mean and dispersions of (13.05 ± 2.04) h for MSLN-CAR.CIK (N = 4 spheroids), (12.85 ± 5.09) h for NTD.CIK (N = 6 spheroids). (** P ≤ 0.01; **** P ≤ 0.0001).

2.1.2 MSLN-CAR.CIK are functional against the floating component of mOC

In order to assess the corresponding cytotoxic activity of MSLN-CAR.CIK in the floating-like setting, we used nuclear fragmentation in mOC spheroids as a surrogate of induced tumor cell death. Tumor nuclear fragmentation after 24 hours of co-culture with MSLN-CAR.CIK was more clearly visible in presence of a forced flow **(Fig. 19A)** than in the static-liquid co-culture **(Fig. 19B).** Correspondingly, cytotoxicity was measured considering the release of Lactate Dehydrogenase in the culture medium by the dying tumor cells, due to cell lysis, as described in Methods, section 9. MSLN-CAR.CIK killing activity was significantly higher in presence of a continuous forced flow coherently with the faster localization of effectors on the target as shown in **Fig. 19C**. The relative enhanced cytotoxicity by MSLN-CAR.CIK vs NTD.CIK was coherent with the stronger tumor localization of MSLN-CAR.CIK thereby yielding a systematically higher cytotoxicity independently of the flow, as shown in **Fig. 19C**. Furthermore, our data indicate that the increased cytotoxic potential of MSLN-CAR.CIK with respect to NTD.CIK observed in a 2D context **(Fig. 15A)** is retained in the 3D context.

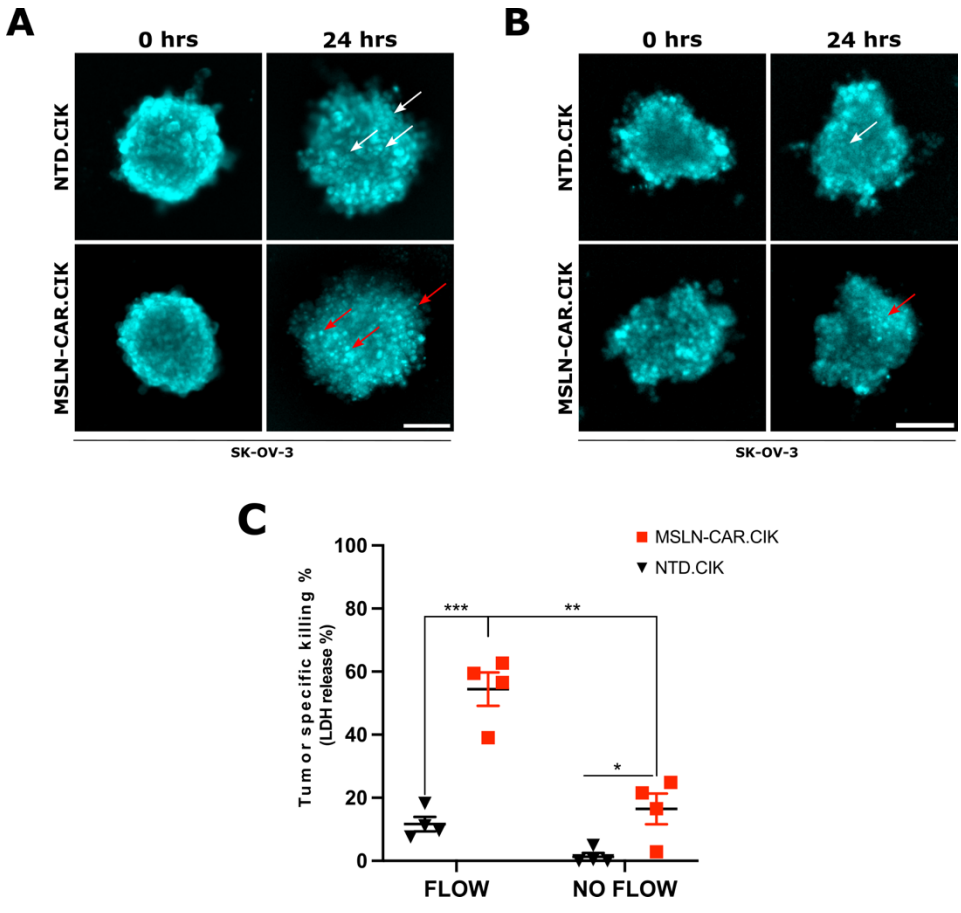

Figure 19. MSLN-CAR.CIK exert a higher anti-tumor activity in presence of fluid flow in floating cultures. (A-B) Representative images of mOC spheroids labeled with NucBlue and cultured with immune effectors in the presence **(A)** or absence **(B)** of flow. Red arrows indicate small and fragmented nuclei, while white arrows indicate intact nuclei. Scale bar: 200 µm. **(C)** MSLN-CAR.CIK target more effectively 3D mOC spheroid in the presence of forced flow. Lactate dehydrogenase (LDH) release from spheroids cultured in the presence or absence of fluid flow (n=4) (mean ± SD). (* $P \leq 0.05$; ** $P \leq 0.01$; *** $P \leq 0.001$; **** $P \leq 0.0001$).

Taken together our results indicate that MSLN-CAR.CIK are more intensely localized on the target than NTD.CIK and such tumor localization is significantly boosted by fluid flow in liquid cultures.

2.2 Solid component of mOC

2.2.1 MSLN-CAR.CIK recruit on the solid component of mOC

As a means to assess whether MSLN-CAR.CIK can effectively reach and kill targets in a more static environment and in presence of an ECM, we set up a solid-like setting by embedding the 3D culture in a hydrogel. Effectors and targets were co-cultured in two different experimental conditions, in which tumor spheroids were generally premixed with a hydrogel and MSLN-CAR.CIK were either added on the liquid–gel interface or embedded within the gel, as shown in **Fig. 20A**, to evaluate their ability to penetrate within the matrix. The latter experimental setup was functional to test immune effectors activity in a more homogeneous and reproducible way.

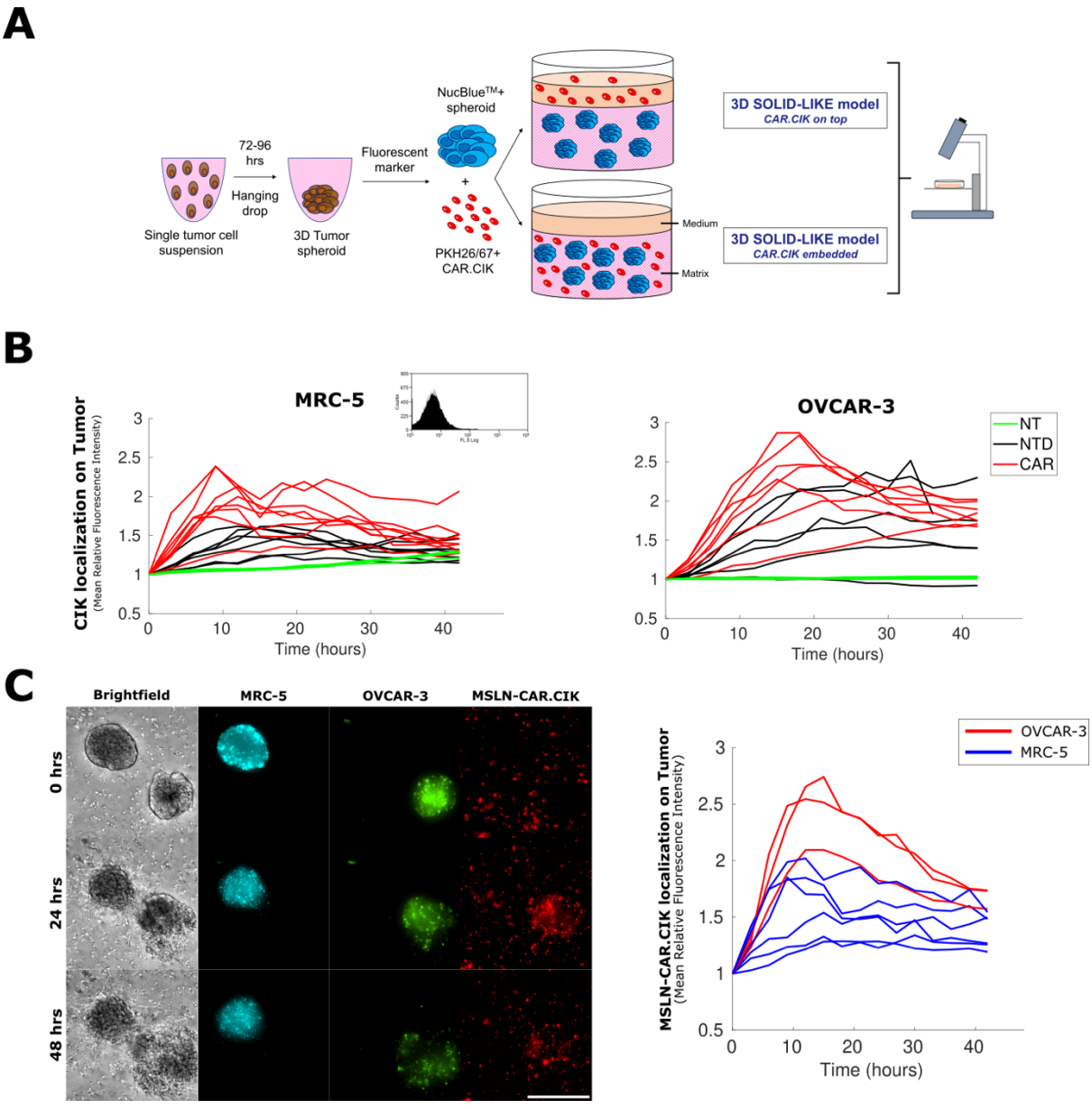

Figure 20. 3D models recapitulating the solid component of PC. (A) Sketch of the reductionistic experimental 3D models recalling peritoneal metastasis. 3D tumor spheroids were generated by hanging drop technique. In the solid-like models, tumor spheroids embedded in a hydrogel were co-cultured with MSLN-CAR.CIK either added on the liquid–gel interface or embedded as well. Live imaging and data analysis were used to monitor the assays. **(B)** MSLN-CAR.CIK recruitment as a function of time on normal fetal lung fibroblast 3D spheroids (MRC-5) **(left)** lacking the expression of MSLN, as shown by the representative histogram, compared to MSLN-CAR.CIK recruitment on high MSLN expressing mOC spheroids **(right)**, when co-culturing tumor or fibroblast spheroids with immune effectors. Each thin line represents a single spheroid. (NT: Untreated; NTD: NTD.CIK; CAR: MSLN-CAR.CIK) **(C)** Representative time lapse microscopy images of MSLN-CAR.CIK localization over 3D targets, when co-embedding in the same hydrogel both mOC and fibroblast spheroids. Fibroblast spheroids are labeled with NucBlue (cyan), mOC spheroids are labeled with PKH67 (green) and effectors are labeled with PKH26 (red). Grayscale images correspond to brightfield images. Scale bar: 200 μm **(left)**. MSLN-CAR.CIK localization on mOC spheroids (red lines) and fibroblast spheroids (blue lines) over time **(right)**. To generate MRC-5 spheroids, a cell suspension of 1200 cells/100 μL per well was plated in ULA 96-well round bottom plates, centrifuged at 300 r.p.m. for 10 minutes and assembled in 1 day, adapting the protocol from the published method (Ivascu A., Kubbies M. SLAS Discovery, 2006).

First, we assessed how MSLN-CAR.CIK target non-tumoral targets with respect to a tumoral one, when challenged embedded in a hydrogel. We considered both co-cultures of immune effectors against tumoral or non-tumoral 3D targets, as well as tri-cultures of immune-effectors and tumoral and non-tumoral 3D targets. By measuring the immune effectors recruitment on targets as a function of time, we detected MSLN-CAR.CIK localization on 3D fibroblasts aggregates to be lower than recruitment over the cancer cell lines **(Fig. 20B-C)**, supporting the notion of a generally limited off-target action for MSLN-CAR.CIK on non-tumoral targets.

Subsequently, we focused on dissecting the dynamics of recruitment of MSLN-CAR.CIK in 3D matrix. Microscopic inspection through live imaging over 3h-intervals indicated that MSLN-CAR.CIK were recruited more rapidly when embedded in the hydrogel since the beginning **(Fig. 21A top - B and Supplementary Video S3)**, presumably due to the smaller average distance to be covered to reach the target, suggesting that the average effector-target distance might be relevant in determining recruitment lag-times**.** MSLN-CAR.CIK also penetrated the hydrogel **(Fig. 21A bottom - C)** from the liquid-matrix interface albeit with more variable recruitment lag times, confirming a potential dependence on the distance of the target from the interface. Coherently, when observed for longer times (72 hours), similar levels of MSLN-CAR.CIK recruitments were reached, independently from where the immune cells were initially located **(Fig. 21D and Supplementary Video S4)**. This observation is corroborated by the direct comparison of the distribution of lag-times in the two different settings (termed top and

embedded, see **Fig. 21E**), which highlights a much broader distribution for top seeded effectors than for embedded effectors.

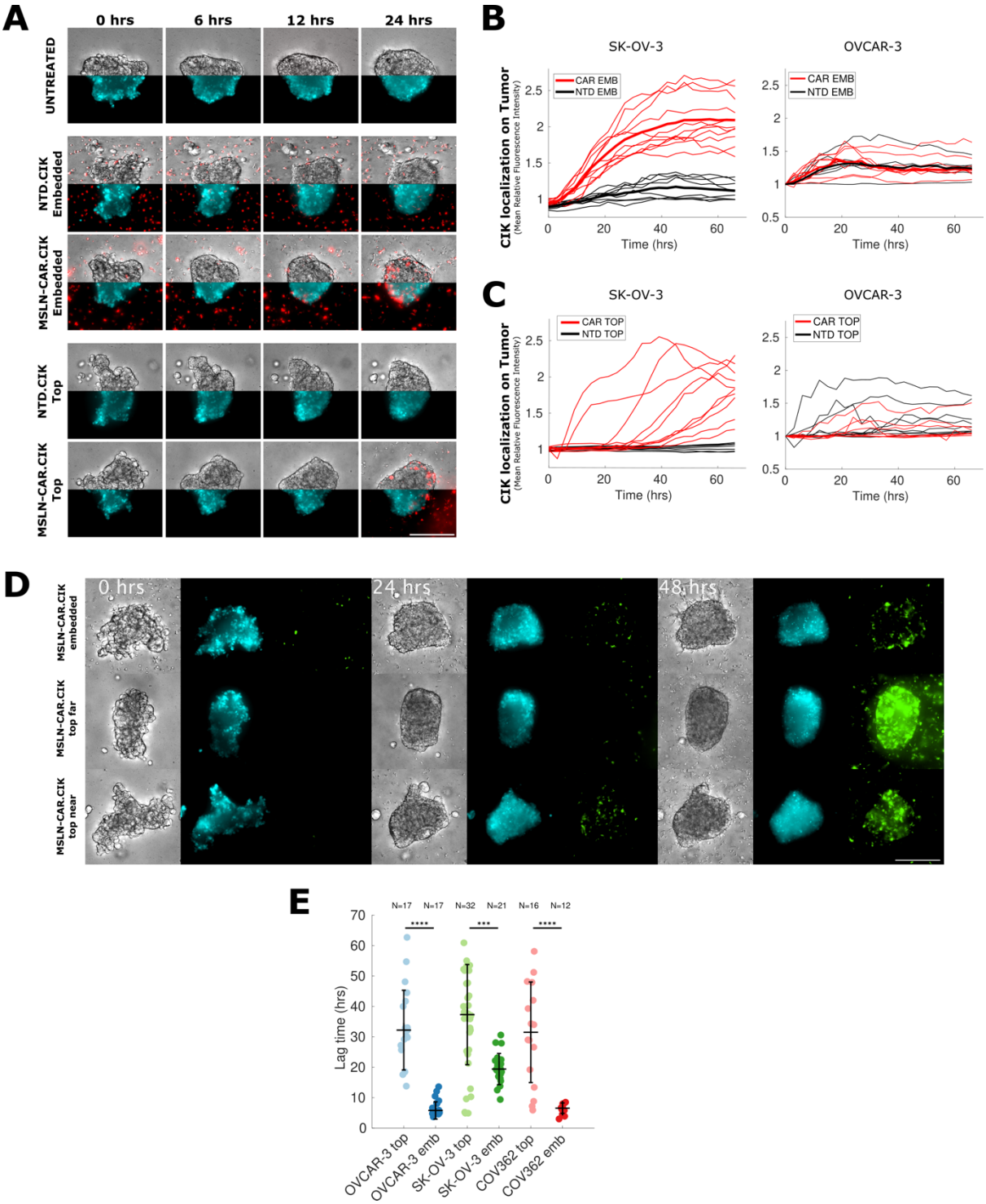

Figure 21. MSLN-CAR.CIK migrate and are recruited on mOC tumor spheroids. (A) MSLN-CAR.CIK and NTD.CIK were monitored by time-lapse imaging when embedded in the hydrogel **(top)** and when seeded on top **(bottom)** against mOC spheroids**.** Representative microscope images refer to snapshots at indicated times where the top half of the image is the bright field channel while the lower part corresponds to tumors labeled with NucBlue, and for both the additional fluorescent channel corresponds to effectors. Scale bar: 200 μm. **(B-C)** Intensity of fluorescence signal in the regions of the image corresponding to the spheroids. The plot shows the recruitment of effector cells on mOC spheroids when MSLN-CAR.CIK or NTD.CIK were embedded **(B)** or seeded on top of the hydrogel **(C)**, as a function of time. Each thin line represents a single spheroid, while the ticker lines represent the median. **(D)** Comparison of MSLN-CAR.CIK monitored by time-lapse imaging when embedded in the hydrogel with respect to when seeded on top of it, targeting mOC spheroids embedded at different distances from the liquid-matrix interface**.** mOC spheroids are labeled with NucBlue (cyan) and effectors labeled with PKH67 (green). Grayscale images correspond to brightfield images. Scale bar: 200 μm. **(E)** Lag time of recruitment on tumor spheroids for MSLN-CAR.CIK embedded or seeded on top of the hydrogel for each considered mOC cell line. For example, OVCAR-3 cell line challenged with MSLN-CAR.CIK, results in a lag time (31.50 ± 16.53) h when embedded (*N* = 17 spheroids), versus (6.55 ± 1.71) h when on top (*N* = 17 spheroids).

Our data suggest that, on average, the time required to reach the mOC spheroids is significantly influenced by the distance traveled by the effectors. In order to corroborate this observation, we calculated the approximate distance of spheroids from the interface where MSLN-CAR.CIK were seeded initially. As expected, recruitment was much faster on those spheroids closer to the interface and delayed on spheroids further away from the effectors, as shown in **Fig. 22A.** The inevitable underlying heterogeneous spatial distribution and the resulting variability in the response is crucial, since it could relate to the situation in patients' metastases within the peritoneal membrane and might indeed suggest that a strategy to minimize the initial distance between effectors and targets, such as in a locoregional approach, might prove beneficial to the treatment.

Along this line of investigation, it is worth noting that other than the paradigmatic liquid-like and solid-like setups, metastatic implants can be found adhered at the liquid-matrix interface [99]. In order to take this case into consideration and to be able to compare it with the other setups we performed experiments where MSLN-CAR.CIK were added on the liquid-gel interface and challenged against mOC spheroids that had been seeded both on top of the hydrogel as well as completely embedded in **(Fig. 22B)**. The intent was to verify first whether MSLN-CAR.CIK could recruit faster over a tumor target with little or no distance to cover. Secondly, and of greater translational relevance, our aim was to assess whether after getting in contact with the tumor targets at the top, immune effectors were still able to invade from the liquid to the matrix and to be recruited over the embedded spheroids. Our results outlined how MSLN-CAR.CIK recruitment over superficial spheroids (CAR OUT) was almost immediate and the presence of these spheroids did not compromise the ability of the MSLN-CAR.CIK to subsequently target inner mOC spheroids (CAR IN) **(Fig. 22B).**

It is worth noting that the typical lag-times obtained in experiments performed in the solid-like model are estimated around one order of magnitude larger than those obtained in the floating-like models **(Fig. 22C),** as predicted by our estimates.

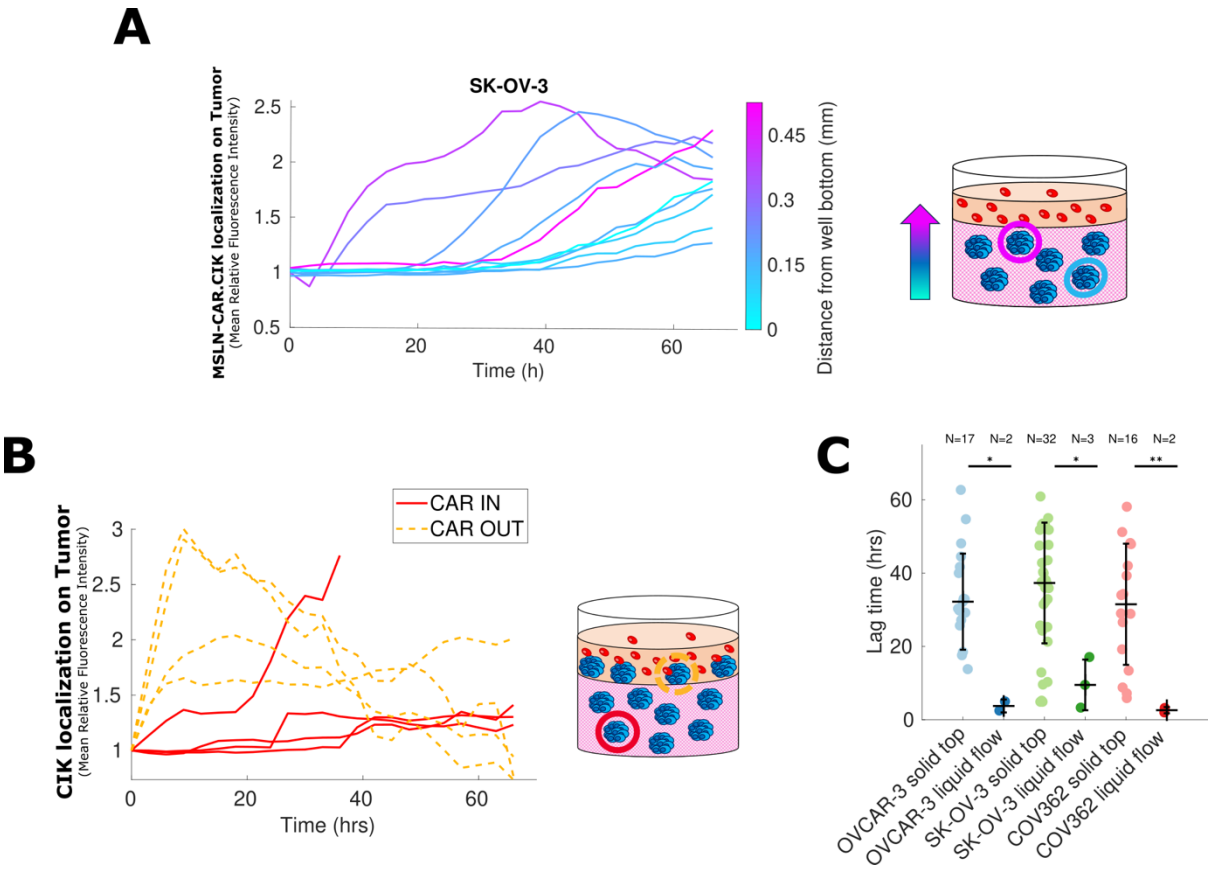

Figure 22. MSLN-CAR.CIK recruitment time is distance-dependent. (A) The plot correlates the recruitment of the MSLN-CAR.CIK on mOC spheroids as reported by the fluorescence signal corresponding to single spheroids over time, with respect to the distance of the single mOC spheroids from the liquid-matrix interface. Blue hues correspond to spheroids more distant from the interface, while violet hues correspond to the closer ones. **(B)** The plot shows the recruitment of MSLN-CAR.CIK when seeded on top of the hydrogel against mOC spheroids seeded both on top of as well (CAR OUT) or completely embedded in (CAR IN). **(C)** Recruitment time of MSLN-CAR.CIK when seeded on top of the hydrogel in a 3D solid-like model or in a 3D floating-like model under a forced fluid flow for each considered mOC cell line. For example, OVCAR-3 cell line challenged with MSLN-CAR.CIK, results in a lag time (31.50 ± 16.53) h when on top of the hydrogel (N = 17 spheroids), versus (2.60 ± 0.85) h in a forced flow (N = 2 spheroids). (* $P \leq 0.05$; ** $P \leq 0.01$; *** $P \leq 0.001$; **** $P \leq 0.0001$).

2.2.2 MSLN-CAR.CIK infiltrate the solid component of mOC

In order to understand whether the cytotoxic activity mediated by MSLN-CAR.CIK was carried out by means of interactions limited to the surface of the tumor spheroids or due to infiltration in mass by immune effectors, we assessed the ability of CAR-redirected cells to infiltrate 3D solid targets, which is a prerequisite for an efficient destruction of solid masses. Confocal analysis of mOC spheroids embedded in the hydrogel and co-cultured with effectors for 16

hours outlined how beyond the fraction of MSLN-CAR.CIK that can adhere to the spheroid surface, there is also a comparable or even greater fraction that manage to penetrate the 3D cell aggregate **(Fig. 23A)**, clearly supporting the notion that MSLN-CAR.CIK can reach and infiltrate in a 3D solid-like biological setting, as shown in different z-planes along the tumor spheroid **(Fig. 23B-D)**.

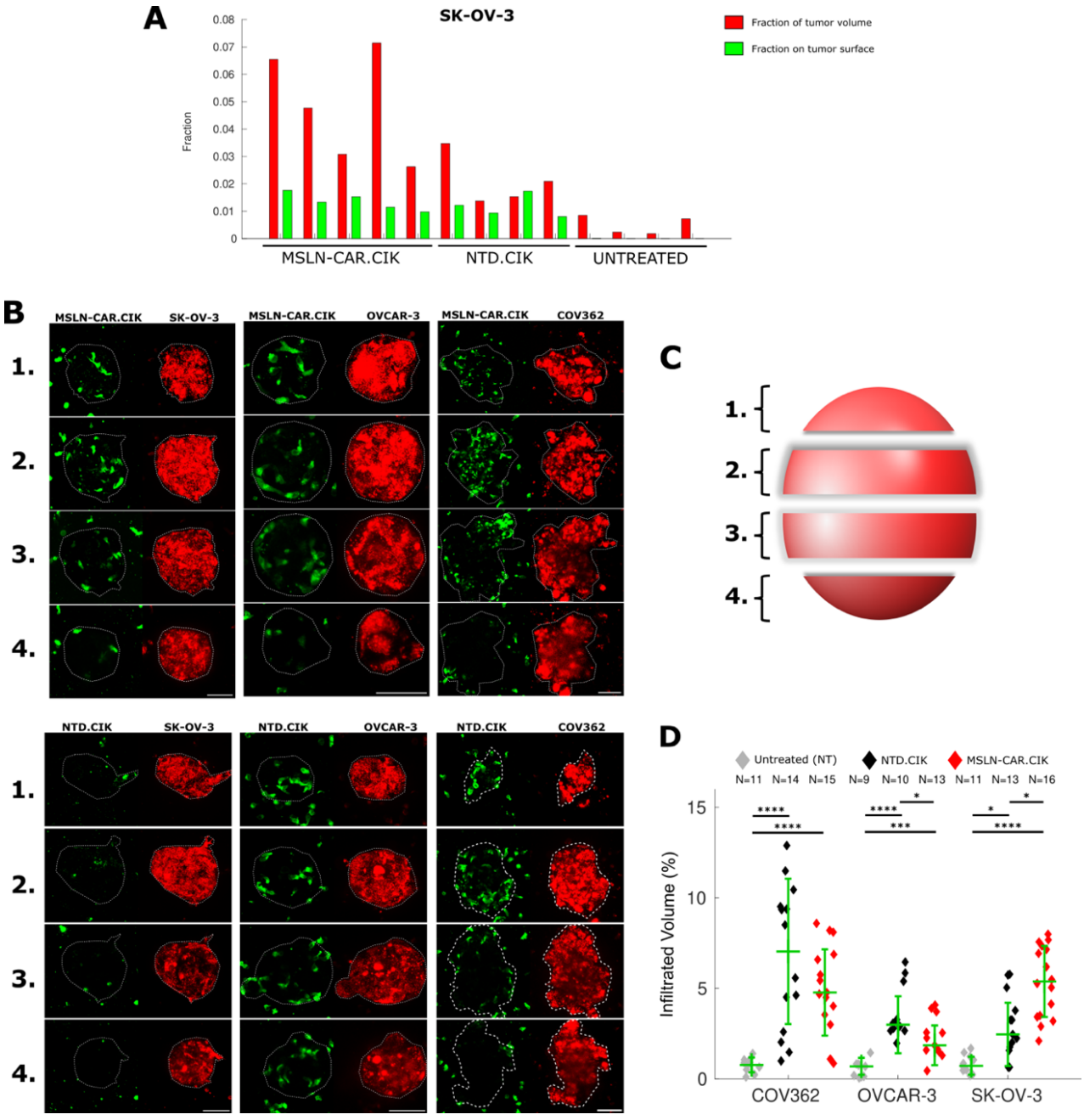

Figure 23. MSLN-CAR.CIK infiltrate the tumor target in a 3D solid-like biological setting. (A) Exemplificatory comparison among the fraction of immune effectors within tumor spheroid volume (red bars) and the fraction on tumor spheroid surface (green bars) obtained by segmenting immune effectors within the spheroid volume for SK-OV-3 cell line. **(B)** Maximum intensity projections of four grouped confocal sections of mOC spheroids challenged with MSLN-CAR.CIK **(top)** or NTD.CIK **(bottom)**, both embedded in 3D hydrogel after 16 h of co-culture. (immune effectors: green - PKH67; mOC spheroid: red - PKH26). Scale bar: 50 μm. **(C)** Sketch of the mOC spheroid sectioning done to

generate four different maximum intensity projections along the z-plane of each spheroid. **(D)** Fraction of mOC spheroid volume occupied by MSLN CAR.CIK or NTD.CIK, obtained by quantifying the segmented signal of immune effectors within the spheroid volume. (* $P \leq 0.05$; ** $P \leq 0.01$; *** $P \leq 0.001$; **** $P \leq 0.0001$).

Our data indicate that MSLN-CAR.CIK are able to be recruited on tumor cell aggregates in a solid-like experimental setting, with variable kinetics depending on the distance between the initial position of the effectors. Furthermore MSLN-CAR.CIK are able to reach the surface of cell spheroids, to penetrate within the cell aggregate and to kill tumor cells.

2.2.3 MSLN-CAR.CIK are functional against the solid component of mOC

Finally, to investigate the MSLN-CAR.CIK cytotoxic activity against tumor targets when challenged in a solid-like environment, we measured the intensity of propidium iodide signal in spheroids treated with MSLN-CAR.CIK and used that as a proxy for cytotoxicity. Representative images are shown in **Fig. 24A**. The quantification of the imaging-based assay confirms that MSLN-CAR.CIK exert a significant cytotoxic effect, ranging from approximately 2- to 4-fold higher than baseline level of spontaneous mortality of untreated tumor spheroids, peaking around 4-fold for OVCAR-3 consistently with 2D killing assays **(Fig. 24B-C)**. Taken together these data indicate that despite a general ability of NTD.CIK to localize on and infiltrate the three-dimensional structure of tumor cell aggregates (as shown in **Fig. 21A** and **23B**), the killing ability of MSLN-CAR.CIK in 3D is systematically and significantly higher than that of NTD.CIK. This observation is coherent with our results on 2D killing assays which indicate MSLN-CAR.CIK as more cytotoxic than NTD.CIK.

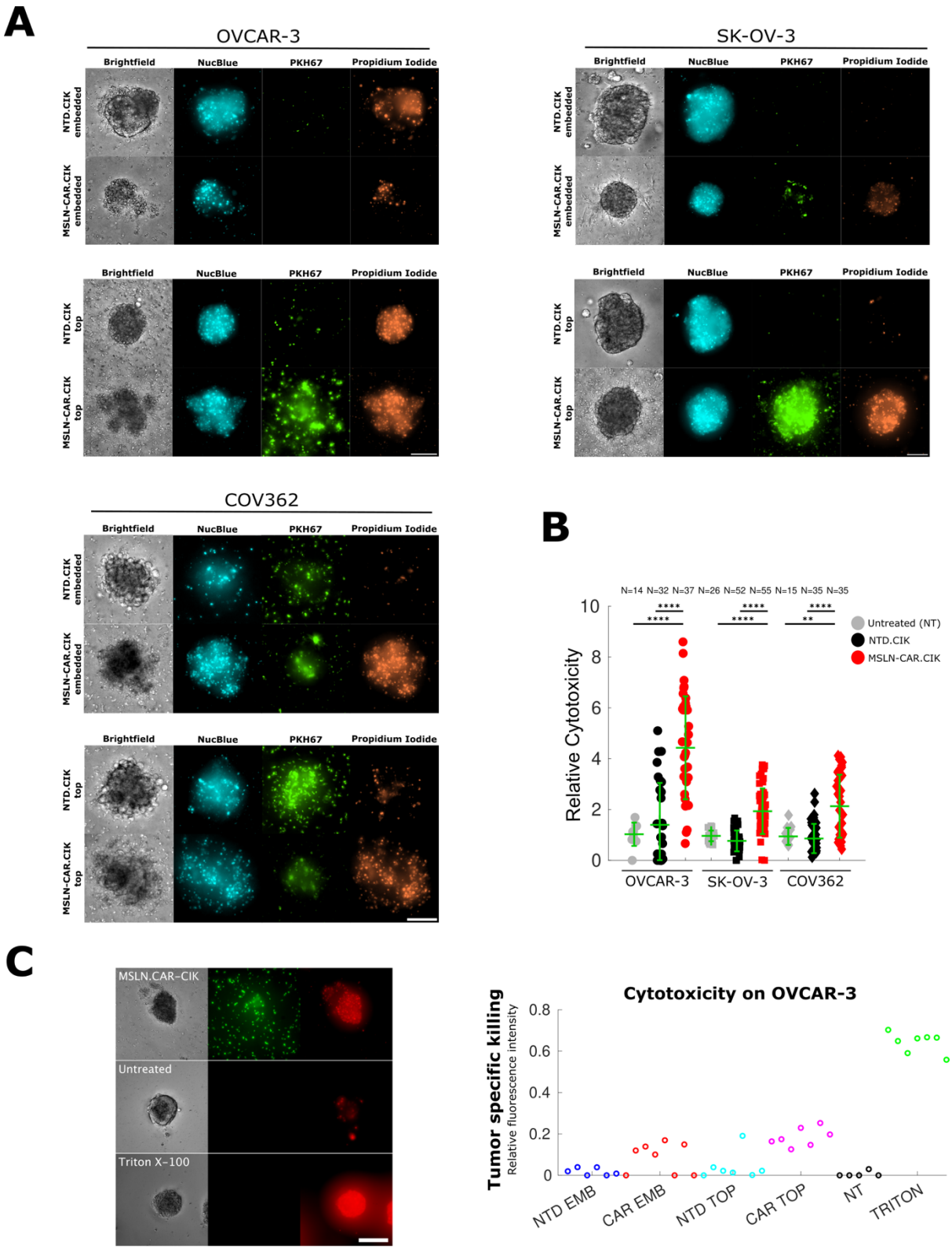

Figure 24. MSLN-CAR.CIK are cytotoxic against the solid component of PC in 3D solid-like biological settings. (A) Comparison of MSLN-CAR.CIK- and NTD.CIK-treated mOC spheroids lapsed after 72 hours of co-culture, when immune effectors are embedded in the hydrogel with respect to when seeded on top of it. mOC spheroids are labeled with NucBlue (cyan), effectors with

PKH67 (green), and the killing effect is shown by propidium iodide labeling (orange). Grayscale images correspond to brightfield images. Scale bar: 100 µm. **(B)** Cytotoxic activity on single mOC spheroids either untreated (gray), co-cultured with MSLN-CAR.CIK (red) or with NTD.CIK (black) in both 3D solid-like models, all related to untreated condition. Green bars correspond to median and SD. (** $P \leq 0.01$; **** $P \leq 0.0001$). **(C)** The representative images compare control untreated OVCAR-3 spheroid, OVCAR-3 spheroid treated with MSLN-CAR.CIK and OVCAR-3 spheroid treated with Triton X-100, used as positive control for maximum cytotoxicity, all referred to the 3D solid-like embedded model. mOC spheroids are labeled with propidium iodide (red) while MSLN-CAR.CIK with PKH67 (green). Gray images correspond to brightfield images. Scale bar: 200 µm **(left)**. Cytotoxic activity in plot corresponding to single mOC spheroids either untreated, co-cultured with MSLN-CAR.CIK or NTD.CIK either embedded or on top, or treated with Triton X-100, the positive control for maximum cytotoxicity **(right)**.

Our data indicate that MSLN-CAR.CIK are able to be recruited on tumor cell aggregates in a solid-like experimental setting, with variable kinetics depending on the distance between the initial position of the effectors and that positioning of the effectors might be crucial for a successful cell-based therapy. Furthermore, MSLN-CAR.CIK are able to reach the surface of cell spheroids, to penetrate within the cell aggregate and to kill tumor cells. These *in vitro* data support the plausibility of our approach and call for further investigations in this direction.

DISCUSSION

Advanced OC patients affected by PC displays poor prognosis and limited responses to conventional treatments. An opportunity to improve PC management is represented by its own peculiar pathophysiology [102], where the administration of drugs in situ could ameliorate the effective targeting of the tumor cells as well as reduce toxicity, as already been tested for chemotherapies [160] and in ongoing or recently concluded testing for CAR-redirected cell therapies [94]. Indeed, CAR-redirected cell-based therapies are among the treatments that could mostly take advantage of it, significantly improving the access to metastatic lesions. However, to reach the most successful application it is necessary the understanding of how the engineered immune cells interact with the different peculiar tumor lesions.

Our work provides evidence of the relevant antitumor activity by MSLN-CAR.CIK within 3D experimental immunotherapy models of PC from advanced OC, shedding light on the impact of peritoneal metastasis complexity on MSLN-CAR.CIK cell-based immunotherapy.

A central aim of our research was the development of a reductionistic and reliable experimental 3D setting that recalled independently the floating-like and solid-like components of PC, to model the spatio-temporal dynamics and anti-tumor activity of MSLN-CAR.CIK therapy. Our intent was to gain insights into specific variables that could be relevant and considerable in optimizing experimental procedures of locoregional treatments with the infusion of CAR.CIK into the peritoneal cavity, as well as for transversal methodological applicability to multiple experimental settings.

In order to model the challenging floating-like environment with tumor cell aggregates floating in the ascites fluid [333], we subjected the 3D co-culture of MSLN-CAR.CIK and mOC spheroids to a fluid flow. In this regard, a relevant aspect that we integrated in our models is the fluid flow mediated transport which is a peculiarity of the floating-like setting. Only few of the current models mimicking advanced OC consider the fluid flow present in the peritoneal cavity [314] and none of those has tested the interaction with any kind of immune effectors as therapy. A fluid flow is instead substantially absent in the solid-like setting, where cell-transport is due to active cell migration through the ECM, and potentially significantly slower. Coherently, our data highlighted the positive contribution of a fluid flow on the kinetics of MSLN-CAR.CIK localization over targets with respect to the case where fluid flow is absent as well as on the ultimate killing function.

Such observation is also coherent with reported effects of fluid flow on increased T cell activation through mechanotransduction induced by SSs, thanks to the mechanically stimulated ion channels present on the surface of the T cells that trigger lymphocytes activation [334,335]. For example, the ion channel Piezo1 is activated by biophysical stimulations, such as fluid SS, and it is involved in the optimization of T cell activation [336]. In this regard, Hope and colleagues correlated the increment of a fluid SS over T or CAR.T cells to an increased activation of those lymphocytes, with higher release of IL-2 and IFN-γ [334].
In the clinical setting of an intraperitoneal infusion, these findings support the idea that MSLN-CAR.CIK might benefit from the liquid compartment dynamics of PC, further speculating an additional contribution from SS that could enhance the functional activation of the immune effectors.

Extending the focus to the interactions with solid components, we observed how MSLN-CAR.CIK were able to move and localize on tumor targets within the ECM, even starting the penetration from the liquid phase.
Overall, the recruitment kinetics for CAR.CIK was slower if compared to the pure liquid condition but however effective, with elapsed time of recruitment dependent on the distance of targets from the interface. Therefore, the experimental results agreed with our initial back of the envelope estimation on the typical timescales for immune effectors-tumor contact, which predicted a several orders of magnitude faster recruitment in a liquid environment, where movement was forced by external fluid flow, than in solid environment, where the interaction is consequent to an active cell migration through the matrix.

We reasoned that the migration of CAR.CIK within the matrix is active and likely sustained by a chemotactic gradient which drives and orient or bias MSLN-CAR.CIK migration over the tumor target, with an additional reported long-range homotypic signaling and positive feedback loops reinforcing the action of immune effectors. Indeed, various analysis including that of Niño J.L. et al. showed how the diffusion of chemokines can account for the cooperative (CAR.)T cell accumulation on tumors and killing, upon engaging of cognate targets which accelerates the recruitment of distant T cells through long-range homotypic signaling and positive intrapopulation feedback loops, whereas in absence of cognate tumor cells (CAR.)T cells exhibited no chemotaxis, but only chemokinesis [255,337,338]. Differently, in a liquid environment and in presence of a flow, MSLN-CAR.CIK localization over the mOC targets originates from passive transport due to the fluid flow and adhesion to the target may be sustained by the higher affinity of the scFv of the MSLN-CAR respect to the less “affine” but more multispecific binding brought by the NKG2D receptor [339,340].

Furthermore, in a fluid forced flow, concentration gradients might be destroyed partially or completely by flow mixing, thereby reducing or eliminating the role of spatially oriented diffusible cues. Such differences between the two conditions determine the diversity in the involved timescales which nonetheless allow MSLN-CAR.CIK to get in contact with and attack the different types of tumor lesions in both experimental settings.
A possible consequence could implicate a time delay in the destruction of the two types of lesions in mOC patients, with the floating ones being likely eliminated first.

It is worth noting how tumor homing, migration and invasion of the ECM are crucial phenotypes for CAR-based cell therapies to be effective and successful against solid tumors. In our model, MSLN-CAR.CIK managed to penetrate the hydrogel and target spheroids over a depth of at least 1.5 mm. The capacity of MSLN-CAR.CIK to infiltrate and destroy 3D mOC targets was clearly demonstrated in our model. In particular, our data indicate that infiltration is not only happening on the external surface of tumor spheroids but also deeper inside, endowing MSLN-CAR.CIK with an even higher killing potential due to geometric aspects. Such observations might also call for deeper investigations on the contribution of cooperative behaviors that add on the individual activity MSLN-CAR.CIK, similarly to what is assessed with T cells [338]. It may be worthy in the future to address immune effectors activity with a greater depth, a higher frequency of time-lapse, and try to detect and correlate simultaneously the mechanisms of recruitment, infiltration and killing at a time-resolved level, rather than at the endpoint.

It is conceivable that MSLN-CAR.CIK-mediated anti-tumor activity involves different degrees of interactions and strategies of killing, in the liquid compartment compared to the solid compartment. Taking the analogy between hematological tumors and solid tumors as a reference, it has been highlighted how CAR.T cells targeting of liquid tumors involves brief interactions, where CAR.T cells are quickly detached from the initial targeted tumor cell to move on to the next cell [341]. Differently, for solid tumors the serial killing exerted by T cells depends on a stable attachment to the tumor target, with a so-called “super engager” behavior exerted by CAR.T cells [278].

Our data support efforts and strategies to minimize the target-to-tumor distance thereby enhancing the chance of interactions between immune effectors and targets, like in the case of intraperitoneal infusions, object of investigation in several preclinical and clinical trials [49,202,203,205,211,213]. A second point of translational relevance suggested by our data is that the presence of a liquid component does not compromise the ability of the immune effectors to

target inner, matrix embedded targets, supporting the notion that the coexistence of both tumor compartments can be tackled by the same therapeutic approach.

Here, we propose MSLN-CAR-redirected CIK lymphocytes as functional immune effectors. The underlying rationale is to explore a possible integrative or alternative option to conventional CAR.T, in consideration of the current hurdles in their application to solid tumors [342]. CIK are usually considered mature and infused from the 3rd week of their *ex vivo* expansion. At that point their phenotype is prevalently CD3+CD8+, with negligent component of NK (CD3- CD56+) elements. The effector memory and terminally differentiated late effector populations are the more represented among the CD3+CD56+ fraction, which bears the higher killing ability [343,344]. CIK remain indeed T lymphocytes but endowed with NK-like intrinsic tumor cell killing potential, HLA-independent and NKG2D mediated, that couples with the CAR-specific activity, ultimately amplifying the antitumor effects of MSLN-CAR.CIK and potentially counteracting escape mechanisms based on heterogeneous expression of CAR targets or tumor clonal selection [77,82]. Furthermore, the activation of MSLN-CAR.CIK by target engagement may prompt a favorable bystander effect against tumor cells with lower or negative MSLN expression, similarly to what reported for T cells [345,346]. However, considering their late differentiated phenotype, it may be crucial to verify whether CAR.CIK acquire an exhaustive phenotype upon prolonged exposure to target.

Within such a framework, our data support and validate MSLN as a suitable tumor target antigen for CAR-therapies against advanced OC, in line with previous evidence reported with CAR.T [243,347]. In fact, we found MSLN mRNA expression across different cancerous cell lines of advanced OC in CCLE database [332] and we confirmed by flow cytometry MSLN protein expression on the same panel. The observed intense antitumor activity, maintained even at unfavorable E:T ratios, is encouraging and relevant and more realistic in the hypothesis of clinical perspective. Moreover, we highlighted a correlation between MSLN membrane protein expression level and MSLN-CAR.CIK anti-tumor activity, which are consistent with data correlating the need of a given tumor target antigen density and the triggering of the CAR activation [348]. Moreover, limited anti-tumor activity was exerted on targets not or lowly expressing MSLN, corroborating previous results reporting lower rates of non-specific toxicity on low-level expression of MSLN in normal tissues, further supporting the glycoprotein as an attractive target for CAR-cell therapy [217].

Furthermore, the experimental model of recruitment kinetics and 3D interactions described in our work can in principle apply to other cell therapies employing different immune effectors (for example T or NK cells), as well as to other solid cancers, such as mesothelioma,

pancreatic or colorectal cancers, where cell immunotherapy approaches with locoregional/intracavitary infusions are being investigated [45,202,349,350].

Overall, our work provides an integrated experimental platform, capable of exploring and monitoring the functionality of CAR.CIK against 3D tumor targets, taking into account elements of both the liquid and solid components of PC. The model allows to expose, consider and longitudinally measure independent variables, striving for a cell-resolved level of analysis, addressing current limitations of standard cell-based immunological assays and murine models. Our findings could elucidate how antitumor immune effectors may behave or be affected in their multiple functions in a mixed complex environment such as PC, therefore supporting further developments and improvements for clinical studies exploring intraperitoneal cellular immunotherapy with CAR.CIK or CAR.T cells, being aware of the different timescales of tumor elimination that may be present.

FUTURE PERSPECTIVES

The multifaceted complexity of advanced OC microenvironment includes a plethora of important parameters that are crucial to investigate at deeper levels in order to understand how the efficacy of an immune cell therapy can be influenced and therefore better optimized. For this reason, future work shall address additional points that may potentially improve the level of resemblance of our 3D models to the real PC pathophysiology and test how CAR.CIK therapies may be positively or negatively affected by.

The starting point will include the generation of a unique 3D model in which both the floating-like environment in presence of a fluid flow as well as the solid-like environment will be challenged concurrently, thus recapitulating the circumstance when MSLN-CAR.CIK are delivered peritoneally. Such an experimental setting would recall the accumulating ascites and the need to target lesions localized on the peritoneum. This set up will help assessing whether MSLN-CAR.CIK maintain their capacity to penetrate from a liquid to an ECM and target effectively the 3D tumoral structure embedded in or laid on top.

Future research will also include the addition over the ECM of layers of epithelial cells derived from the mesothelium, in the attempt to better recall the composition of the peritoneum [100] and explore the ability of MSLN-CAR.CIK to reach and target lesions infiltrated at even deeper levels. This could be done by exploiting the normal epithelial cell line Met-5A (ATCC [351]), established from the mesothelium of non-cancerous individuals isolated from the pleural fluids. The mesothelial layer is anticipated to be expressing the target antigen MSLN although at lower levels and would be a perfect obstacle to assess how MSLN-CAR.CIK may act in presence of both non-tumoral and tumoral target expressing various levels of MSLN.

Mechanistically, to characterize deeper how MSLN-CAR.CIK may be recruited on the 3D tumor target, it will be necessary to implement a live imaging approach able to track individually the immune effectors with higher resolution in space and time, as already mentioned above.

In a translational perspective, it is necessary to acknowledge that our findings were generated with tumor spheroids derived from commercial cancer cell lines. While cell lines allow for a very robust and reliable experimental model, it will be necessary to verify the therapy performance against malignant ascites samples of advanced-stage OC patients, by performing dedicated experiments co-culturing MSLN-CAR.CIK with the 3D heterogeneous MCAs isolated from ascites. An important feature that our biological model lacks is indeed the

heterogeneous composition reported in ascites, which goes beyond the metastatic OC cells [352].

Along the same line, the acellular composition of the malignant ascites could impair MSLN-CAR.CIK functionality, i.e. by favoring the upregulation of exhaustive markers or persistence and how we could overcome the potential obstacles. Thus, it would be interesting to test the functional changes of MSLN-CAR.CIK upon exposure to malignant ascites supernatant and characterize the different molecular components of the sample secretome. It has been already reported how the activity of NK and T cells are impaired by malignant ascites, probably due to the high sodium content as well as a low content of chloride and potassium [353]. Nevertheless, the CAR arming of a population of cytokine/induced memory-like NK cells has been shown to reduce the dysfunction led by patient-derived ascites [354]. Therefore, a deeper understanding of how the TME of PC may influence the functional behavior of CAR-cell therapies in the peritoneal cavity, in particular of CAR-redirected CIK, will help rationalizing the design of effective immunotherapeutic approaches for advanced or recurrent OC patients. A last series of improvements concerns the possibility to investigate combinatorial approaches with PARP inhibitors or ICIs that may improve patients' outcome. Along this line, these investigations could also help to identify the best way to armor MSLN-CAR.CIK with cytokine signal functional to enhance their antitumor capacity in a complex environment, thus turning a second-generation CAR into a fourth-generation [355].

To further sustain the spatio-temporal dynamic evaluations inspected in our 3D models, we are aware of the relevance of trying to recall events also in preclinical *in vivo* models of peritoneally disseminated OC, despite acknowledging the difference between human and mouse peritoneum, the latter characterized by a smaller omentum [356-358]. Different groups have already tested and proved the greater efficacy of delivering locoregionally a CAR-redirected immune cell therapy in orthotopic xenograft or syngeneic mouse models of disseminated OC forming ascites [347,359,360].

The goal of an *in vivo* evaluation consistent with our project would be to assess the different timescale required for the proposed locoregional CAR-cell therapy to promote the reduction of ascites formation/accumulation *vs* metastatic tumor nodes localized along the peritoneum, likely sacrificing treated mice developing ascites at progressive time points. However, differently from our established *in vitro* models, it would be more complex to perform real-time measurements and tracking of immune-cellular behaviors.

Altogether, all these additional evaluations will be functional to support the reliability of MSLN-CAR.CIK therapy in targeting PC from advanced OC.

BIBLIOGRAPHY

1 Chen, Daniel S. & Mellman, I. Oncology Meets Immunology: The Cancer-Immunity Cycle. *Immunity* **39**, 1-10 (2013). https://doi.org/https://doi.org/10.1016/j.immuni.2013.07.012

2 Hanahan, D. Hallmarks of Cancer: New Dimensions. *Cancer Discovery* **12**, 31-46 (2022). https://doi.org/10.1158/2159-8290.Cd-21-1059

3 Fenis, A., Demaria, O., Gauthier, L., Vivier, E. & Narni-Mancinelli, E. New immune cell engagers for cancer immunotherapy. *Nature Reviews Immunology* (2024). https://doi.org/10.1038/s41577-023-00982-7

4 Waldman, A. D., Fritz, J. M. & Lenardo, M. J. A guide to cancer immunotherapy: from T cell basic science to clinical practice. *Nature Reviews Immunology* **20**, 651-668 (2020). https://doi.org/10.1038/s41577-020-0306-5

5 Ma, W. *et al.* Increasing cure rates of solid tumors by immune checkpoint inhibitors. *Experimental Hematology & Oncology* **12**, 10 (2023). https://doi.org/10.1186/s40164-023-00372-8

6 Tang, L., Huang, Z., Mei, H. & Hu, Y. Immunotherapy in hematologic malignancies: achievements, challenges and future prospects. *Signal Transduction and Targeted Therapy* **8**, 306 (2023). https://doi.org/10.1038/s41392-023-01521-5

7 Havel, J. J., Chowell, D. & Chan, T. A. The evolving landscape of biomarkers for checkpoint inhibitor immunotherapy. *Nature Reviews Cancer* **19**, 133-150 (2019). https://doi.org/10.1038/s41568-019-0116-x

8 Brunet, J.-F. *et al.* A new member of the immunoglobulin superfamily—CTLA-4. *Nature* **328**, 267-270 (1987). https://doi.org/10.1038/328267a0

9 Linsley, P. S. *et al.* CTLA-4 is a second receptor for the B cell activation antigen B7. *Journal of Experimental Medicine* **174**, 561-569 (1991). https://doi.org/10.1084/jem.174.3.561

10 Walunas, T. L. *et al.* CTLA-4 can function as a negative regulator of T cell activation. *Immunity* **1**, 405-413 (1994). https://doi.org/10.1016/1074-7613(94)90071-X

11 Hodi, F. S. *et al.* Improved Survival with Ipilimumab in Patients with Metastatic Melanoma. *New England Journal of Medicine* **363**, 711-723 (2010). https://doi.org/10.1056/NEJMoa1003466

12 Korman, A. J., Garrett-Thomson, S. C. & Lonberg, N. The foundations of immune checkpoint blockade and the ipilimumab approval decennial. *Nature Reviews Drug Discovery* **21**, 509-528 (2022). https://doi.org/10.1038/s41573-021-00345-8

13 Patel, T. H. *et al.* FDA Approval Summary: Tremelimumab in Combination with Durvalumab for the Treatment of Patients with Unresectable Hepatocellular Carcinoma. *Clinical Cancer Research* **30**, 269-273 (2024). https://doi.org/10.1158/1078-0432.Ccr-23-2124

14 Francisco, L. M., Sage, P. T. & Sharpe, A. H. The PD-1 pathway in tolerance and autoimmunity. *Immunological Reviews* **236**, 219-242 (2010). https://doi.org/https://doi.org/10.1111/j.1600-065X.2010.00923.x

15 McLane, L. M., Abdel-Hakeem, M. S. & Wherry, E. J. CD8 T Cell Exhaustion During Chronic Viral Infection and Cancer. *Annual Review of Immunology* **37**, 457-495 (2015). https://doi.org/10.1146/annurev-immunol-041015-055318

16 Rosenberg, J. E. *et al.* Atezolizumab in patients with locally advanced and metastatic urothelial carcinoma who have progressed following treatment with platinum-based chemotherapy: a single-arm, multicentre, phase 2 trial. *The Lancet* **387**, 1909-1920 (2016). https://doi.org/10.1016/S0140-6736(16)00561-4

17 Mathieu, L. N. *et al.* FDA Approval Summary: Atezolizumab as Adjuvant Treatment following Surgical Resection and Platinum-Based Chemotherapy for Stage II to IIIA NSCLC. *Clinical Cancer Research* **29**, 2973-2978 (2023). https://doi.org/10.1158/1078-0432.Ccr-22-3699

18 Suzman, D. L. *et al.* FDA Approval Summary: Atezolizumab or Pembrolizumab for the Treatment of Patients with Advanced Urothelial Carcinoma Ineligible for Cisplatin-Containing Chemotherapy. *The Oncologist* **24**, 563-569 (2018). https://doi.org/10.1634/theoncologist.2018-0084
19 Jenkins, R. W., Barbie, D. A. & Flaherty, K. T. Mechanisms of resistance to immune checkpoint inhibitors. *British Journal of Cancer* **118**, 9-16 (2018). https://doi.org/10.1038/bjc.2017.434
20 Finn, O. J. The dawn of vaccines for cancer prevention. *Nature Reviews Immunology* **18**, 183-194 (2018). https://doi.org/10.1038/nri.2017.140
21 Guo, C. *et al.* in *Advances in Cancer Research* Vol. 119 (eds Kenneth D. Tew & Paul B. Fisher) 421-475 (Academic Press, 2013).
22 Castle, J. C. *et al.* Exploiting the Mutanome for Tumor Vaccination. *Cancer Research* **72**, 1081-1091 (2012). https://doi.org/10.1158/0008-5472.Can-11-3722
23 Rohaan, M. W., Berg, J. H. v. d., Kvistborg, P. & Haanen, J. B. A. G. Adoptive transfer of tumor-infiltrating lymphocytes in melanoma: a viable treatment option. *Journal for ImmunoTherapy of Cancer* **6**, 102 (2018). https://doi.org/10.1186/s40425-018-0391-1
24 Urbansky, A., Lenshof, A., Dykes, J., Laurell, T. & Scheding, S. -Separation of Lymphocyte Populations from Peripheral Blood Progenitor Cell Products Using Affinity Bead Acoustophoresis. *Blood* **124**, 315-315 (2014). https://doi.org/10.1182/blood.V124.21.315.315
25 Tsimberidou, A.-M. *et al.* T-cell receptor-based therapy: an innovative therapeutic approach for solid tumors. *Journal of Hematology & Oncology* **14**, 102 (2021). https://doi.org/10.1186/s13045-021-01115-0
26 Sadelain, M., Brentjens, R. & Rivière, I. The Basic Principles of Chimeric Antigen Receptor Design. *Cancer Discovery* **3**, 388-398 (2013). https://doi.org/10.1158/2159-8290.Cd-12-0548
27 Mitra, A. *et al.* From bench to bedside: the history and progress of CAR T cell therapy. *Frontiers in Immunology* **14** (2023). https://doi.org/10.3389/fimmu.2023.1188049
28 Maalej, K. M. *et al.* CAR-cell therapy in the era of solid tumor treatment: current challenges and emerging therapeutic advances. *Molecular Cancer* **22**, 20 (2023). https://doi.org/10.1186/s12943-023-01723-z
29 Dougé, A., El Ghazzi, N., Lemal, R. & Rouzaire, P. Adoptive T Cell Therapy in Solid Tumors: State-of-the Art, Current Challenges, and Upcoming Improvements. *Molecular Cancer Therapeutics* **23**, 272-284 (2024). https://doi.org/10.1158/1535-7163.Mct-23-0310
30 Sarnaik, A. A. *et al.* Lifileucel, a Tumor-Infiltrating Lymphocyte Therapy, in Metastatic Melanoma. *Journal of Clinical Oncology* **39**, 2656-2666 (2021). https://doi.org/10.1200/JCO.21.00612
31 Julve, M., Lythgoe, M. P., Larkin, J. & Furness, A. J. S. Lifileucel: the first cellular therapy approved for solid tumours. *Trends in Cancer* **10**, 475-477 (2024). https://doi.org/10.1016/j.trecan.2024.04.003
32 Adaptimmune. *Adaptimmune receives U.S. FDA accelerated approval of TECELRA® (afamitresgene autoleucel), the first approved engineered cell therapy for a solid tumor.*, <https://tinyurl.com/tch2emrw> (2024).
33 D'Angelo, S. P. *et al.* Afamitresgene autoleucel for advanced synovial sarcoma and myxoid round cell liposarcoma (SPEARHEAD-1): an international, open-label, phase 2 trial. *The Lancet* **403**, 1460-1471 (2024). https://doi.org/10.1016/S0140-6736(24)00319-2
34 Mortezaee, K. Immune escape: A critical hallmark in solid tumors. *Life Sciences* **258**, 118110 (2020). https://doi.org/https://doi.org/10.1016/j.lfs.2020.118110
35 Martinez, M. & Moon, E. K. CAR T Cells for Solid Tumors: New Strategies for Finding, Infiltrating, and Surviving in the Tumor Microenvironment. *Frontiers in Immunology* **10** (2019). https://doi.org/10.3389/fimmu.2019.00128

36 Hiltensperger, M. & Krackhardt, A. M. Current and future concepts for the generation and application of genetically engineered CAR-T and TCR-T cells. *Frontiers in Immunology* **14** (2023). https://doi.org/10.3389/fimmu.2023.1121030
37 Rafiq, S., Hackett, C. S. & Brentjens, R. J. Engineering strategies to overcome the current roadblocks in CAR T cell therapy. *Nature Reviews Clinical Oncology* **17**, 147-167 (2020). https://doi.org/10.1038/s41571-019-0297-y
38 Imai, C. *et al.* Chimeric receptors with 4-1BB signaling capacity provoke potent cytotoxicity against acute lymphoblastic leukemia. *Leukemia* **18**, 676-684 (2004). https://doi.org/10.1038/sj.leu.2403302
39 Karlsson, H. *et al.* Evaluation of Intracellular Signaling Downstream Chimeric Antigen Receptors. *PLOS ONE* **10**, e0144787 (2015). https://doi.org/10.1371/journal.pone.0144787
40 Chmielewski, M. & Abken, H. TRUCKs: the fourth generation of CARs. *Expert Opinion on Biological Therapy* **15**, 1145-1154 (2015). https://doi.org/10.1517/14712598.2015.1046430
41 Kagoya, Y. *et al.* A novel chimeric antigen receptor containing a JAK–STAT signaling domain mediates superior antitumor effects. *Nature Medicine* **24**, 352-359 (2018). https://doi.org/10.1038/nm.4478
42 Vargas, J. E. *et al.* Retroviral vectors and transposons for stable gene therapy: advances, current challenges and perspectives. *Journal of Translational Medicine* **14**, 288 (2016). https://doi.org/10.1186/s12967-016-1047-x
43 Monjezi, R. *et al.* Enhanced CAR T-cell engineering using non-viral Sleeping Beauty transposition from minicircle vectors. *Leukemia* **31**, 186-194 (2017). https://doi.org/10.1038/leu.2016.180
44 Hu, Z. *et al.* LunX-CAR T Cells as a Targeted Therapy for Non-Small Cell Lung Cancer. *Molecular Therapy - Oncolytics* **17**, 361-370 (2020). https://doi.org/10.1016/j.omto.2020.04.008
45 Adusumilli, P. S. *et al.* A Phase I Trial of Regional Mesothelin-Targeted CAR T-cell Therapy in Patients with Malignant Pleural Disease, in Combination with the Anti–PD-1 Agent Pembrolizumab. *Cancer Discovery* **11**, 2748-2763 (2021). https://doi.org/10.1158/2159-8290.CD-21-0407
46 Ahmed, N. *et al.* HER2-Specific Chimeric Antigen Receptor–Modified Virus-Specific T Cells for Progressive Glioblastoma: A Phase 1 Dose-Escalation Trial. *JAMA Oncology* **3**, 1094-1101 (2017). https://doi.org/10.1001/jamaoncol.2017.0184
47 Safarzadeh Kozani, P. *et al.* Recent Advances in Solid Tumor CAR-T Cell Therapy: Driving Tumor Cells From Hero to Zero? *Frontiers in Immunology* **13** (2022). https://doi.org/10.3389/fimmu.2022.795164
48 Dagar, G. *et al.* Harnessing the potential of CAR-T cell therapy: progress, challenges, and future directions in hematological and solid tumor treatments. *Journal of Translational Medicine* **21**, 449 (2023). https://doi.org/10.1186/s12967-023-04292-3
49 Pennsylvania, U. o., Health, N. I. o. & Tmunity Therapeutics, a. w. o. s. o. K. P. (https://classic.clinicaltrials.gov/show/NCT03054298, 2017).
50 Sterner, R. C. & Sterner, R. M. CAR-T cell therapy: current limitations and potential strategies. *Blood Cancer Journal* **11**, 69 (2021). https://doi.org/10.1038/s41408-021-00459-7
51 Mao, R., Kong, W. & He, Y. The affinity of antigen-binding domain on the antitumor efficacy of CAR T cells: Moderate is better. *Frontiers in Immunology* **13** (2022).
52 Liu, X. *et al.* Affinity-Tuned ErbB2 or EGFR Chimeric Antigen Receptor T Cells Exhibit an Increased Therapeutic Index against Tumors in Mice. *Cancer Research* **75**, 3596-3607 (2015). https://doi.org/10.1158/0008-5472.CAN-15-0159
53 Lin, L. *et al.* Preclinical evaluation of CD8+ anti-BCMA mRNA CAR T cells for treatment of multiple myeloma. *Leukemia* **35**, 752-763 (2021). https://doi.org/10.1038/s41375-020-0951-5

54 Safarzadeh Kozani, P., Safarzadeh Kozani, P., Rahbarizadeh, F. & Khoshtinat Nikkhoi, S. Strategies for Dodging the Obstacles in CAR T Cell Therapy. *Frontiers in Oncology* **11** (2021).
55 Stock, S., Schmitt, M. & Sellner, L. Optimizing Manufacturing Protocols of Chimeric Antigen Receptor T Cells for Improved Anticancer Immunotherapy. *International Journal of Molecular Sciences* **20** (2019).
56 Jaggers, J. L. *et al.* Characterizing inclusion and exclusion criteria in clinical trials for chimeric antigen receptor (CAR) T-cell therapy among adults with hematologic malignancies. *Journal of Geriatric Oncology* **12**, 235-238 (2021). https://doi.org/https://doi.org/10.1016/j.jgo.2020.08.004
57 Morris, E. C., Neelapu, S. S., Giavridis, T. & Sadelain, M. Cytokine release syndrome and associated neurotoxicity in cancer immunotherapy. *Nature Reviews Immunology* **22**, 85-96 (2022). https://doi.org/10.1038/s41577-021-00547-6
58 Depil, S., Duchateau, P., Grupp, S. A., Mufti, G. & Poirot, L. 'Off-the-shelf' allogeneic CAR T cells: development and challenges. *Nature Reviews Drug Discovery* **19**, 185-199 (2020). https://doi.org/10.1038/s41573-019-0051-2
59 Liu, E. *et al.* Use of CAR-Transduced Natural Killer Cells in CD19-Positive Lymphoid Tumors. *New England Journal of Medicine* **382**, 545-553 (2020). https://doi.org/10.1056/NEJMoa1910607
60 Albinger, N., Hartmann, J. & Ullrich, E. Current status and perspective of CAR-T and CAR-NK cell therapy trials in Germany. *Gene Therapy* **28**, 513-527 (2021). https://doi.org/10.1038/s41434-021-00246-w
61 Kim, R. *et al.* 951 A phase 1 first in human study of adenovirally transduced anti-HER2 CAR macrophages in subjects with HER2 overexpressing solid tumors: preliminary safety, pharmacokinetics, and TME reprogramming data. *Journal for ImmunoTherapy of Cancer* **9**, A1000 (2021). https://doi.org/10.1136/jitc-2021-SITC2021.951
62 Pan, K. *et al.* CAR race to cancer immunotherapy: from CAR T, CAR NK to CAR macrophage therapy. *Journal of Experimental & Clinical Cancer Research* **41**, 119 (2022). https://doi.org/10.1186/s13046-022-02327-z
63 Sangiolo, D. Cytokine Induced Killer Cells as Promising Immunotherapy for Solid Tumors. *Journal of Cancer* **2**, 363-368 (2011). https://doi.org/10.7150/jca.2.363
64 Schmidt-Wolf, I. G., Negrin, R. S., Kiem, H. P., Blume, K. G. & Weissman, I. L. Use of a SCID mouse/human lymphoma model to evaluate cytokine-induced killer cells with potent antitumor cell activity. *Journal of Experimental Medicine* **174**, 139-149 (1991). https://doi.org/10.1084/jem.174.1.139
65 Gao, X. *et al.* Cytokine-Induced Killer Cells As Pharmacological Tools for Cancer Immunotherapy. *Frontiers in Immunology* **8** (2017). https://doi.org/10.3389/fimmu.2017.00774
66 Schmidt-Wolf, I. G. H. *et al.* Propagation of large numbers of T cells with natural killer cell markers. *British Journal of Haematology* **87**, 453-458 (1994). https://doi.org/https://doi.org/10.1111/j.1365-2141.1994.tb08297.x
67 Lu, P. H. & Negrin, R. S. A novel population of expanded human CD3+CD56+ cells derived from T cells with potent in vivo antitumor activity in mice with severe combined immunodeficiency. *The Journal of Immunology* **153**, 1687-1696 (1994). https://doi.org/10.4049/jimmunol.153.4.1687
68 Cappuzzello, E., Sommaggio, R., Zanovello, P. & Rosato, A. Cytokines for the induction of antitumor effectors: The paradigm of Cytokine-Induced Killer (CIK) cells. *Cytokine & Growth Factor Reviews* **36**, 99-105 (2017). https://doi.org/https://doi.org/10.1016/j.cytogfr.2017.06.003
69 Schmidt-Wolf, I. G. *et al.* Phenotypic characterization and identification of effector cells involved in tumor cell recognition of cytokine-induced killer cells. *Exp Hematol* **21**, 1673-1679 (1993).
70 Mehta, B. A., Schmidt-Wolf, I. G. H., Weissman, I. L. & Negrin, R. S. Two Pathways of Exocytosis of Cytoplasmic Granule Contents and Target Cell Killing by Cytokine-

Induced CD3+CD56+ Killer Cells. *Blood* **86**, 3493-3499 (1995). https://doi.org/https://doi.org/10.1182/blood.V86.9.3493.bloodjournal8693493

71 Cappuzzello, E., Tosi, A., Zanovello, P., Sommaggio, R. & Rosato, A. Retargeting cytokine-induced killer cell activity by CD16 engagement with clinical-grade antibodies. *OncoImmunology* **5**, e1199311 (2016). https://doi.org/10.1080/2162402X.2016.1199311

72 Sommaggio, R. *et al.* Adoptive cell therapy of triple negative breast cancer with redirected cytokine-induced killer cells. *OncoImmunology* **9**, 1777046 (2020). https://doi.org/10.1080/2162402X.2020.1777046

73 Dalla Pietà, A. *et al.* Innovative therapeutic strategy for B-cell malignancies that combines obinutuzumab and cytokine-induced killer cells. *J Immunother Cancer* **9** (2021). https://doi.org/10.1136/jitc-2021-002475

74 Schmidt-Wolf, I. G. H. *et al.* Phase I clinical study applying autologous immunological effector cells transfected with the interleukin-2 gene in patients with metastatic renal cancer, colorectal cancer and lymphoma. *British Journal of Cancer* **81**, 1009-1016 (1999). https://doi.org/10.1038/sj.bjc.6690800

75 Zhang, Y. & Schmidt-Wolf, I. G. H. Ten-year update of the international registry on cytokine-induced killer cells in cancer immunotherapy. *Journal of Cellular Physiology* **235**, 9291-9303 (2020). https://doi.org/https://doi.org/10.1002/jcp.29827

76 Hontscha, C., Borck, Y., Zhou, H., Messmer, D. & Schmidt-Wolf, I. G. H. Clinical trials on CIK cells: first report of the international registry on CIK cells (IRCC). *Journal of Cancer Research and Clinical Oncology* **137**, 305-310 (2011). https://doi.org/10.1007/s00432-010-0887-7

77 Cappuzzello, E. *et al.* How can Cytokine-induced killer cells overcome CAR-T cell limits. *Frontiers in Immunology* **14** (2023). https://doi.org/10.3389/fimmu.2023.1229540

78 Albelda, S. M. Tumor Antigen Heterogeneity: The “Elephant in the Room” of Adoptive T-cell Therapy for Solid Tumors. *Cancer Immunology Research* **8**, 2-2 (2020). https://doi.org/10.1158/2326-6066.CIR-19-0801

79 Gill, S. & June, C. H. Going viral: chimeric antigen receptor T-cell therapy for hematological malignancies. *Immunological Reviews* **263**, 68-89 (2015). https://doi.org/https://doi.org/10.1111/imr.12243

80 Magnani, C. F. *et al.* Sleeping Beauty–engineered CAR T cells achieve antileukemic activity without severe toxicities. *The Journal of Clinical Investigation* **130**, 6021-6033 (2020). https://doi.org/10.1172/JCI138473

81 Merker, M. *et al.* Generation and characterization of ErbB2-CAR-engineered cytokine-induced killer cells for the treatment of high-risk soft tissue sarcoma in children. *Oncotarget; Vol 8, No 39* (2017).

82 Merker, M. *et al.* ERBB2-CAR-Engineered Cytokine-Induced Killer Cells Exhibit Both CAR-Mediated and Innate Immunity Against High-Risk Rhabdomyosarcoma. *Frontiers in Immunology* **11** (2020). https://doi.org/10.3389/fimmu.2020.581468

83 Leuci, V. *et al.* CD44v6 as innovative sarcoma target for CAR-redirected CIK cells. *OncoImmunology* **7**, e1423167 (2018). https://doi.org/10.1080/2162402X.2017.1423167

84 Leuci, V. *et al.* CSPG4-Specific CAR.CIK Lymphocytes as a Novel Therapy for the Treatment of Multiple Soft-Tissue Sarcoma Histotypes. *Clinical Cancer Research* **26**, 6321-6334 (2020). https://doi.org/10.1158/1078-0432.CCR-20-0357

85 Giraudo, L. *et al.* CSPG4 CAR-redirected Cytokine Induced Killer lymphocytes (CIK) as effective cellular immunotherapy for HLA class I defective melanoma. *Journal of Experimental & Clinical Cancer Research* **42**, 310 (2023). https://doi.org/10.1186/s13046-023-02884-x

86 Magnani, C. F. *et al.* Preclinical Efficacy and Safety of CD19CAR Cytokine-Induced Killer Cells Transfected with Sleeping Beauty Transposon for the Treatment of Acute Lymphoblastic Leukemia. *Human Gene Therapy* **29**, 602-613 (2018). https://doi.org/10.1089/hum.2017.207

87 Perriello, V. M. *et al.* IL-3-zetakine combined with a CD33 costimulatory receptor as a dual CAR approach for safer and selective targeting of AML. *Blood Advances* **7**, 2855-2871 (2023). https://doi.org/10.1182/bloodadvances.2022008762
88 Ren, X. *et al.* Modification of cytokine-induced killer cells with chimeric antigen receptors (CARs) enhances antitumor immunity to epidermal growth factor receptor (EGFR)-positive malignancies. *Cancer Immunology, Immunotherapy* **64**, 1517-1529 (2015). https://doi.org/10.1007/s00262-015-1757-6
89 Zuo, S. *et al.* Modification of cytokine-induced killer cells with folate receptor alpha (FRα)-specific chimeric antigen receptors enhances their antitumor immunity toward FRα-positive ovarian cancers. *Molecular Immunology* **85**, 293-304 (2017). https://doi.org/https://doi.org/10.1016/j.molimm.2017.03.017
90 Onlus, F. M. T. M. D. M. (https://classic.clinicaltrials.gov/show/NCT03389035, 2017).
91 Andrea Biondi, M. & Onlus, F. M. T. M. D. M. (https://classic.clinicaltrials.gov/show/NCT05869279, 2023).
92 Andrea Biondi, M., Alessandro Rambaldi, M. & Onlus, F. M. T. M. D. M. (https://clinicaltrials.gov/study/NCT05252403, 2021).
93 Cherkassky, L., Hou, Z., Amador-Molina, A. & Adusumilli, P. S. Regional CAR T cell therapy: An ignition key for systemic immunity in solid tumors. *Cancer Cell* **40**, 569-574 (2022). https://doi.org/10.1016/j.ccell.2022.04.006
94 Sagnella, S. M. *et al.* Locoregional delivery of CAR-T cells in the clinic. *Pharmacological Research* **182**, 106329 (2022). https://doi.org/https://doi.org/10.1016/j.phrs.2022.106329
95 Vitanza, N. A. *et al.* Locoregional infusion of HER2-specific CAR T cells in children and young adults with recurrent or refractory CNS tumors: an interim analysis. *Nature Medicine* (2021). https://doi.org/10.1038/s41591-021-01404-8
96 Del Baldo, G. *et al.* The peculiar challenge of bringing CAR-T cells into the brain: Perspectives in the clinical application to the treatment of pediatric central nervous system tumors. *Frontiers in Immunology* **14** (2023). https://doi.org/10.3389/fimmu.2023.1142597
97 Donovan, L. K. *et al.* Locoregional delivery of CAR T cells to the cerebrospinal fluid for treatment of metastatic medulloblastoma and ependymoma. *Nature Medicine* **26**, 720-731 (2020). https://doi.org/10.1038/s41591-020-0827-2
98 Katz, S. C. *et al.* HITM-SIR: phase Ib trial of intraarterial chimeric antigen receptor T-cell therapy and selective internal radiation therapy for CEA+ liver metastases. *Cancer Gene Therapy* **27**, 341-355 (2020). https://doi.org/10.1038/s41417-019-0104-z
99 van Baal, J. O. A. M. *et al.* Development of Peritoneal Carcinomatosis in Epithelial Ovarian Cancer: A Review. *Journal of Histochemistry & Cytochemistry* **66**, 67-83 (2017). https://doi.org/10.1369/0022155417742897
100 van Baal, J. O. A. M. *et al.* The histophysiology and pathophysiology of the peritoneum. *Tissue and Cell* **49**, 95-105 (2017). https://doi.org/https://doi.org/10.1016/j.tice.2016.11.004
101 Thomassen, I. *et al.* Peritoneal carcinomatosis of gastric origin: A population-based study on incidence, survival and risk factors. *International Journal of Cancer* **134**, 622-628 (2014). https://doi.org/https://doi.org/10.1002/ijc.28373
102 Coccolini, F. *et al.* Peritoneal carcinomatosis. *World J Gastroenterol* **19**, 6979-6994 (2013). https://doi.org/10.3748/wjg.v19.i41.6979
103 Cortés-Guiral, D. *et al.* Primary and metastatic peritoneal surface malignancies. *Nature Reviews Disease Primers* **7**, 91 (2021). https://doi.org/10.1038/s41572-021-00326-6
104 Slatnik, C. L. P. & Duff, E. Ovarian cancer: Ensuring early diagnosis. *The Nurse Practitioner* **40** (2015).
105 Siegel, R. L., Miller, K. D. & Jemal, A. Cancer statistics, 2020. *CA: A Cancer Journal for Clinicians* **70**, 7-30 (2020). https://doi.org/https://doi.org/10.3322/caac.21590
106 Bethesda, M. N. C. I. *Ovarian Epithelial, Fallopian Tube, and Primary Peritoneal Cancer Treatment (PDQ®)–Health Professional Version*, <https://www.cancer.gov/types/ovarian/hp/ovarian-epithelial-treatment-pdq> (2024).

107 Jayson, G. C., Kohn, E. C., Kitchener, H. C. & Ledermann, J. A. Ovarian cancer. *The Lancet* **384**, 1376-1388 (2014). https://doi.org/https://doi.org/10.1016/S0140-6736(13)62146-7

108 Veneziani, A. C. *et al.* Heterogeneity and treatment landscape of ovarian carcinoma. *Nature Reviews Clinical Oncology* **20**, 820-842 (2023). https://doi.org/10.1038/s41571-023-00819-1

109 McCluggage, W. G. Morphological subtypes of ovarian carcinoma: a review with emphasis on new developments and pathogenesis. *Pathology* **43**, 420-432 (2011). https://doi.org/https://doi.org/10.1097/PAT.0b013e328348a6e7

110 Zhang, Y. *et al.* Current Advances in PD-1/PD-L1 Blockade in Recurrent Epithelial Ovarian Cancer. *Frontiers in Immunology* **13** (2022). https://doi.org/10.3389/fimmu.2022.901772

111 Burg, L. *et al.* Incidence and predictors of peritoneal metastases of gynecological origin: a population-based study in the Netherlands. *J Gynecol Oncol* **31** (2020).

112 Köbel, M. *et al.* Differences in tumor type in low-stage versus high-stage ovarian carcinomas. *Int J Gynecol Pathol* **29**, 203-211 (2010). https://doi.org/10.1097/PGP.0b013e3181c042b6

113 Matulonis, U. A. *et al.* Ovarian cancer. *Nature Reviews Disease Primers* **2**, 16061 (2016). https://doi.org/10.1038/nrdp.2016.61

114 Pokhriyal, R., Hariprasad, R., Kumar, L. & Hariprasad, G. Chemotherapy Resistance in Advanced Ovarian Cancer Patients. *Biomarkers in Cancer* **11**, 1179299X19860815 (2019). https://doi.org/10.1177/1179299X19860815

115 Cancer Research Institute. *How is Immunotherapy for Ovarian Cancer Changing the Outlook for Patients?*, <https://www.cancerresearch.org/cancer-types/ovarian-cancer> (n.d.).

116 Tan, D. S. P., Agarwal, R. & Kaye, S. B. Mechanisms of transcoelomic metastasis in ovarian cancer. *The Lancet Oncology* **7**, 925-934 (2006). https://doi.org/https://doi.org/10.1016/S1470-2045(06)70939-1

117 Bella, Á. *et al.* in *International Review of Cell and Molecular Biology* Vol. 371 (eds Fernando Aranda, Pedro Berraondo, & Lorenzo Galluzzi) 117-131 (Academic Press, 2022).

118 Anwar, A. & Kasi, A. *Peritoneal Cancer*. (StatPearls Publishing, Treasure Island (FL), 2023).

119 Katdare, N., Prabhu, R. & Bhatt, A. in *Management of Peritoneal Metastases-Cytoreductive Surgery, HIPEC and Beyond* (ed Aditi Bhatt) 527-559 (Springer Singapore, 2018).

120 Al Habyan, S., Kalos, C., Szymborski, J. & McCaffrey, L. Multicellular detachment generates metastatic spheroids during intra-abdominal dissemination in epithelial ovarian cancer. *Oncogene* **37**, 5127-5135 (2018). https://doi.org/10.1038/s41388-018-0317-x

121 Patel, I. S., Madan, P., Getsios, S., Bertrand, M. A. & MacCalman, C. D. Cadherin switching in ovarian cancer progression. *International Journal of Cancer* **106**, 172-177 (2003). https://doi.org/https://doi.org/10.1002/ijc.11086

122 Elloul, S. *et al.* Snail, Slug, and Smad-interacting protein 1 as novel parameters of disease aggressiveness in metastatic ovarian and breast carcinoma. *Cancer* **103**, 1631-1643 (2005). https://doi.org/https://doi.org/10.1002/cncr.20946

123 Hayashi, K. *et al.* Real-time Imaging of Tumor-Cell Shedding and Trafficking in Lymphatic Channels. *Cancer Research* **67**, 8223-8228 (2007). https://doi.org/10.1158/0008-5472.CAN-07-1237

124 Burleson, K. M. *et al.* Ovarian carcinoma ascites spheroids adhere to extracellular matrix components and mesothelial cell monolayers. *Gynecologic Oncology* **93**, 170-181 (2004). https://doi.org/10.1016/j.ygyno.2003.12.034

125 Kenny, H. A. *et al.* Mesothelial cells promote early ovarian cancer metastasis through fibronectin secretion. *The Journal of Clinical Investigation* **124**, 4614-4628 (2014). https://doi.org/10.1172/JCI74778

126 Ayantunde, A. A. & Parsons, S. L. Pattern and prognostic factors in patients with malignant ascites: a retrospective study. *Annals of Oncology* **18**, 945-949 (2007). https://doi.org/10.1093/annonc/mdl499
127 Krugmann, J. *et al.* Malignant ascites occurs most often in patients with high-grade serous papillary ovarian cancer at initial diagnosis: a retrospective analysis of 191 women treated at Bayreuth Hospital, 2006–2015. *Archives of Gynecology and Obstetrics* **299**, 515-523 (2019). https://doi.org/10.1007/s00404-018-4952-9
128 Kipps, E., Tan, D. S. P. & Kaye, S. B. Meeting the challenge of ascites in ovarian cancer: new avenues for therapy and research. *Nature Reviews Cancer* **13**, 273-282 (2013). https://doi.org/10.1038/nrc3432
129 Szender, J. B. *et al.* Impact of ascites volume on clinical outcomes in ovarian cancer: A cohort study. *Gynecologic Oncology* **146**, 491-497 (2017). https://doi.org/10.1016/j.ygyno.2017.06.008
130 Holm-Nielsen, P. PATHOGENESIS OF ASCITES IN PERITONEAL CARCINOMATOSIS1. *Acta Pathologica Microbiologica Scandinavica* **33**, 10-21 (1953). https://doi.org/https://doi.org/10.1111/j.1699-0463.1953.tb04805.x
131 Nagy, J. A., Herzberg, K. T., Dvorak, J. M. & Dvorak, H. F. Pathogenesis of malignant ascites formation: initiating events that lead to fluid accumulation. *Cancer Res* **53**, 2631-2643 (1993).
132 Miyoshi, A. *et al.* Etiology of Ascites and Pleural Effusion Associated with Ovarian Tumors: Literature Review and Case Reports of Three Ovarian Tumors Presenting with Massive Ascites, but without Peritoneal Dissemination. *Case Reports in Obstetrics and Gynecology* **2015**, 414019 (2015). https://doi.org/10.1155/2015/414019
133 Zebrowski, B. K. *et al.* Markedly Elevated Levels of Vascular Endothelial Growth Factor in Malignant Ascites. *Annals of Surgical Oncology* **6**, 373-378 (1999). https://doi.org/10.1007/s10434-999-0373-0
134 Raptopoulos, V. & Gourtsoyiannis, N. Peritoneal carcinomatosis. *European Radiology* **11**, 2195-2206 (2001). https://doi.org/10.1007/s003300100998
135 MEYERS, M. A. DISTRIBUTION OF INTRA-ABDOMINAL MALIGNANT SEEDING: DEPENDENCY ON DYNAMICS OF FLOW OF ASCITIC FLUID. *American Journal of Roentgenology* **119**, 198-206 (1973). https://doi.org/10.2214/ajr.119.1.198
136 Hyler, A. R. *et al.* Fluid shear stress impacts ovarian cancer cell viability, subcellular organization, and promotes genomic instability. *PLOS ONE* **13**, e0194170 (2018). https://doi.org/10.1371/journal.pone.0194170
137 Reynolds, O. III. An experimental investigation of the circumstances which determine whether the motion of water shall be direct or sinuous, and of the law of resistance in parallel channels. *Proceedings of the Royal Society of London* **35**, 84-99 (1883). https://doi.org/doi:10.1098/rspl.1883.0018
138 Reneman, R. S. & Hoeks, A. P. G. Wall shear stress as measured in vivo: consequences for the design of the arterial system. *Medical & Biological Engineering & Computing* **46**, 499-507 (2008). https://doi.org/10.1007/s11517-008-0330-2
139 Piché, A. Malignant peritoneal effusion acting as a tumor environment in ovarian cancer progression: Impact and significance. *World J Clin Oncol* **9**, 167-171 (2018). https://doi.org/10.5306/wjco.v9.i8.167
140 Milliken, D., Scotton, C., Raju, S., Balkwill, F. & Wilson, J. Analysis of chemokines and chemokine receptor expression in ovarian cancer ascites. *Clin Cancer Res* **8**, 1108-1114 (2002).
141 Im, H. *et al.* Label-free detection and molecular profiling of exosomes with a nano-plasmonic sensor. *Nature Biotechnology* **32**, 490-495 (2014). https://doi.org/10.1038/nbt.2886
142 Boylan, K. L. M. *et al.* The expression of Nectin-4 on the surface of ovarian cancer cells alters their ability to adhere, migrate, aggregate, and proliferate. *Oncotarget* **8** (2016).

143 Latifi, A. *et al.* Isolation and Characterization of Tumor Cells from the Ascites of Ovarian Cancer Patients: Molecular Phenotype of Chemoresistant Ovarian Tumors. *PLOS ONE* **7**, e46858 (2012). https://doi.org/10.1371/journal.pone.0046858
144 Gao, Q. *et al.* Heterotypic CAF-tumor spheroids promote early peritoneal metastasis of ovarian cancer. *Journal of Experimental Medicine* **216**, 688-703 (2019). https://doi.org/10.1084/jem.20180765
145 Matte, I. *et al.* Mesothelial cells interact with tumor cells for the formation of ovarian cancer multicellular spheroids in peritoneal effusions. *Clinical & Experimental Metastasis* **33**, 839-852 (2016). https://doi.org/10.1007/s10585-016-9821-y
146 Izar, B. *et al.* A single-cell landscape of high-grade serous ovarian cancer. *Nature Medicine* **26**, 1271-1279 (2020). https://doi.org/10.1038/s41591-020-0926-0
147 Mei, S., Chen, X., Wang, K. & Chen, Y. Tumor microenvironment in ovarian cancer peritoneal metastasis. *Cancer Cell International* **23**, 11 (2023). https://doi.org/10.1186/s12935-023-02854-5
148 Kim, S. I. & Kim, J. W. Role of surgery and hyperthermic intraperitoneal chemotherapy in ovarian cancer☆. *ESMO Open* **6**, 100149 (2021). https://doi.org/https://doi.org/10.1016/j.esmoop.2021.100149
149 Nag, S., Aggarwal, S., Rauthan, A. & Warrier, N. Maintenance therapy for newly diagnosed epithelial ovarian cancer– a review. *Journal of Ovarian Research* **15**, 88 (2022). https://doi.org/10.1186/s13048-022-01020-1
150 Verschraegen, C. F. *et al.* Docetaxel for Patients With Paclitaxel-Resistant Müllerian Carcinoma. *Journal of Clinical Oncology* **18**, 2733-2739 (2000). https://doi.org/10.1200/JCO.2000.18.14.2733
151 Le Saux, O., Ray-Coquard, I. & Labidi-Galy, S. I. Challenges for immunotherapy for the treatment of platinum resistant ovarian cancer. *Seminars in Cancer Biology* **77**, 127-143 (2021). https://doi.org/https://doi.org/10.1016/j.semcancer.2020.08.017
152 Gerestein, C. G. *et al.* The prediction of progression-free and overall survival in women with an advanced stage of epithelial ovarian carcinoma. *Bjog* **116**, 372-380 (2009). https://doi.org/10.1111/j.1471-0528.2008.02033.x
153 Ozols, R. F. *et al.* Phase III trial of carboplatin and paclitaxel compared with cisplatin and paclitaxel in patients with optimally resected stage III ovarian cancer: a Gynecologic Oncology Group study. *J Clin Oncol* **21**, 3194-3200 (2003). https://doi.org/10.1200/jco.2003.02.153
154 Lengyel, E. Ovarian cancer development and metastasis. *Am J Pathol* **177**, 1053-1064 (2010). https://doi.org/10.2353/ajpath.2010.100105
155 Caruso, G. *et al.* Poly (ADP-ribose) polymerase inhibitors (PARPi) in ovarian cancer: lessons learned and future directions. *International Journal of Gynecologic Cancer* **33**, 431-443 (2023). https://doi.org/10.1136/ijgc-2022-004149
156 Bhamidipati, D., Haro-Silerio, J. I., Yap, T. A. & Ngoi, N. PARP inhibitors: enhancing efficacy through rational combinations. *British Journal of Cancer* **129**, 904-916 (2023). https://doi.org/10.1038/s41416-023-02326-7
157 Ray-Coquard, I. *et al.* Olaparib plus Bevacizumab as First-Line Maintenance in Ovarian Cancer. *New England Journal of Medicine* **381**, 2416-2428 (2019). https://doi.org/10.1056/NEJMoa1911361
158 Katarina, C. & Borut, K. in *Ovarian Cancer* (eds Devaja Omer & Papadopoulos Andreas) Ch. 9 (IntechOpen, 2017).
159 Harding, V. *et al.* Safety, cost-effectiveness and feasibility of daycase paracentesis in the management of malignant ascites with a focus on ovarian cancer. *British Journal of Cancer* **107**, 925-930 (2012). https://doi.org/10.1038/bjc.2012.343
160 Breusa, S. *et al.* Localized chemotherapy approaches and advanced drug delivery strategies: a step forward in the treatment of peritoneal carcinomatosis from ovarian cancer. *Frontiers in Oncology* **13** (2023). https://doi.org/10.3389/fonc.2023.1125868
161 de Bree, E. & Tsiftsis, D. D. in *Advances in Peritoneal Surface Oncology* (ed Santiago González-Moreno) 39-51 (Springer Berlin Heidelberg, 2007).

162 van Stein, R. M., Aalbers, A. G. J., Sonke, G. S. & van Driel, W. J. Hyperthermic Intraperitoneal Chemotherapy for Ovarian and Colorectal Cancer: A Review. *JAMA Oncology* **7**, 1231-1238 (2021). https://doi.org/10.1001/jamaoncol.2021.0580

163 Filis, P. *et al.* Hyperthermic intraperitoneal chemotherapy (HIPEC) for the management of primary advanced and recurrent ovarian cancer: a systematic review and meta-analysis of randomized trials. *ESMO Open* **7**, 100586 (2022). https://doi.org/https://doi.org/10.1016/j.esmoop.2022.100586

164 van Driel, W. J. *et al.* Hyperthermic Intraperitoneal Chemotherapy in Ovarian Cancer. *New England Journal of Medicine* **378**, 230-240 (2018). https://doi.org/10.1056/NEJMoa1708618

165 Ohno, S., Siddik, Z. H., Kido, Y., Zwelling, L. A. & Bull, J. M. C. Thermal enhancement of drug uptake and DNA adducts as a possible mechanism for the effect of sequencing hyperthermia on cisplatin-induced cytotoxicity in L1210 cells. *Cancer Chemotherapy and Pharmacology* **34**, 302-306 (1994). https://doi.org/10.1007/BF00686037

166 Francis, P. *et al.* Phase I feasibility and pharmacologic study of weekly intraperitoneal paclitaxel: a Gynecologic Oncology Group pilot Study. *Journal of Clinical Oncology* **13**, 2961-2967 (1995). https://doi.org/10.1200/JCO.1995.13.12.2961

167 Wright, A. A. *et al.* Use and Effectiveness of Intraperitoneal Chemotherapy for Treatment of Ovarian Cancer. *Journal of Clinical Oncology* **33**, 2841-2847 (2015). https://doi.org/10.1200/jco.2015.61.4776

168 Alyami, M. *et al.* Pressurised intraperitoneal aerosol chemotherapy: rationale, evidence, and potential indications. *The Lancet Oncology* **20**, e368-e377 (2019). https://doi.org/https://doi.org/10.1016/S1470-2045(19)30318-3

169 Solass, W. *et al.* Intraperitoneal Chemotherapy of Peritoneal Carcinomatosis Using Pressurized Aerosol as an Alternative to Liquid Solution: First Evidence for Efficacy. *Annals of Surgical Oncology* **21**, 553-559 (2014). https://doi.org/10.1245/s10434-013-3213-1

170 Kakchekeeva, T. *et al.* In Vivo Feasibility of Electrostatic Precipitation as an Adjunct to Pressurized Intraperitoneal Aerosol Chemotherapy (ePIPAC). *Annals of Surgical Oncology* **23**, 592-598 (2016). https://doi.org/10.1245/s10434-016-5108-4

171 Hwang, W.-T., Adams, S. F., Tahirovic, E., Hagemann, I. S. & Coukos, G. Prognostic significance of tumor-infiltrating T cells in ovarian cancer: A meta-analysis. *Gynecologic Oncology* **124**, 192-198 (2012). https://doi.org/https://doi.org/10.1016/j.ygyno.2011.09.039

172 Wefers, C., Lambert, L. J., Torensma, R. & Hato, S. V. Cellular immunotherapy in ovarian cancer: Targeting the stem of recurrence. *Gynecologic Oncology* **137**, 335-342 (2015). https://doi.org/https://doi.org/10.1016/j.ygyno.2015.02.019

173 Zhang, L. *et al.* Intratumoral T Cells, Recurrence, and Survival in Epithelial Ovarian Cancer. *New England Journal of Medicine* **348**, 203-213 (2003). https://doi.org/doi:10.1056/NEJMoa020177

174 Blanc-Durand, F., Clemence Wei Xian, L. & Tan, D. S. P. Targeting the immune microenvironment for ovarian cancer therapy. *Frontiers in Immunology* **14** (2023). https://doi.org/10.3389/fimmu.2023.1328651

175 Chalmers, Z. R. *et al.* Analysis of 100,000 human cancer genomes reveals the landscape of tumor mutational burden. *Genome Medicine* **9**, 34 (2017). https://doi.org/10.1186/s13073-017-0424-2

176 Schumacher, T. N. & Schreiber, R. D. Neoantigens in cancer immunotherapy. *Science* **348**, 69-74 (2015). https://doi.org/10.1126/science.aaa4971

177 Rizvi, N. A. *et al.* Mutational landscape determines sensitivity to PD-1 blockade in non–small cell lung cancer. *Science* **348**, 124-128 (2015). https://doi.org/10.1126/science.aaa1348

178 Ojalvo, L. S., Nichols, P. E., Jelovac, D. & Emens, L. A. Emerging immunotherapies in ovarian cancer. *Discov Med* **20**, 97-109 (2015).

179 Emens, L. A., Kok, M. & Ojalvo, L. S. Targeting the programmed cell death-1 pathway in breast and ovarian cancer. *Current Opinion in Obstetrics and Gynecology* **28** (2016).

180 Odunsi, K. Immunotherapy in ovarian cancer. *Annals of Oncology* **28**, viii1-viii7 (2017). https://doi.org/https://doi.org/10.1093/annonc/mdx444
181 Weir, G. M. *et al.* Metronomic cyclophosphamide enhances HPV16E7 peptide vaccine induced antigen-specific and cytotoxic T-cell mediated antitumor immune response. *OncoImmunology* **3**, e953407 (2014). https://doi.org/10.4161/21624011.2014.953407
182 Odunsi, K. *et al.* Epigenetic Potentiation of NY-ESO-1 Vaccine Therapy in Human Ovarian Cancer. *Cancer Immunology Research* **2**, 37-49 (2014). https://doi.org/10.1158/2326-6066.Cir-13-0126
183 Patel, B. K. *et al.* Cowpea Mosaic Virus (CPMV)-Based Cancer Testis Antigen NY-ESO-1 Vaccine Elicits an Antigen-Specific Cytotoxic T Cell Response. *ACS Applied Bio Materials* **3**, 4179-4187 (2020). https://doi.org/10.1021/acsabm.0c00259
184 Odunsi, K. *et al.* Efficacy of vaccination with recombinant vaccinia and fowlpox vectors expressing NY-ESO-1 antigen in ovarian cancer and melanoma patients. *Proceedings of the National Academy of Sciences* **109**, 5797-5802 (2012). https://doi.org/doi:10.1073/pnas.1117208109
185 Deng, M. *et al.* Immunotherapy for Ovarian Cancer: Disappointing or Promising? *Molecular Pharmaceutics* **21**, 454-466 (2024). https://doi.org/10.1021/acs.molpharmaceut.3c00986
186 Barve, M. *et al.* Pilot Study of Combination Gemogenovatucel-T (Vigil) and Durvalumab in Women With Relapsed BRCA-wt Triple-Negative Breast or Ovarian Cancer. *Clinical Medicine Insights: Oncology* **16**, 11795549221110501 (2022). https://doi.org/10.1177/11795549221110501
187 Matulonis, U. A. *et al.* Antitumor activity and safety of pembrolizumab in patients with advanced recurrent ovarian cancer: results from the phase II KEYNOTE-100 study. *Annals of Oncology* **30**, 1080-1087 (2019). https://doi.org/10.1093/annonc/mdz135
188 Won-Hee, Y., Anna, D. & Lawrence, K. Immune checkpoint inhibitors in ovarian cancer: where do we go from here? *Cancer Drug Resistance* **6**, 358-377 (2023). https://doi.org/10.20517/cdr.2023.13
189 Germano, G. *et al.* Inactivation of DNA repair triggers neoantigen generation and impairs tumour growth. *Nature* **552**, 116-120 (2017). https://doi.org/10.1038/nature24673
190 Shen, J. *et al.* PARPi Triggers the STING-Dependent Immune Response and Enhances the Therapeutic Efficacy of Immune Checkpoint Blockade Independent of BRCAness. *Cancer Research* **79**, 311-319 (2019). https://doi.org/10.1158/0008-5472.CAN-18-1003
191 Moore, K. N. *et al.* Mirvetuximab Soravtansine in FRα-Positive, Platinum-Resistant Ovarian Cancer. *New England Journal of Medicine* **389**, 2162-2174 (2023). https://doi.org/10.1056/NEJMoa2309169
192 Tsikouras, P. *et al.* The contribution of catumaxomab in the treatment of malignant ascites in patients with ovarian cancer: a review of the literature. *Archives of Gynecology and Obstetrics* **288**, 581-585 (2013). https://doi.org/10.1007/s00404-013-2868-y
193 Fujita, K. *et al.* Prolonged disease-free period in patients with advanced epithelial ovarian cancer after adoptive transfer of tumor-infiltrating lymphocytes. *Clin Cancer Res* **1**, 501-507 (1995).
194 Aoki, Y. *et al.* Use of adoptive transfer of tumor-infiltrating lymphocytes alone or in combination with cisplatin-containing chemotherapy in patients with epithelial ovarian cancer. *Cancer Res* **51**, 1934-1939 (1991).
195 PAN, Y. *et al.* Cytokine-induced Killer T Cells Enhance the Cytotoxicity Against Carboplatin-resistant Ovarian Cancer Cells. *Anticancer Research* **40**, 3865-3872 (2020). https://doi.org/10.21873/anticanres.14376
196 Liu, J., Wang, L., Wang, Y., Zhang, W. & Cao, Y. Phenotypic characterization and anticancer capacity of CD8+ cytokine-induced killer cells after antigen-induced expansion. *PLOS ONE* **12**, e0175704 (2017). https://doi.org/10.1371/journal.pone.0175704

197 Capellero, S. *et al.* Preclinical immunotherapy with Cytokine-Induced Killer lymphocytes against epithelial ovarian cancer. *Scientific Reports* **10**, 6478 (2020). https://doi.org/10.1038/s41598-020-63634-z
198 Nasiri, F. *et al.* CAR-T cell immunotherapy for ovarian cancer: hushing the silent killer. *Frontiers in Immunology* **14** (2023). https://doi.org/10.3389/fimmu.2023.1302307
199 Koneru, M., O'Cearbhaill, R., Pendharkar, S., Spriggs, D. R. & Brentjens, R. J. A phase I clinical trial of adoptive T cell therapy using IL-12 secreting MUC-16ecto directed chimeric antigen receptors for recurrent ovarian cancer. *Journal of Translational Medicine* **13**, 102 (2015). https://doi.org/10.1186/s12967-015-0460-x
200 Thistlethwaite, F. C. *et al.* The clinical efficacy of first-generation carcinoembryonic antigen (CEACAM5)-specific CAR T cells is limited by poor persistence and transient pre-conditioning-dependent respiratory toxicity. *Cancer Immunology, Immunotherapy* **66**, 1425-1436 (2017). https://doi.org/10.1007/s00262-017-2034-7
201 Rodriguez-Garcia, A., Minutolo, N. G., Robinson, J. M. & Powell, D. J. T-cell target antigens across major gynecologic cancers. *Gynecologic Oncology* **145**, 426-435 (2017). https://doi.org/10.1016/j.ygyno.2017.03.510
202 Katz, S. C. *et al.* Regional CAR-T cell infusions for peritoneal carcinomatosis are superior to systemic delivery. *Cancer Gene Therapy* **23**, 142-148 (2016). https://doi.org/10.1038/cgt.2016.14
203 Xia Ang, W. *et al.* Intraperitoneal immunotherapy with T cells stably and transiently expressing anti-EpCAM CAR in xenograft models of peritoneal carcinomatosis. *Oncotarget; Vol 8, No 8* (2017).
204 Deshet-Unger, N. *et al.* Comparing Intraperitoneal and Intravenous Personalized ErbB2CAR-T for the Treatment of Epithelial Ovarian Cancer. *Biomedicines* **10**, 2216 (2022).
205 Murad, J. P. *et al.* Effective Targeting of TAG72+ Peritoneal Ovarian Tumors via Regional Delivery of CAR-Engineered T Cells. *Frontiers in Immunology* **9** (2018).
206 Yeku, O. O., Purdon, T. J., Koneru, M., Spriggs, D. & Brentjens, R. J. Armored CAR T cells enhance antitumor efficacy and overcome the tumor microenvironment. *Scientific Reports* **7**, 10541 (2017). https://doi.org/10.1038/s41598-017-10940-8
207 Xu, X., Qiu, J. & Sun, Y. The basics of CAR T design and challenges in immunotherapy of solid tumors — Ovarian cancer as a model. *Human Vaccines & Immunotherapeutics* **13**, 1548-1555 (2017). https://doi.org/10.1080/21645515.2017.1291473
208 Mole, R. H. Whole Body Irradiation—Radiobiology or Medicine? *The British Journal of Radiology* **26**, 234-241 (1953). https://doi.org/10.1259/0007-1285-26-305-234
209 Adusumilli, P. S. *et al.* Regional delivery of mesothelin-targeted CAR T cell therapy generates potent and long-lasting CD4-dependent tumor immunity. *Science Translational Medicine* **6**, 261ra151 (2014). https://doi.org/10.1126/scitranslmed.3010162
210 Sampson, J. H. *et al.* EGFRvIII mCAR-Modified T-Cell Therapy Cures Mice with Established Intracerebral Glioma and Generates Host Immunity against Tumor-Antigen Loss. *Clinical Cancer Research* **20**, 972-984 (2014). https://doi.org/10.1158/1078-0432.CCR-13-0709
211 Center, H. L. M. C., Institute, R. & Anixa Biosciences, I. (https://classic.clinicaltrials.gov/show/NCT05316129, 2022).
212 Center, C. o. H. M. & Institute, N. C. (https://classic.clinicaltrials.gov/show/NCT05225363, 2022).
213 Center, U. L. C. C. & Health, N. I. o. (https://classic.clinicaltrials.gov/show/NCT04670068, 2021).
214 MaxCyte, I., Trial, C. C. & Services, C. (https://classic.clinicaltrials.gov/show/NCT03608618, 2018).
215 Annunziata, C. M. *et al.* Feasibility and preliminary safety and efficacy of first-in-human intraperitoneal delivery of MCY-M11, anti-human-mesothelin CAR mRNA transfected into peripheral blood mononuclear cells, for ovarian cancer and malignant peritoneal

mesothelioma. *Journal of Clinical Oncology* **38**, 3014-3014 (2020). https://doi.org/10.1200/JCO.2020.38.15_suppl.3014

216 O'Hara, M., Stashwick, C., Haas, A. R. & Tanyi, J. L. Mesothelin as a target for chimeric antigen receptor-modified T cells as anticancer therapy. *Immunotherapy* **8**, 449-460 (2016). https://doi.org/10.2217/imt.16.4

217 Morello, A., Sadelain, M. & Adusumilli, P. S. Mesothelin-Targeted CARs: Driving T Cells to Solid Tumors. *Cancer Discovery* **6**, 133-146 (2016). https://doi.org/10.1158/2159-8290.CD-15-0583

218 Chang, K., Pastan, I. & Willingham, M. C. Isolation and characterization of a monoclonal antibody, K1, reactive with ovarian cancers and normal mesothelium. *International Journal of Cancer* **50**, 373-381 (1992). https://doi.org/https://doi.org/10.1002/ijc.2910500308

219 Ordóñez, N. G. Application of mesothelin immunostaining in tumor diagnosis. *Am J Surg Pathol* **27**, 1418-1428 (2003). https://doi.org/10.1097/00000478-200311000-00003

220 Lamberts, L. E., de Groot, D. J. A., Bense, R. D., de Vries, E. G. E. & Fehrmann, R. S. N. Functional genomic mRNA profiling of a large cancer data base demonstrates mesothelin overexpression in a broad range of tumor types. *Oncotarget; Vol 6, No 29* (2015).

221 Chang, K. & Pastan, I. Molecular cloning of mesothelin, a differentiation antigen present on mesothelium, mesotheliomas, and ovarian cancers. *Proceedings of the National Academy of Sciences* **93**, 136-140 (1996). https://doi.org/doi:10.1073/pnas.93.1.136

222 Hassan, R., Kreitman, R. J., Pastan, I. & Willingham, M. C. Localization of Mesothelin in Epithelial Ovarian Cancer. *Applied Immunohistochemistry & Molecular Morphology* **13** (2005).

223 Kachala, S. S. *et al.* Mesothelin Overexpression Is a Marker of Tumor Aggressiveness and Is Associated with Reduced Recurrence-Free and Overall Survival in Early-Stage Lung Adenocarcinoma. *Clinical Cancer Research* **20**, 1020-1028 (2014). https://doi.org/10.1158/1078-0432.CCR-13-1862

224 Rizk, N. P. *et al.* Tissue and Serum Mesothelin Are Potential Markers of Neoplastic Progression in Barrett's Associated Esophageal Adenocarcinoma. *Cancer Epidemiology, Biomarkers & Prevention* **21**, 482-486 (2012). https://doi.org/10.1158/1055-9965.EPI-11-0993

225 Tozbikian, G. *et al.* Mesothelin Expression in Triple Negative Breast Carcinomas Correlates Significantly with Basal-Like Phenotype, Distant Metastases and Decreased Survival. *PLOS ONE* **9**, e114900 (2014). https://doi.org/10.1371/journal.pone.0114900

226 Weidemann, S. *et al.* Mesothelin Expression in Human Tumors: A Tissue Microarray Study on 12,679 Tumors. *Biomedicines* **9** (2021).

227 Bera, T. K. & Pastan, I. Mesothelin is not required for normal mouse development or reproduction. *Mol Cell Biol* **20**, 2902-2906 (2000). https://doi.org/10.1128/mcb.20.8.2902-2906.2000

228 Cheng, W. F. *et al.* High mesothelin correlates with chemoresistance and poor survival in epithelial ovarian carcinoma. *Br J Cancer* **100**, 1144-1153 (2009). https://doi.org/10.1038/sj.bjc.6604964

229 Bharadwaj, U., Marin-Muller, C., Li, M., Chen, C. & Yao, Q. Mesothelin confers pancreatic cancer cell resistance to TNF-α-induced apoptosis through Akt/PI3K/NF-κB activation and IL-6/Mcl-1 overexpression. *Molecular Cancer* **10**, 106 (2011). https://doi.org/10.1186/1476-4598-10-106

230 Chen, S.-H., Hung, W.-C., Wang, P., Paul, C. & Konstantopoulos, K. Mesothelin Binding to CA125/MUC16 Promotes Pancreatic Cancer Cell Motility and Invasion via MMP-7 Activation. *Scientific Reports* **3**, 1870 (2013). https://doi.org/10.1038/srep01870

231 Rump, A. *et al.* Binding of Ovarian Cancer Antigen CA125/MUC16 to Mesothelin Mediates Cell Adhesion*. *Journal of Biological Chemistry* **279**, 9190-9198 (2004). https://doi.org/https://doi.org/10.1074/jbc.M312372200
232 Gubbels, J. A. A. *et al.* Mesothelin-MUC16 binding is a high affinity, N-glycan dependent interaction that facilitates peritoneal metastasis of ovarian tumors. *Molecular Cancer* **5**, 50 (2006). https://doi.org/10.1186/1476-4598-5-50
233 Coelho, R. *et al.* Regulation of invasion and peritoneal dissemination of ovarian cancer by mesothelin manipulation. *Oncogenesis* **9**, 61 (2020). https://doi.org/10.1038/s41389-020-00246-2
234 Chang, M.-C. *et al.* Mesothelin enhances invasion of ovarian cancer by inducing MMP-7 through MAPK/ERK and JNK pathways. *Biochemical Journal* **442**, 293-302 (2012). https://doi.org/10.1042/BJ20110282
235 Servais, E. L. *et al.* Mesothelin Overexpression Promotes Mesothelioma Cell Invasion and MMP-9 Secretion in an Orthotopic Mouse Model and in Epithelioid Pleural Mesothelioma Patients. *Clinical Cancer Research* **18**, 2478-2489 (2012). https://doi.org/10.1158/1078-0432.CCR-11-2614
236 Weidemann, S. *et al.* High Homogeneity of Mesothelin Expression in Primary and Metastatic Ovarian Cancer. *Applied Immunohistochemistry & Molecular Morphology* **31** (2023).
237 Pastan, I. & Hassan, R. Discovery of mesothelin and exploiting it as a target for immunotherapy. *Cancer Res* **74**, 2907-2912 (2014). https://doi.org/10.1158/0008-5472.Can-14-0337
238 Katz, S. I. *et al.* Serum soluble mesothelin-related protein (SMRP) and fibulin-3 levels correlate with baseline malignant pleural mesothelioma (MPM) tumor volumes but are not useful as biomarkers of response in an immunotherapy trial. *Lung Cancer* **154**, 5-12 (2021). https://doi.org/10.1016/j.lungcan.2021.01.011
239 Sapede, C. *et al.* Aberrant splicing and protease involvement in mesothelin release from epithelioid mesothelioma cells. *Cancer Science* **99**, 590-594 (2008). https://doi.org/https://doi.org/10.1111/j.1349-7006.2007.00715.x
240 Hellstrom, I. *et al.* Anti-Mesothelin Antibodies and Circulating Mesothelin Relate to the Clinical State in Ovarian Cancer Patients. *Cancer Epidemiology, Biomarkers & Prevention* **17**, 1520-1526 (2008). https://doi.org/10.1158/1055-9965.Epi-08-0039
241 Hassan, R. *et al.* Detection and Quantitation of Serum Mesothelin, a Tumor Marker for Patients with Mesothelioma and Ovarian Cancer. *Clinical Cancer Research* **12**, 447-453 (2006). https://doi.org/10.1158/1078-0432.CCR-05-1477
242 Scholler, N. *et al.* Soluble member(s) of the mesothelin/megakaryocyte potentiating factor family are detectable in sera from patients with ovarian carcinoma. *Proceedings of the National Academy of Sciences* **96**, 11531-11536 (1999). https://doi.org/10.1073/pnas.96.20.11531
243 Lanitis, E. *et al.* Redirected Antitumor Activity of Primary Human Lymphocytes Transduced With a Fully Human Anti-mesothelin Chimeric Receptor. *Molecular Therapy* **20**, 633-643 (2012). https://doi.org/10.1038/mt.2011.256
244 Carpenito, C. *et al.* Control of large, established tumor xenografts with genetically retargeted human T cells containing CD28 and CD137 domains. *Proceedings of the National Academy of Sciences* **106**, 3360-3365 (2009). https://doi.org/doi:10.1073/pnas.0813101106
245 González, P. A. *et al.* Modulation of Tumor Immunity by Soluble and Membrane-Bound Molecules at the Immunological Synapse. *Clinical and Developmental Immunology* **2013**, 450291 (2013). https://doi.org/10.1155/2013/450291
246 Liu, X. F. *et al.* Tumor resistance to anti-mesothelin CAR-T cells caused by binding to shed mesothelin is overcome by targeting a juxtamembrane epitope. *Proceedings of the National Academy of Sciences* **121**, e2317283121 (2024). https://doi.org/doi:10.1073/pnas.2317283121

247 Rodrigues, J., Heinrich, M. A., Teixeira, L. M. & Prakash, J. 3D In Vitro Model (R)evolution: Unveiling Tumor–Stroma Interactions. *Trends in Cancer* **7**, 249-264 (2021). https://doi.org/10.1016/j.trecan.2020.10.009
248 Zhou, Z. *et al.* Harnessing 3D in vitro systems to model immune responses to solid tumours: a step towards improving and creating personalized immunotherapies. *Nature Reviews Immunology* (2023). https://doi.org/10.1038/s41577-023-00896-4
249 Shelton, S. E., Nguyen, H. T., Barbie, D. A. & Kamm, R. D. Engineering approaches for studying immune-tumor cell interactions and immunotherapy. *iScience* **24**, 101985 (2021). https://doi.org/https://doi.org/10.1016/j.isci.2020.101985
250 Wegner, A. Chimeric antigen receptor T cells for the treatment of cancer and the future of preclinical models for predicting their toxicities. *Immunotherapy* **9**, 669-680 (2017). https://doi.org/10.2217/imt-2017-0028
251 Long, A. H. *et al.* 4-1BB costimulation ameliorates T cell exhaustion induced by tonic signaling of chimeric antigen receptors. *Nature Medicine* **21**, 581-590 (2015). https://doi.org/10.1038/nm.3838
252 Grunewald, L. *et al.* A Reproducible Bioprinted 3D Tumor Model Serves as a Preselection Tool for CAR T Cell Therapy Optimization. *Frontiers in Immunology* **12** (2021). https://doi.org/10.3389/fimmu.2021.689697
253 Pavesi, A. *et al.* Using microfluidics to investigate tumor cell extravasation and T-cell immunotherapies. *Annu Int Conf IEEE Eng Med Biol Soc* **2015**, 1853-1856 (2015). https://doi.org/10.1109/embc.2015.7318742
254 Pavesi, A. *et al.* A 3D microfluidic model for preclinical evaluation of TCR-engineered T cells against solid tumors. *JCI Insight* **2** (2017). https://doi.org/10.1172/jci.insight.89762
255 Galeano Niño, J. L. *et al.* Cytotoxic T cells swarm by homotypic chemokine signalling. *eLife* **9**, e56554 (2020). https://doi.org/10.7554/eLife.56554
256 Schnalzger, T. E. *et al.* 3D model for CAR-mediated cytotoxicity using patient-derived colorectal cancer organoids. *The EMBO Journal* **38**, e100928 (2019). https://doi.org/10.15252/embj.2018100928
257 Zanoni, M., Pignatta, S., Arienti, C., Bonafè, M. & Tesei, A. Anticancer drug discovery using multicellular tumor spheroid models. *Expert Opinion on Drug Discovery* **14**, 289-301 (2019). https://doi.org/10.1080/17460441.2019.1570129
258 Costa, E. C. *et al.* 3D tumor spheroids: an overview on the tools and techniques used for their analysis. *Biotechnology Advances* **34**, 1427-1441 (2016). https://doi.org/https://doi.org/10.1016/j.biotechadv.2016.11.002
259 Attieh, Y. *et al.* Cancer-associated fibroblasts lead tumor invasion through integrin-β3–dependent fibronectin assembly. *Journal of Cell Biology* **216**, 3509-3520 (2017). https://doi.org/10.1083/jcb.201702033
260 Zanoni, M. *et al.* Modeling neoplastic disease with spheroids and organoids. *Journal of Hematology & Oncology* **13**, 97 (2020). https://doi.org/10.1186/s13045-020-00931-0
261 Drost, J. & Clevers, H. Organoids in cancer research. *Nature Reviews Cancer* **18**, 407-418 (2018). https://doi.org/10.1038/s41568-018-0007-6
262 Weeber, F. *et al.* Preserved genetic diversity in organoids cultured from biopsies of human colorectal cancer metastases. *Proceedings of the National Academy of Sciences* **112**, 13308-13311 (2015). https://doi.org/10.1073/pnas.1516689112
263 Yao, Y. *et al.* Patient-Derived Organoids Predict Chemoradiation Responses of Locally Advanced Rectal Cancer. *Cell Stem Cell* **26**, 17-26.e16 (2020). https://doi.org/10.1016/j.stem.2019.10.010
264 Veninga, V. & Voest, E. E. Tumor organoids: Opportunities and challenges to guide precision medicine. *Cancer Cell* **39**, 1190-1201 (2021). https://doi.org/https://doi.org/10.1016/j.ccell.2021.07.020
265 Aref, A. R. *et al.* 3D microfluidic ex vivo culture of organotypic tumor spheroids to model immune checkpoint blockade. *Lab on a Chip* **18**, 3129-3143 (2018). https://doi.org/10.1039/C8LC00322J

266 Dijkstra, K. K. *et al.* Generation of Tumor-Reactive T Cells by Co-culture of Peripheral Blood Lymphocytes and Tumor Organoids. *Cell* **174**, 1586-1598.e1512 (2018). https://doi.org/10.1016/j.cell.2018.07.009
267 Yuki, K., Cheng, N., Nakano, M. & Kuo, C. J. Organoid Models of Tumor Immunology. *Trends in Immunology* **41**, 652-664 (2020). https://doi.org/10.1016/j.it.2020.06.010
268 Fitzgerald, A. A., Li, E. & Weiner, L. M. 3D Culture Systems for Exploring Cancer Immunology. *Cancers* **13**, 56 (2021).
269 Salmon, H. *et al.* Matrix architecture defines the preferential localization and migration of T cells into the stroma of human lung tumors. *The Journal of Clinical Investigation* **122**, 899-910 (2012). https://doi.org/10.1172/JCI45817
270 Wolf, K., Müller, R., Borgmann, S., Bröcker, E. B. & Friedl, P. Amoeboid shape change and contact guidance: T-lymphocyte crawling through fibrillar collagen is independent of matrix remodeling by MMPs and other proteases. *Blood* **102**, 3262-3269 (2003). https://doi.org/10.1182/blood-2002-12-3791
271 Talkenberger, K., Cavalcanti-Adam, E. A., Voss-Böhme, A. & Deutsch, A. Amoeboid-mesenchymal migration plasticity promotes invasion only in complex heterogeneous microenvironments. *Scientific Reports* **7**, 9237 (2017). https://doi.org/10.1038/s41598-017-09300-3
272 Gaylo, A., Schrock, D. C., Fernandes, N. R. J. & Fowell, D. J. T Cell Interstitial Migration: Motility Cues from the Inflamed Tissue for Micro- and Macro-Positioning. *Frontiers in Immunology* **7** (2016). https://doi.org/10.3389/fimmu.2016.00428
273 Tooley, A. J. *et al.* Amoeboid T lymphocytes require the septin cytoskeleton for cortical integrity and persistent motility. *Nature Cell Biology* **11**, 17-26 (2009). https://doi.org/10.1038/ncb1808
274 Krummel, M. F., Bartumeus, F. & Gérard, A. T cell migration, search strategies and mechanisms. *Nature Reviews Immunology* **16**, 193-201 (2016). https://doi.org/10.1038/nri.2015.16
275 Koeck, S. *et al.* The influence of stromal cells and tumor-microenvironment-derived cytokines and chemokines on CD3+CD8+ tumor infiltrating lymphocyte subpopulations. *OncoImmunology* **6**, e1323617 (2017). https://doi.org/10.1080/2162402X.2017.1323617
276 Ando, Y., Oh, J. M., Zhao, W., Tran, M. & Shen, K. Engineering a Vascularized Hypoxic Tumor Model for Therapeutic Assessment. *Cells* **10**, 2201 (2021).
277 Wallstabe, L. *et al.* ROR1-CAR T cells are effective against lung and breast cancer in advanced microphysiologic 3D tumor models. *JCI Insight* **4** (2019). https://doi.org/10.1172/jci.insight.126345
278 Dekkers, J. F. *et al.* Uncovering the mode of action of engineered T cells in patient cancer organoids. *Nature Biotechnology* **41**, 60-69 (2023). https://doi.org/10.1038/s41587-022-01397-w
279 Kim, H., Kim, S., Lim, H. & Chung, A. J. Expanding CAR-T cell immunotherapy horizons through microfluidics. *Lab on a Chip* (2024). https://doi.org/10.1039/D3LC00622K
280 Li, Y. *et al.* Microfluidic devices: The application in TME modeling and the potential in immunotherapy optimization. *Frontiers in Genetics* **13** (2022). https://doi.org/10.3389/fgene.2022.969723
281 Mulas, C. *et al.* Microfluidic platform for 3D cell culture with live imaging and clone retrieval. *Lab on a Chip* **20**, 2580-2591 (2020). https://doi.org/10.1039/D0LC00165A
282 Park, D. *et al.* High-Throughput Microfluidic 3D Cytotoxicity Assay for Cancer Immunotherapy (CACI-IMPACT Platform). *Frontiers in Immunology* **10** (2019). https://doi.org/10.3389/fimmu.2019.01133
283 Ando, Y. *et al.* Evaluating CAR-T Cell Therapy in a Hypoxic 3D Tumor Model. *Advanced Healthcare Materials* **8**, 1900001 (2019). https://doi.org/https://doi.org/10.1002/adhm.201900001

284 Carvalho, M. R., Lima, D., Reis, R. L., Correlo, V. M. & Oliveira, J. M. Evaluating Biomaterial- and Microfluidic-Based 3D Tumor Models. *Trends in Biotechnology* **33**, 667-678 (2015). https://doi.org/10.1016/j.tibtech.2015.09.009
285 Cai, L. *et al.* Engineered biomaterials for cancer immunotherapy. *MedComm* **1**, 35-46 (2020). https://doi.org/https://doi.org/10.1002/mco2.8
286 Smith, T. T. *et al.* Biopolymers codelivering engineered T cells and STING agonists can eliminate heterogeneous tumors. *The Journal of Clinical Investigation* **127**, 2176-2191 (2017). https://doi.org/10.1172/JCI87624
287 Huang, Q. *et al.* The frontier of live tissue imaging across space and time. *Cell Stem Cell* **28**, 603-622 (2021). https://doi.org/10.1016/j.stem.2021.02.010
288 Stephens, D. J. & Allan, V. J. Light Microscopy Techniques for Live Cell Imaging. *Science* **300**, 82-86 (2003). https://doi.org/doi:10.1126/science.1082160
289 Specht, E. A., Braselmann, E. & Palmer, A. E. A Critical and Comparative Review of Fluorescent Tools for Live-Cell Imaging. *Annual Review of Physiology* **79**, 93-117 (2017). https://doi.org/https://doi.org/10.1146/annurev-physiol-022516-034055
290 Edlund, C. *et al.* LIVECell—A large-scale dataset for label-free live cell segmentation. *Nature Methods* **18**, 1038-1045 (2021). https://doi.org/10.1038/s41592-021-01249-6
291 Hu, C. *et al.* Live-dead assay on unlabeled cells using phase imaging with computational specificity. *Nature Communications* **13**, 713 (2022). https://doi.org/10.1038/s41467-022-28214-x
292 Zaritsky, A. *et al.* Interpretable deep learning uncovers cellular properties in label-free live cell images that are predictive of highly metastatic melanoma. *Cell Systems* **12**, 733-747.e736 (2021). https://doi.org/10.1016/j.cels.2021.05.003
293 van Ineveld, R. L. *et al.* Multispectral confocal 3D imaging of intact healthy and tumor tissue using mLSR-3D. *Nature Protocols* **17**, 3028-3055 (2022). https://doi.org/10.1038/s41596-022-00739-x
294 Yang, J.-M. *et al.* Deciphering cell signaling networks with massively multiplexed biosensor barcoding. *Cell* **184**, 6193-6206.e6114 (2021). https://doi.org/https://doi.org/10.1016/j.cell.2021.11.005
295 Borlinghaus, R. T. MRT letter: High speed scanning has the potential to increase fluorescence yield and to reduce photobleaching. *Microscopy Research and Technique* **69**, 689-692 (2006). https://doi.org/https://doi.org/10.1002/jemt.20363
296 Iaia, I. *et al.* Recruitment, Infiltration, and Cytotoxicity of HLA-Independent Killer Lymphocytes in Three-Dimensional Melanoma Models. *Cancers* **13** (2021).
297 Spiller, E. R. *et al.* Imaging-Based Machine Learning Analysis of Patient-Derived Tumor Organoid Drug Response. *Frontiers in Oncology* **11** (2021). https://doi.org/10.3389/fonc.2021.771173
298 Shroff, H., Testa, I., Jug, F. & Manley, S. Live-cell imaging powered by computation. *Nature Reviews Molecular Cell Biology* (2024). https://doi.org/10.1038/s41580-024-00702-6
299 Jupyter Book (Zenodo, 2021).
300 Sarder, P. & Nehorai, A. Deconvolution methods for 3-D fluorescence microscopy images. *IEEE Signal Processing Magazine* **23**, 32-45 (2006). https://doi.org/10.1109/MSP.2006.1628876
301 Meijering, E. Cell Segmentation: 50 Years Down the Road [Life Sciences]. *IEEE Signal Processing Magazine* **29**, 140-145 (2012). https://doi.org/10.1109/MSP.2012.2204190
302 Meijering, E., Dzyubachyk, O., Smal, I. & van Cappellen, W. A. Tracking in cell and developmental biology. *Seminars in Cell & Developmental Biology* **20**, 894-902 (2009). https://doi.org/https://doi.org/10.1016/j.semcdb.2009.07.004
303 Ravindran, S. Five ways deep learning has transformed image analysis. *Nature* **609**, 864-866 (2022). https://doi.org/10.1038/d41586-022-02964-6
304 Meijering, E., Carpenter, A. E., Peng, H., Hamprecht, F. A. & Olivo-Marin, J.-C. Imagining the future of bioimage analysis. *Nature Biotechnology* **34**, 1250-1255 (2016). https://doi.org/10.1038/nbt.3722

305 Li, X., Zhang, Y., Wu, J. & Dai, Q. Challenges and opportunities in bioimage analysis. *Nature Methods* **20**, 958-961 (2023). https://doi.org/10.1038/s41592-023-01900-4

306 Berg, S. *et al.* ilastik: interactive machine learning for (bio)image analysis. *Nature Methods* **16**, 1226-1232 (2019). https://doi.org/10.1038/s41592-019-0582-9

307 Ershov, D. *et al.* TrackMate 7: integrating state-of-the-art segmentation algorithms into tracking pipelines. *Nature Methods* **19**, 829-832 (2022). https://doi.org/10.1038/s41592-022-01507-1

308 Stirling, D. R. *et al.* CellProfiler 4: improvements in speed, utility and usability. *BMC Bioinformatics* **22**, 433 (2021). https://doi.org/10.1186/s12859-021-04344-9

309 Straehle, C. N. *et al.* in *2012 IEEE Conference on Computer Vision and Pattern Recognition.* 765-772.

310 Kimmel, J. C., Brack, A. S. & Marshall, W. F. Deep Convolutional and Recurrent Neural Networks for Cell Motility Discrimination and Prediction. *IEEE/ACM Transactions on Computational Biology and Bioinformatics* **18**, 562-574 (2021). https://doi.org/10.1109/TCBB.2019.2919307

311 Freckmann, E. C. *et al.* Traject3d allows label-free identification of distinct co-occurring phenotypes within 3D culture by live imaging. *Nature Communications* **13**, 5317 (2022). https://doi.org/10.1038/s41467-022-32958-x

312 Buggenthin, F. *et al.* Prospective identification of hematopoietic lineage choice by deep learning. *Nature Methods* **14**, 403-406 (2017). https://doi.org/10.1038/nmeth.4182

313 McKenzie, A. J. *et al.* The mechanical microenvironment regulates ovarian cancer cell morphology, migration, and spheroid disaggregation. *Scientific Reports* **8**, 7228 (2018). https://doi.org/10.1038/s41598-018-25589-0

314 Rickard, B. P. *et al.* Malignant Ascites in Ovarian Cancer: Cellular, Acellular, and Biophysical Determinants of Molecular Characteristics and Therapy Response. *Cancers* **13**, 4318 (2021).

315 Carduner, L. *et al.* Ovarian cancer ascites-derived vitronectin and fibronectin: Combined purification, molecular features and effects on cell response. *Biochimica et Biophysica Acta (BBA) - General Subjects* **1830**, 4885-4897 (2013). https://doi.org/https://doi.org/10.1016/j.bbagen.2013.06.023

316 Bascetin, R. *et al.* A biomimetic model of 3D fluid extracellular macromolecular crowding microenvironment fine-tunes ovarian cancer cells dissemination phenotype. *Biomaterials* **269**, 120610 (2021). https://doi.org/https://doi.org/10.1016/j.biomaterials.2020.120610

317 Gokturk, H. S. *et al.* The Role of Ascitic Fluid Viscosity in the Differential Diagnosis of Ascites. *Canadian Journal of Gastroenterology* **24**, 896786 (2010). https://doi.org/10.1155/2010/896786

318 Shurbaji, S., G. Anlar, G., A. Hussein, E., Elzatahry, A. & C. Yalcin, H. Effect of Flow-Induced Shear Stress in Nanomaterial Uptake by Cells: Focus on Targeted Anti-Cancer Therapy. *Cancers* **12** (2020).

319 Gotlieb, W. H. *et al.* Intraperitoneal Pressures and Clinical Parameters of Total Paracentesis for Palliation of Symptomatic Ascites in Ovarian Cancer. *Gynecologic Oncology* **71**, 381-385 (1998). https://doi.org/10.1006/gyno.1998.5215

320 Asem, M. *et al.* Ascites-induced compression alters the peritoneal microenvironment and promotes metastatic success in ovarian cancer. *Scientific Reports* **10**, 11913 (2020). https://doi.org/10.1038/s41598-020-68639-2

321 Ingber, D. E. TENSEGRITY: THE ARCHITECTURAL BASIS OF CELLULAR MECHANOTRANSDUCTION. *Annual Review of Physiology* **59**, 575-599 (1997). https://doi.org/10.1146/annurev.physiol.59.1.575

322 Xin, Y. *et al.* Biophysics in tumor growth and progression: from single mechano-sensitive molecules to mechanomedicine. *Oncogene* **42**, 3457-3490 (2023). https://doi.org/10.1038/s41388-023-02844-x

323 Klymenko, Y. *et al.* Modeling the effect of ascites-induced compression on ovarian cancer multicellular aggregates. *Disease Models & Mechanisms* **11** (2018). https://doi.org/10.1242/dmm.034199

324 Rizvi, I. *et al.* Flow induces epithelial-mesenchymal transition, cellular heterogeneity and biomarker modulation in 3D ovarian cancer nodules. *Proceedings of the National Academy of Sciences of the United States of America* **110**, E1974-E1983 (2013). https://doi.org/10.1073/pnas.1216989110

325 Ip, C. K. M. *et al.* Stemness and chemoresistance in epithelial ovarian carcinoma cells under shear stress. *Scientific Reports* **6**, 26788 (2016). https://doi.org/10.1038/srep26788

326 Nath, S. *et al.* Flow-induced Shear Stress Confers Resistance to Carboplatin in an Adherent Three-Dimensional Model for Ovarian Cancer: A Role for EGFR-Targeted Photoimmunotherapy Informed by Physical Stress. *Journal of Clinical Medicine* **9**, 924 (2020).

327 Medico, E. *et al.* The molecular landscape of colorectal cancer cell lines unveils clinically actionable kinase targets. *Nature Communications* **6**, 7002 (2015). https://doi.org/10.1038/ncomms8002

328 Amendola, M., Venneri, M. A., Biffi, A., Vigna, E. & Naldini, L. Coordinate dual-gene transgenesis by lentiviral vectors carrying synthetic bidirectional promoters. *Nature Biotechnology* **23**, 108-116 (2005). https://doi.org/10.1038/nbt1049

329 Au - Naber, H. P. H., Au - Wiercinska, E., Au - ten Dijke, P. & Au - van Laar, T. Spheroid Assay to Measure TGF-β-induced Invasion. *JoVE*, e3337 (2011). https://doi.org/doi:10.3791/3337

330 Berg, H. C. & Purcell, E. M. Physics of chemoreception. *Biophysical journal* **20**, 193-219 (1977). https://doi.org/10.1016/S0006-3495(77)85544-6

331 Schindelin, J. *et al.* Fiji: an open-source platform for biological-image analysis. *Nature Methods* **9**, 676-682 (2012). https://doi.org/10.1038/nmeth.2019

332 Barretina, J. *et al.* The Cancer Cell Line Encyclopedia enables predictive modelling of anticancer drug sensitivity. *Nature* **483**, 603-607 (2012). https://doi.org/10.1038/nature11003

333 Shield, K., Ackland, M. L., Ahmed, N. & Rice, G. E. Multicellular spheroids in ovarian cancer metastases: Biology and pathology. *Gynecologic Oncology* **113**, 143-148 (2009). https://doi.org/10.1016/j.ygyno.2008.11.032

334 Hope, J. M. *et al.* Fluid shear stress enhances T cell activation through Piezo1. *BMC Biology* **20**, 61 (2022). https://doi.org/10.1186/s12915-022-01266-7

335 Zhuang, C., Gould, J. E., Enninful, A., Shao, S. & Mak, M. Biophysical and mechanobiological considerations for T-cell-based immunotherapy. *Trends in Pharmacological Sciences* **44**, 366-378 (2023). https://doi.org/10.1016/j.tips.2023.03.007

336 Liu, C. S. C. *et al.* Cutting Edge: Piezo1 Mechanosensors Optimize Human T Cell Activation. *The Journal of Immunology* **200**, 1255-1260 (2018). https://doi.org/10.4049/jimmunol.1701118

337 Weninger, W., Biro, M. & Jain, R. Leukocyte migration in the interstitial space of non-lymphoid organs. *Nature Reviews Immunology* **14**, 232-246 (2014). https://doi.org/10.1038/nri3641

338 Ronteix, G. *et al.* High resolution microfluidic assay and probabilistic modeling reveal cooperation between T cells in tumor killing. *Nature Communications* **13**, 3111 (2022). https://doi.org/10.1038/s41467-022-30575-2

339 Culpepper, D. J., Maddox, M. K., Caldwell, A. B. & McFarland, B. J. Systematic mutation and thermodynamic analysis of central tyrosine pairs in polyspecific NKG2D receptor interactions. *Molecular Immunology* **48**, 516-523 (2011). https://doi.org/https://doi.org/10.1016/j.molimm.2010.10.007

340 Muñoz-López, P. *et al.* Single-Chain Fragment Variable: Recent Progress in Cancer Diagnosis and Therapy. *Cancers* **14** (2022).

341 Romain, G. *et al.* Multidimensional single-cell analysis identifies a role for CD2-CD58 interactions in clinical antitumor T cell responses. *The Journal of Clinical Investigation* **132** (2022). https://doi.org/10.1172/JCI159402

342 Albelda, S. M. CAR T cell therapy for patients with solid tumours: key lessons to learn and unlearn. *Nature Reviews Clinical Oncology* **21**, 47-66 (2024). https://doi.org/10.1038/s41571-023-00832-4
343 Pievani, A. *et al.* Dual-functional capability of CD3+CD56+ CIK cells, a T-cell subset that acquires NK function and retains TCR-mediated specific cytotoxicity. *Blood* **118**, 3301-3310 (2011). https://doi.org/10.1182/blood-2011-02-336321
344 Franceschetti, M. *et al.* Cytokine-induced killer cells are terminallydifferentiated activated CD8 cytotoxic T-EMRA lymphocytes. *Experimental Hematology* **37**, 616-628.e612 (2009). https://doi.org/https://doi.org/10.1016/j.exphem.2009.01.010
345 Upadhyay, R. *et al.* A Critical Role for Fas-Mediated Off-Target Tumor Killing in T-cell Immunotherapy. *Cancer Discovery* **11**, 599-613 (2021). https://doi.org/10.1158/2159-8290.CD-20-0756
346 DeSelm, C. *et al.* Low-Dose Radiation Conditioning Enables CAR T Cells to Mitigate Antigen Escape. *Molecular Therapy* **26**, 2542-2552 (2018). https://doi.org/10.1016/j.ymthe.2018.09.008
347 Esther, S. *et al.* Tuned activation of MSLN-CAR T cells induces superior antitumor responses in ovarian cancer models. *Journal for ImmunoTherapy of Cancer* **11**, e005691 (2023). https://doi.org/10.1136/jitc-2022-005691
348 Walker, A. J. *et al.* Tumor Antigen and Receptor Densities Regulate Efficacy of a Chimeric Antigen Receptor Targeting Anaplastic Lymphoma Kinase. *Molecular Therapy* **25**, 2189-2201 (2017). https://doi.org/10.1016/j.ymthe.2017.06.008
349 Katz, S. C. *et al.* Phase I Hepatic Immunotherapy for Metastases Study of Intra-Arterial Chimeric Antigen Receptor–Modified T-cell Therapy for CEA+ Liver Metastases. *Clinical Cancer Research* **21**, 3149-3159 (2015). https://doi.org/10.1158/1078-0432.CCR-14-1421
350 Chongqing Precision Biotech Co., L. (https://classic.clinicaltrials.gov/show/NCT05415475, 2021).
351 Institute of Medicine (US) Committee on Resource Sharing in Biomedical Research. in *Resource Sharing in Biomedical Research* (ed Bond EC Berns KI, Manning FJ) Ch. 2, (1996).
352 Capellero, S. *et al.* Ovarian Cancer Cells in Ascites Form Aggregates That Display a Hybrid Epithelial-Mesenchymal Phenotype and Allows Survival and Proliferation of Metastasizing Cells. *International Journal of Molecular Sciences* **23**, 833 (2022).
353 Hrvat, A. *et al.* Electrolyte imbalance causes suppression of NK and T cell effector function in malignant ascites. *Journal of Experimental & Clinical Cancer Research* **42**, 235 (2023). https://doi.org/10.1186/s13046-023-02798-8
354 Tarannum, M. *et al.* CAR memory–like NK cells targeting the membrane proximal domain of mesothelin demonstrate promising activity in ovarian cancer. *Science Advances* **10**, eadn0881 (2024). https://doi.org/doi:10.1126/sciadv.adn0881
355 Tang, L., Pan, S., Wei, X., Xu, X. & Wei, Q. Arming CAR-T cells with cytokines and more: Innovations in the fourth-generation CAR-T development. *Molecular Therapy* **31**, 3146-3162 (2023). https://doi.org/https://doi.org/10.1016/j.ymthe.2023.09.021
356 Wilkosz, S. *et al.* A comparative study of the structure of human and murine greater omentum. *Anatomy and Embryology* **209**, 251-261 (2005). https://doi.org/10.1007/s00429-004-0446-6
357 Bella, Á. *et al.* Mouse Models of Peritoneal Carcinomatosis to Develop Clinical Applications. *Cancers* **13** (2021).
358 Okabe, Y. Development and organization of omental milky spots. *Immunological Reviews* **324**, 68-77 (2024). https://doi.org/https://doi.org/10.1111/imr.13337
359 Ranoa, D. R. E. *et al.* Single CAR-T cell treatment controls disseminated ovarian cancer in a syngeneic mouse model. *Journal for ImmunoTherapy of Cancer* **11**, e006509 (2023). https://doi.org/10.1136/jitc-2022-006509
360 Casey, N. P. *et al.* Efficient CAR T cell targeting of the CA125 extracellular repeat domain of MUC16. *Journal for ImmunoTherapy of Cancer* **12**, e008179 (2024). https://doi.org/10.1136/jitc-2023-008179